Master thesis : Mould compensation for thermoset composites parts

Auteur : Pareja Muñoz, Miguel Alejandro
Promoteur(s) : Bruyneel, Michael; Georges, Arnaud
Faculté : Faculté des Sciences appliquées
Diplôme : Master en ingénieur civil en aérospatiale, à finalité spécialisée en "aerospace engineering"
Année académique : 2016-2017
URI/URL : http://hdl.handle.net/2268.2/2638

University of Liège
Faculty of Applied Sciences
Promotor: Michaël Bruyneel

Mold compensation for thermoset composites parts

Graduation Studies conducted for obtaining the Master's degree in Aerospace Engineering by

Miguel Alejandro Pareja Muñoz

Academic year 2016 - 2017

Dedicado a mi abuelo Miguel

"Ours is the commencement of a flying age, and I am happy to have popped into existence at a period so interesting."

Amelia Earhart (1897-1937)

Abstract

Samtech, a company whose main activity is the development of a FE software named `Samcef`, is interested in gaining know-how about mold compensation techniques for thermoset composites parts. For the latter purpose, an internship stage of 4 months has been dedicated to study the subject with Siemens's software `NX`, which includes `Samcef` capabilities.

A bibliographical research on the mold compensation techniques has been performed. Several aspects have been studied: the necessity of these compensation methods on the modern industry, the manufacturing processes of thermoset composite materials, the change in properties they experience (curing process), the origin of the geometrical deviations of the produced part from the desired geometry, the available numerical solutions to model the latter phenomena, and the already employed mold compensation techniques available in the literature: CAD-based and mesh-based strategies.

After that, a first numerical model has been developed in order for the identified mold compensation techniques to be implemented. An easy geometry with a predictable deformation has been selected – the deformation mode has been controlled with the composition of the employed laminate on the part. After refinement of the model, the mold compensation techniques have been carried out for the first time and a methodology, i.e. a set of steps and tasks, has been defined for each of them.

With the first simple geometry and laminate, the compensated mold has been found with the different compensation strategies. With these results, a first comparison of the methods has been done. Following that, different geometries with different deformation modes have been studied: the first geometry and a different one have been used with 4 different laminates. The compensation methods have suffered some modifications to adapt the new geometries and deformation modes, and success has not always been achieved. Besides, some restrictive factors have limited the application of some methods to some cases.

The results obtained have been valuable and varied enough to extract thorough conclusions on the strengths and weaknesses of the methods: their robustness, universality, accuracy, total time necessary or complexity have been analyzed. Finally, some proposals on the future continuation of the thesis have been discussed.

Acknowledgements

I would like to express my sincere gratitude to my academic advisor Dr. Michaël Bruyneel for his continuous support during the making of this thesis. He has provided me with uncountable and constructive suggestions which have greatly helped me in the development of the investigation carried out on mold compensation techniques. Furthermore, his feedback during the writing of the thesis has allowed me to improve the final outcome of this document.

I am also sincerely grateful to Dr. Frédéric Pascon, my industrial advisor, with whom I have spent many hours in the office in Samtech's headquarters. His patience, motivation, and immense knowledge have allowed me to overcome the many barriers I have encountered during the past 4 months. He has always been willing to dedicate time to solve my doubts, and his guidance has been key to properly set the limits and objectives of this thesis.

My sincere thanks also goes to Dr. Tom van Eekelen, who has selflessly dedicated his time to assist to the meetings we have had with Michaël and Frédéric. His opinions and experience on this thesis' subject, as well as his encouragement, are greatly appreciated.

I also want to acknowledge my internship colleague Cédric Laruelle for his every-day company at the office, in which we both have spent several hours working on our thesis. His energy has always motivated me and influenced me very positively. A warm appreciation also goes to all employees at Samtech, who have always been very kind with me during my stage there.

Lastly, my highest appreciation goes to my family and friends, without whom I would not be who I am today. Special thanks goes to my mom, as she has supported me wholeheartedly throughout the making of this thesis.

Contents

Introduction

This chapter briefly presents the motivation, objectives and the scope of this thesis. It also introduces the contents and organization of the document and it ends with the global methodology followed.

The main objective of this thesis is the study and development of mold compensation techniques for thermoset composite parts. The present study is done in collaboration with the company Samtech and serves as the master thesis project to complete the Master in Aerospace Engineering coursed by the author at the Université de Liège.

Samtech's main activity is the development of `Samcef` (*Système pour l'Analyse des Milieux Continus par Eléments Finis*) FE software, as well as the Caesam platform, which is a high-level integration platform in CAE. The company was recently acquired by Siemens PLM Software, one of whose leading products is `NX`, a CAD/CAM/CAE[1] software. Part of Samtech's activities is now the implementation of all `Samcef` capabilities into `NX` software. The software that will be used in this thesis will therefore be `NX` 11.0, in accordance with the current business orientation of Samtech.

The motivation of the project is the interest of Samtech to investigate the subject of mold compensation with `NX` and `Samcef` for the first time. The latter interest has turned into an internship of 4 months and a master thesis, which suited the author's curiosity.

The ultimate goals of this thesis are to implement and study the main mold compensation techniques found in the literature with `NX`. The latter consist in developing a numerical tool for the user to obtain the mold shape with which a desired composite material part can be manufactured within desired tolerances. To do so, the curing process of a certain thermoset composite material must be modeled and diverse methods that account for the cured-induced distortions must be considered to modify the final mold geometry.

The scope of the study is the implementation and test of the most used compensation techniques in `NX` and finding their strengths and weaknesses by compensating different geometries with different types of themroset composite laminates.

The thesis is organized in 5 chapters: Introduction; State of the Art, where a bibliographical research on the mold compensation techniques has been done; Numerical Model and Methodology, where the employed numerical models and the methodology, i.e. steps and tasks, followed to implement the compensation techniques are detailed;

[1] CAD stands for computer-aided design; CAM stands for computer-aided manufacturing; and CAE stands for computer-aided engineering.

Results, where the compensation results of the tested geometries and laminates with the different methods are presented; and finally, the Conclusions chapter with a summary of the conclusions deduced from the results and experience achieved.

Additionally, three appendices have been added to support the document: one on the Classical Lamination Theory (CLT), which describes the stress-strain behaviour of composite laminates; another in which a numerical verification of `Samcef` is made by comparing an analytic known case with a numerical model; and the last one is a brief explanation on how to obtain a CAD model from a mesh in `NX`.

For last, the methodology followed to develop the objectives of this thesis is presented below:

1. Get experience with the employed software: `NX` (`Samcef`); and do a bibliographical research in order to know the state of the art regarding mold compensation techniques and everything related to them: cure kinetics, cure distortions, modelling approaches, etc.

2. With a known geometry and unidirectional (UD) thermoset composite material properties, build an efficient thermo-mechanical model in order to try the mold compensation strategies on it.

3. Implement the main mold compensation techniques on an easy and predictable configuration.

4. Apply and modify in accordance the methods to compensate more complex deformation modes.

5. From the results obtained, extract conclusions on every method with regard to the geometry, deformation mode, easiness of application and other relevant features.

State of the Art

In this chapter, a bibliographic research on mold compensation techniques for thermoset composite material parts is presented. The industrial context in which this methods can be necessary is firstly introduced. After, the main distortions for which molds require compensation are detailed, preceded by an explanation of the main composite manufacturing processes and the curing process. The chapter ends with the exposition of the numerical modeling of the process and the main compensation strategies found in the literature.

2.1 Industrial Context

Composite materials[2] offer a number of advantages over traditional materials. They contribute to the development of durable, lightweight and high-performance structures; they help reducing the environmental impact of vehicles that use such structures, e.g. aircrafts or cars, as the weight reduction leads to less fuel consumption; and they are revolutionizing high value industrial sectors such as aerospace, automotive, wind energy, marine and construction.

Increasing demand for international travels has lead to a huge employment of these materials in the aerospace sector, having exceeded the symbolic threshold of 50% of the total structure weight in the Boeing 787 Dreamliner and the Airbus 350 XWB. Car chassis are also being manufactured with composites, with the main challenge to overcome being the production rate and cost optimization. Meanwhile, large-scale composite wind turbine blades face the challenge of having a reliable process at such scales respecting the desired tolerances.

Designing and manufacturing composite materials is a challenge for the industry. The composites industry has only been successful on individual cases, and the latter success has proven to be inadequate for the development of a coherent industry with deep expertise and volume production [1]. This difficulty to establish a solid industry is greatly related to the properties of composites and how those suppose a problem when manufacturing composite parts.

Composite material properties such as heterogeneity or anisotropy lead to interaction of the different scales that exist within these materials. There are meso/microscopic defects such as fiber misalignment, delaminations, porosity, resin-rich zones or internal stresses, among others. Conversely, macroscopic defects, e.g. cure-induced distortions, are the ones that play a crucial role in the final properties and shape of the composite part (studied in depth in this thesis).

Cure-induced distortions are deviations exhibited when the composite material is removed from the mold at the end of the manufacturing process. They are caused by different phenomena such as thermal and chemical shrinkage, material anisotropy, temperature heterogeneity, mold/part interaction or unsuitable process conditions. These

[2]Composite materials are also referred as *composites*.

distortions usually result in spring-in (angles in curved regions tend to close) or warpage (curvature or twist of initially flat regions) – see Figure 2.1 (a) and (b).

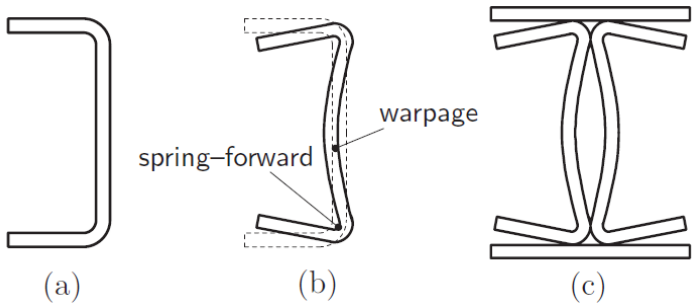

Figure 2.1: Typical distortions of a C-shpaed part: (a) intended geometry, (b) distorted geometry and (c) potential assembling problem [2].

This post-cure deformations can lead to different problems such as:

- Assembly of parts may be difficult or lead to failure: distortions may require a high effort to match two parts together – see Figure 2.1 (c).
- Reduced in-service loads as internal stresses are generated in the parts. The overall mechanical properties obtained are worsen.
- Shape non-conformities can have a crucial impact on the usefulness of the part. In terms of aerodynamic performance, a wind turbine blade can be completely useless if the final shape is far away from the targeted shape.

A recognised solution to tackle this phenomena, which is employed in the industry, is the use of stiffeners. The latter help reduce the amount of distortions but at the same time they are difficult to assemble and make it harder to anticipate the distortion modes [2]. An alternative to the use of stiffeners are mold compensation techniques, i.e. numerical tools capable of predicting the shape of the mold which minimizes the deviations with respect to the target design.

Despite numerous studies about cure-induced distortions, the literature still lacks tried-and-tested methodologies for their reduction. The increasing complexity of the designs makes rules of thumb obsolete, while relying on experimental trial-and-error sequences results in prohibitive additional costs and delays [2]. Thus, there exists a necessity of developing such mold compensation technique that can be easy to implement for different geometries and curing conditions.

2.2 Composite Manufacturing Processes

Several manufacturing techniques exist for thermoset composite processing. The choice of one over the other will be driven by the advantages and disadvantages of each technique. Some features to consider that are important to take this decision are detailed next:

Geometric accuracy	**Structural requirements**
Economical context	**Materials at hand**
Part dimensions & shape	**Production rate**
Laminate resulting mechanical properties	

Table 2.1: Some features relevant when choosing a manufacturing process.

However, a few common points serve as a basis for all manufacturing processes:

- **Molding** to shape the composite is always required. The characteristics of the mold will be decisive to accomplish some of the features detailed in Table 2.1.
- A **curing** cycle is undergone: resin changes from a liquid or viscous state to a solid state. The evolution of the curing temperature is crucial for the final mechanical properties and shape of the manufactured part.

2.2.1 The Autoclave Process

In an autoclave the composite, initially a prepreg[3], is subjected to elevated pressures (compaction of the laminate) and a temperature cycle (curing or polymerization process). The temperature of the prepreg is regulated owing to convective heat exchange with circulating hot air, following the pre-determined curing cycle. The prepreg is secured by a vacuum bag sealed at the periphery of the part [3]. The latter allows a high fiber to resin ratio and a good removal of air voids. In Figure 2.2, a depiction of the process is shown.

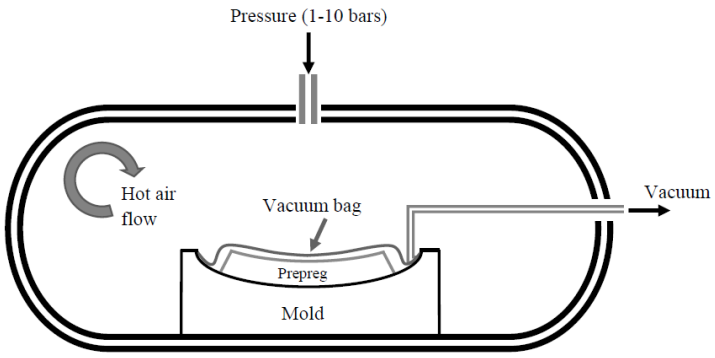

Figure 2.2: Schematic depiction of the autoclave process [2].

The advantages and disadvantages of this process are detailed in Table 2.2:

Advantages	Disadvantages
Only a lower mold is necessary	Very expensive
High quality of the final part	Size is limited by the manufacturing capabilities of the autoclave and mold

Table 2.2: Advantages and disadvantages of the autoclave process.

[3]Prepreg refers to pre-impregnated composite fibers where a thermoset polymer matrix is already present.

2.2.2 The RTM Process

The resin transfer molding (RTM) process is an alternative to produce high quality parts. A two-part, matched, closed mold, which is made of metal or composite material is used. Dry reinforcement (typically a preform) is placed into the closed mold and the two half molds are sealed together by a clamping force, normally exerted by a press. If the mold is not self-heating, the press has to play this role. Resin and catalyst are injected and mixed in dispensing equipment, then pumped into the mold under low to moderate pressure through injection ports, following predesigned paths through the preform [4] – the cure is performed inside the mold. Extremely low-viscosity resin is used in RTM applications for thick parts to permeate preforms quickly and evenly before cure.

Figure 2.3 depicts the above explained process. An alternative process is the Same Qualified RTM (SQRTM) process, where the dry fabric is replaced by prepregs and where the injected resin serves only as in-mold compaction pressure.

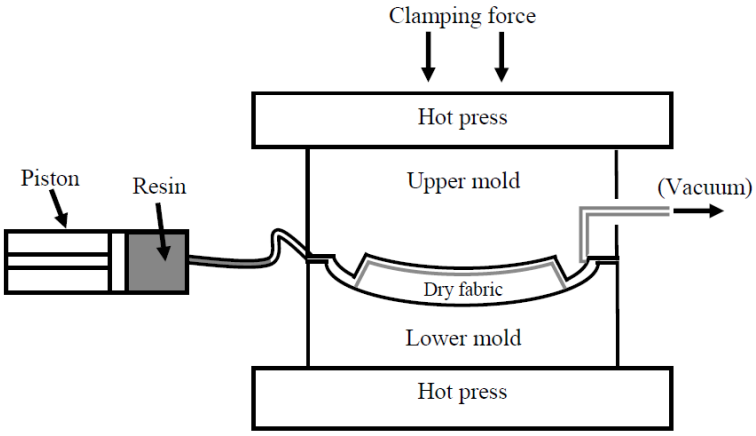

Figure 2.3: Schematic depiction of the RTM process [2].

The advantages and disadvantages of this process are detailed in Table 2.3:

Advantages	Disadvantages
Smooth surface finish on all exposed surfaces	Self-heating molds are expensive
Dry fabrics and resins are less expensive than prepregs	Using a press limits the size of the parts
Low void content	

Table 2.3: Advantages and disadvantages of the RTM process.

2.2.3 The VARTM Process

The vacuum-assisted resin transfer molding (VARTM) process is a low-cost alternative to the RTM process. In this process the resin flow is driven by the atmospheric pressure. This drastically reduces the impregnation speed, and a low-facilitating medium is generally needed on top of the fabric, which prevents the use of an upper mold [2] – see Figure 2.4.

The lower pressure also results in a higher void content, excluding this process for high performance applications – using a double bag technique helps improve the latter aspect.

Fiber reinforcements are placed in a one-sided mold, and a cover, typically a plastic bagging film, is placed over the top to form a vacuum-tight seal. The resin typically enters the structure (by vacuum) through strategically placed ports and feed lines, that facilitate wetout of the fibers [4]. The part size is, in theory, not limited – this process is used in the naval or wind turbine industries. VARTM operates with low-cost tooling, making it possible to inexpensively produce large, complex parts in one shot.

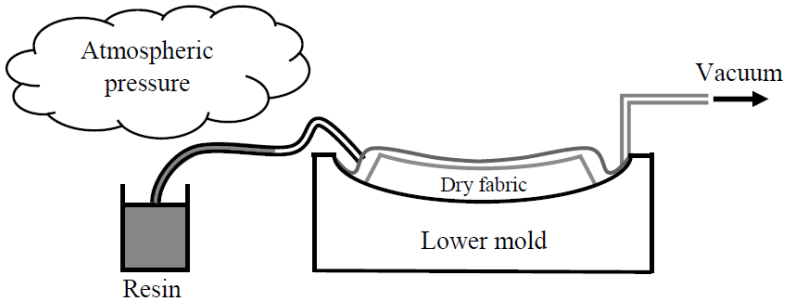

Figure 2.4: Schematic depiction of the VARTM process [2].

The advantages and disadvantages of this process are detailed in Table 2.4:

Advantages	Disadvantages
Size is not limited	Higher void content than RTM
Cheaper than RTM	Fails to produce high performance parts

Table 2.4: Advantages and disadvantages of the VARTM process.

2.3 Cure Development

The curing of a composite material is actually that of the matrix, i.e. the thermoset resin. During the curing process, the resin changes from a liquid/viscous state to a solid state. The solidification of the resin consists in the cross-linking of the polymer chains, which is an irreversible process. The curing process is a heat-activated auto-catalytic exothermic chemical reaction.

The temperature required to activate the reaction ranges from room temperature for low-cost resins, to about 180°C for the high performance epoxy resins. The typical processing time is a few hours [2]. The degree of cure X ($X \in [0, 1]$) is a fundamental parameter to understand the curing process, and it drives the change in stiffness in the resin, its thermal expansion and its chemical shrinkage. The resin is liquid until the gel point X_{gel} (gelation). This value is assumed to be a constant characteristic of the resin. After, the resin is in a rubbery state, i.e. can withstand some stresses, until the glassy or solid state is reached (vitrification).

An important parameter to be defined is the glass transition temperature T_g, which is the temperature of transition between the glassy and rubbery state. It evolves (increasingly) with the curing process. When T_g is higher than the temperature of the material, the mobility of the polymer drops drastically, i.e. the glassy state is reached. After that, the reaction becomes diffusion-controlled and the cure slows down and eventually stagnates – see Figure 2.5.

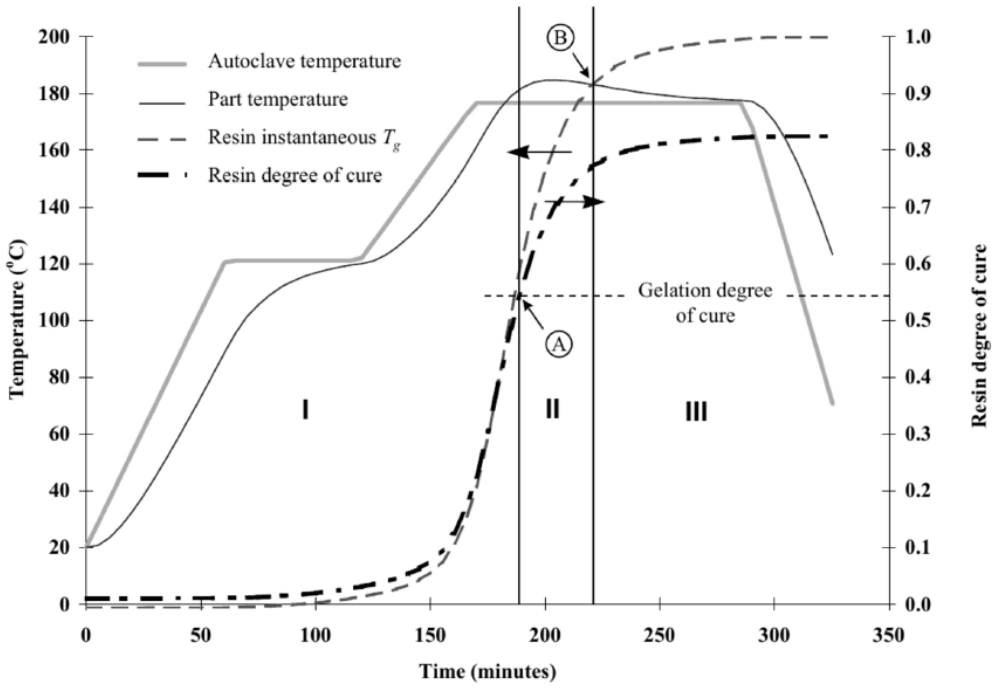

Figure 2.5: Typical curing cycle and cure development for a high performance epoxy. Point A is gelation, point B is vitrification. Phases I to III refer to liquid, rubbery and glassy states, respectively [2].

A first temperature dwell at a lower temperature (in Figure 2.5 is 120°C) is commonly applied to limit the amount of exothermic heat and to lower the viscosity of the resin in order to degas it more easily. Then the material is heated and maintained at the cure temperature until a desired degree of cure is reached. A higher final degree of cure can then be reached by increasing the cure temperature or by performing a post-cure step, leading to improved material properties [2].

2.4 Manufacturing-induced Distortions

The distortions of the composite material after the curing process can have different origins. The variables or phenomena that influence the manufacturing-induced distortions are: chemical shrinkage, thermal shrinkage, temperature cycle (curing cycle), anisotropy and stacking sequence, mold/part interaction and inhomogeneities of the process or in the laminate.

The latter produce the development of a non-reversible dilatational strain. These phenomena are briefly explained next, and they serve for a better understanding of how to model such distortions (Section 2.5) and as a starting point to develop the mold compensation techniques (Section 2.6).

2.4.1 Chemical Shrinkage

As the curing progresses, the density of the resin increases. That is due to the conversion of secondary bonds between monomer molecules into covalent bonds, the latter being shorter than the former [2]. This is an irreversible process that lead to residual stresses and shape distortions.

2.4.2 Thermal Shrinkage

The thermal shrinkage is caused by the different behaviours of the resin during the evolution through three material states – i.e. different coefficient of thermal expansion (CTE).

- **Liquid state**: the resin just flows through the fibers. Generally the CTE is very close to 0 and it is usually considered null.
- **Rubbery state**: there is an expansion that creates residual stresses and shape distortion. The CTE is not null anymore.
- **Glassy state**: the CTE is usually smaller than in the rubbery state.

The expansion and contractions that the resin experiences throughout the process are different during the heating and the cooling phases. Therefore, the deformations do not cancel out and at the end of the curing process permanent distortions remain in the cured part. Figure 2.6 schematically depicts the development of the dilatational strain ε^E, to which the chemical and thermal shrinkage contribute.

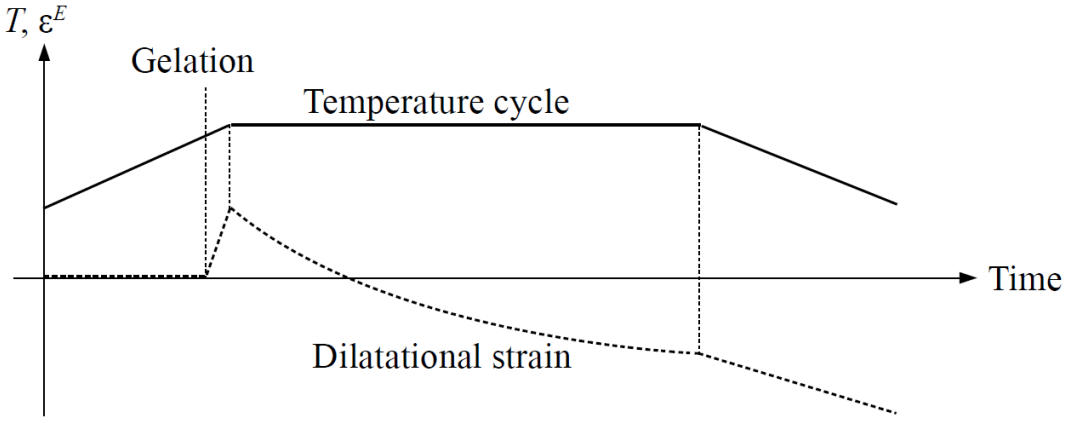

Figure 2.6: Development of dilatational strain with the curing cycle resulting in residual stresses [2].

2.4.3 Temperature Cycle

The temperature cycle followed during the curing process influences the total dilatational strain. Reaching gelation at a lower temperature leads to a larger thermal expansion in the rubbery state (see Figure 2.6), which can balance out the thermal and chemical shrinking, leading to less distortions.

2.4.4 Anisotropy and Stacking Sequence

Anisotropy is the main cause of spring-in deformations. Fibers are chemically inert and exhibit a lower CTE than resins. Since the tangential strain is constrained by the fibers, the radial strain is the one that has the greatest contribution, resulting in the spring-in effect – see Figure 2.7.

The in-plane anisotropy of composites enhances the ability of the material to avoid or reduce spring-in, as a reduction of the through-thickness (radial direction in Figure 2.7) contraction is obtained.

Then, regarding the stacking sequence of the laminate, asymmetrical layups lead to warpage due to the anisotropy of the mechanical properties of each layer.

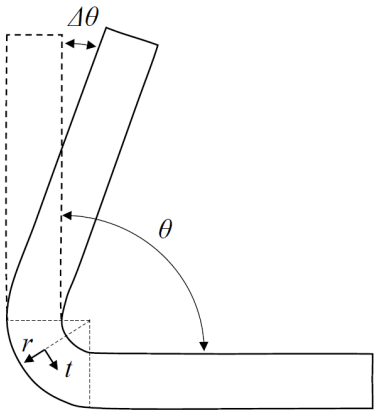

Figure 2.7: Spring-in resulting from the anisotropic nature of composite materials (r stands for the radial direction and t for the tangential direction) [2].

2.4.5 Mold/part Interaction

When the mold and the composite part are in contact, there is a traction applied by the mold to the laminate due to the CTE mismatch between the two materials. If one-sided mold is used (autoclave or VARTM processes), asymmetrical in-plane forces appear on the composite material which finally lead to friction between the metal (mold) and composite (part).

This phenomena may lead to inappropriate contact between the mold and the part. The latter implies an heterogeneous temperature distribution along the material (due to the contact mismatch) which leads to different curing ratios and therefore, different resin final properties and permanent deformations. A way to mitigate this phenomenon is decreasing the mentioned friction: the use of Mylar or propylene sheets at the interface can help reduce that negative phenomenon [2].

2.4.6 Inhomogeneities

Inhomogeneities on the composite material during the curing process lead to distortions. One of the major inhomogeneities that can be found in the manufacturing process are temperature gradients. Temperature gradients in massive metal molds lead to an imbalance in the residual stresses, and therefore warpage appears on the laminate. The latter temperature gradients may origin from poor contact between the mold and the part, or from an uneven heating of the mold or the chamber the mold is in (autoclave process).

Other sources of inhomogeneities are: fiber volume gradients, fiber misalignment, corner thickening or void content. All these phenomena depend on the proper execution of manufacturing process, e.g. void content can be avoided with a proper vacuum and with an even pressure distributed on the prepreg.

2.5 Process Modeling

In order to predict the cure-induced distortions, numerical models are necessary to describe the evolution of the main variables involved in the manufacturing process of thermoset composite parts: the degree of cure X, the glass transition cycle temperature T_g, the cycle temperature T, the coefficients of thermal expansion α and of chemical shrinkage β of the composite and the mechanical properties of the composite.

The mechanical behaviour of the thermoset composites during curing must also be modeled, which must take into account the coupling with the thermal process and the consequent change in resin properties.

2.5.1 Cure Kinetics

Cure kinetics deals with the evolution of the degree of cure X during the hardening of the composite material – that is, the hardening of the thermoset resin. The degree of cure X is defined as the ratio between the heat released by the cure reaction and the maximum possible heat per unit mass released by the reaction H_T:

$$X(t) = X_0 + \frac{1}{H_T}\int_0^t \frac{\mathrm{d}H}{\mathrm{d}\tau}\mathrm{d}\tau, \tag{2.1}$$

where X_0 is the degree of cure at the beginning of the experiment (usually zero), and $\mathrm{d}H/\mathrm{d}\tau$ is the instantaneous heat flux per unit mass released by the reaction. X is a dimensionless variable varying between 0 and 1.

Most phenomenological models assume that the cure rate is solely a function of the degree of cure and of the temperature, i.e. $\dot{X} = f(X,T)$. The models that perform best are the ones that account for the auto-catalytic nature of the reaction and for the diffusion effect which limits the cure in the glassy state.

The model proposed in `Samcef` is the following [5]:

$$\dot{X}(X,T) = [K_1(1-X)^{n_1} + K_2X^m(1-X)^{n_2}]f_d, \tag{2.2}$$

where n_1, m, n_2 are partial orders of the reaction, and K_1 and K_2 are kinetic constants related to the temperature through Arrhenius-type equations $K_i = A_i e^{-S_i/RT}$, in which A_i are frequencies and S_i are activation energies. The term X^m guides the aforementioned auto-catalytic aspect. Regarding f_d, it represents a diffusion function which tends to zero when the mobility of the polymer chains prevents further cure.

`Samcef` includes the rate-limiting effect of vitrification using two different approaches: the diffusion function is dependent on the degree of cure X [$f_d(X)$] or the glass transition temperature T_g [$f_d(T_g)$]. The former option has been chosen with the following diffusion function:

$$f_d(X) = \frac{2}{1+\exp(\frac{X-X_{max}}{b_D})} - 1 \tag{2.3}$$

where b_D is a fitting parameter for each specific curing cycle. The parameters of a kinetic model are most commonly fitted from Differential Scanning Calorimetry (DSC) measurements, monitoring the heat flux released during curing reactions.

2.5.2 Glass Transition Temperature

The glass transition temperature T_g is an increasing function of X. `Samcef` implements the evolution of T_g as proposed by Di Benedetto [5]:

$$T_g(X) = T_{g0} + (T_{g\infty} - T_{g0})\frac{\lambda X}{1-(1-\lambda)X}, \tag{2.4}$$

where T_{g0} is the T_g of an uncured sample ($X = 0$), $T_{g\infty}$ is the T_g of a fully-cured sample ($X = 1$), and λ is a fitting parameter. The glass transition temperature can be measured by DSC or Dynamic Mechanical Analysis (DMA).

2.5.3 Cycle Temperature

Defining the cycle temperature T in `Samcef` can be approached in two ways:

- Define the curing cycle with respect to time and space $T(t, x)$ and apply it to the numerical domain.
- Define thermal boundary conditions that will in turn define the cycle temperature of the composite part: convection, conduction or radiation and its respective properties or associated parameters as the convection/conduction/radiation thermal coefficients or the heat fluxes.

2.5.4 Thermal Expansion and Chemical Shrinkage

2.5.4.1 Thermal Expansion

The thermal expansion of the resin is related to the increment of temperature as follows: $\Delta\varepsilon_{th} = \alpha\Delta T$, being α the CTE of the composite material. As explained in Section 2.4.2, the CTE of thermoset resins changes dramatically during the curing process. `Samcef` uses separate values for the three states that the resin undergoes, being the CTE constant for each state.

The CTE of both components of the composite material (matrix and fibers) are introduced separately, then homogenized. For the matrix, three different values must be introduced:

$$\alpha_m(T, X, T_g) = \begin{cases} \alpha_{ml} & \forall X \leq X_{gel} \\ \alpha_{mr} & \forall X > X_{gel},\ T_g < T \\ \alpha_{mg} & \forall X > X_{gel},\ T_g \geq T \end{cases} \tag{2.5}$$

Regarding the fibers, their CTE is assumed transversely isotropic: α_{f1} is the coefficient in the fibers direction and $\alpha_{f2} = \alpha_{f3}$ are the ones in the two transverse directions. Then, the CTE α_i of a unidirectional (UD) ply is computed using the following homogenization rules:

$$\alpha_1 = \frac{\alpha_m E_m(1-V_f) + \alpha_{f1} V_f E_f}{E_m(1-V_f) + V_f E_f} \tag{2.6}$$

$$\alpha_2 = \alpha_3 = \alpha_m(1-V_f) + \alpha_{f2} V_f \tag{2.7}$$

which must be computed for the three states that the resin undergoes throughout the curing process (equation 2.5). V_f is the fiber volume fraction.

2.5.4.2 Chemical Shrinkage

Another matrix property to be defined is the chemically-induced shrinkage coefficient, denoted by β_m. This coefficient is linking the chemical shrinkage of the resin to the degree of cure as follows [5]: $\Delta\varepsilon_{ch} = -\beta_m \Delta X$, with β_m implemented in `Samcef` as

$$\beta_m(T, X, T_g) = \begin{cases} \beta_{ml} & \forall X \leq X_{gel} \\ \beta_{mr} & \forall X > X_{gel},\ T_g < T \\ \beta_{mg} & \forall X > X_{gel},\ T_g \geq T \end{cases} \tag{2.8}$$

A positive β_m induces an isotropic shortening of a piece of resin in the three directions for any increase of the degree of cure ($\Delta X > 0$). Then, since only the matrix is undergoing chemical shrinkage, the β_i of a composite UD ply is computed using the following homogenization rules:

$$\beta_1 = \frac{\beta_m E_m (1 - V_f)}{E_m(1 - V_f) + V_f E_f} \tag{2.9}$$

$$\beta_2 = \beta_3 = \beta_m (1 - V_f) \tag{2.10}$$

which must be computed for the three states that the resin undergoes throughout the curing process (equation 2.8).

2.5.5 Properties of Thermoset Composites during Cure

The mechanical properties of a UD ply of composite material are calculated in `Samcef` as explained below.

2.5.5.1 Resin (Matrix) Properties

The matrix is assumed to be a thermoset resin. Its mechanical behavior is evolving with the cycle temperature T, the degree of cure X and the glass transition temperature T_g. At any time, the temperature, degree of cure and glass transition temperature fields must be defined. There are two ways to do this:

- To run first a thermal analysis of curing. Then, the corresponding results – i.e. T(t,x), X(t,x) and T_g(t,x) – are stored in a .u18 file (model definition and results) and they are reloaded during the mechanical analysis using:
  - Identical meshes.
  - Mapping process – dissimilar meshes.
- A second method is to explicitly define the cycle temperature T, the degree of cure X and the glass transition temperature T_g. These values can be defined as constant or as functions of time. And then they are used in the mechanical analysis as inputs.

The resin matrix is assumed to behave like an isotropic elastic material, characterized by a Young's modulus E_m and a Poisson's ratio ν_m. For both the Young's modulus and Poisson's ratio, three values must be defined: E_{mg}/ν_{mg}, E_{mr}/ν_{mr}, and E_{ml}/ν_{ml} for the glassy, the rubbery, and the liquid states, respectively.

Those three Young's moduli and Poisson's ratios will be used according to current values of cycle temperature T, the degree of cure X and the glass transition temperature T_g. All three can be defined as functions of T and/or X and/or T_g.

The Young's modulus E_m and the Poisson's ratio ν_m of the matrix, which will be used for the homogenization of the stiffness properties of the composite, are therefore defined as:

$$E_m(T,X,T_g) = \begin{cases} E_{ml}(T,X,T_g) & \forall X \leq X_{gel} \\ E_{mr}(T,X,T_g) & \forall X > X_{gel},\ T_g < T \\ E_{mg}(T,X,T_g) & \forall X > X_{gel},\ T_g \geq T \end{cases} \tag{2.11}$$

$$\nu_m(T,X,T_g) = \begin{cases} \nu_{ml}(T,X,T_g) & \forall X \leq X_{gel} \\ \nu_{mr}(T,X,T_g) & \forall X > X_{gel},\ T_g < T \\ \nu_{mg}(T,X,T_g) & \forall X > X_{gel},\ T_g \geq T \end{cases} \tag{2.12}$$

2.5.5.2 Fibers Properties

The fibers are assumed to be all aligned to the direction 1 of the UD ply (see Figure 2.8) and such is considered in the computation of homogenized properties. The elastic properties of the fibers are isotropic: Young's modulus E_f, Poisson's ratio ν_f and shear modulus G_f.

2.5.5.3 Homogenized Properties

The homogenized elastic properties are computed considering isotropic properties for the fibers and matrix. The model presented below is valid for unidirectional systems only, since transverse isotropy is assumed for the fibers. Its formulation is based on the laws of mixture originally established by *R. Hill* [6] and *Z. Hashin* [7].

Let V_f, E_f, ν_f, G_f and V_m, E_m, ν_m, G_m denote the volume fractions, Young's moduli, Poisson's ratios and shear moduli of the fibers and matrix material respectively. The hydrostatic compressive modulus of the fibers (K_f) and the matrix (K_m) are first defined:

$$K_f = \frac{E_f}{2(1-2\nu_f)(1+\nu_f)} \tag{2.13}$$

$$K_m = \frac{E_m}{2(1-2\nu_m)(1+\nu_m)} \tag{2.14}$$

The latter are used to determine the transverse bulk modulus K_t:

$$K_t = K_m + \frac{V_f}{\frac{1}{K_f - K_m} + \frac{1-V_f}{K_m + G_m}} \tag{2.15}$$

The 9 elastic coefficients are then successively derived from the following expressions:

- Longitudinal modulus (aligned with the fibers – see Figure 2.8)

$$E_1 = E_f V_f + E_m(1-V_f) + \frac{4V_f(1-V_f)(\nu_f - \nu_m)^2}{\frac{V_f}{K_m} + \frac{1}{G_m} + \frac{1-V_f}{K_f}} \tag{2.16}$$

- In-plane Poisson's ratio

$$\nu_{12} = \nu_f V_f + \nu_m(1 - V_f) + \frac{V_f(1 - V_f)(\nu_f - \nu_m)(\frac{1}{K_m} - \frac{1}{K_f})}{\frac{V_f}{K_m} + \frac{1}{G_m} + \frac{1-V_f}{K_f}} \tag{2.17}$$

- In-plane shear modulus

$$G_{12} = G_m \frac{G_f(1 + V_f) + G_m(1 - V_f)}{G_f(1 - V_f) + G_m(1 + V_f)} \tag{2.18}$$

- Transverse shear modulus

$$G_{23} = G_m + \frac{G_m V_f}{\frac{G_m}{G_f - G_m} + \frac{(K_m + 2G_m)(1-V_f)}{2K_m + 2G_m}} \tag{2.19}$$

- In-plane transverse Young's modulus (aligned with the matrix – see Figure 2.8)

$$E_2 = \frac{2}{\frac{1}{2K_t} + \frac{1}{2G_{23}} + \frac{2\nu_{23}^2}{E_1}} \tag{2.20}$$

- Transverse Poisson's ratio:

$$\nu_{23} = \frac{E_2}{2G_{23}} - 1 \tag{2.21}$$

- The three other coefficients are obtained from the transverse isotropy assumption:

$$\begin{cases} E_3 = E_2 \\ \nu_{13} = \nu_{12} \\ G_{13} = G_{12} \end{cases} \tag{2.22}$$

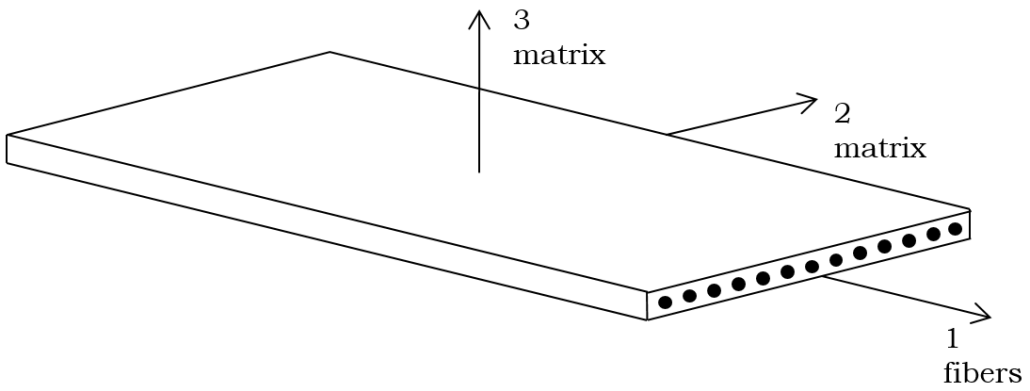

Figure 2.8: Schematic representation of a UD ply.

2.5.6 Mechanical Behavior of Thermoset Composites during Cure

There are different models proposed to model the mechanical behavior of thermoset resins during the curing process. They can be classified in two groups: cure-hardening instantaneous linear elasticity (CHILE) models and viscoelastic models.

Viscoelastic models consider the resin as viscoelastic, thus introducing the viscous effects (relaxation). CHILE models, on their side, neglect relaxation effects and consider the material as linear elastic at every point in time:

$$\sigma_{ij}(t) = \int_0^t C_{ijkl}(\tau) \frac{\partial(\varepsilon_{kl} - \varepsilon_{kl}^E)}{\partial \tau} \mathrm{d}\tau; \tag{2.23}$$

where C is the elastic tensor, which will be varying according to the evolution of the resin properties, σ is the stress, ε is the total strain and ε^E is the dilatational strain resulting from the thermal expansion and chemical shrinkage.

The default model implemented in `Samcef` is a CHILE model in which C_{ijkl} has three constant values, one for each state that the matrix undergoes. Thus, the change of C_{ijkl} is driven by the evolution of X. The latter model is the one employed in this thesis.

2.5.7 Thermo-mechanical Coupling

The curing cycle that leads to the process-induced distortions (coupling between thermal, chemical and mechanical phenomena) is solved as follows:

Starting from an initial state, the heat equation is solved in conjunction with the chosen kinetics model. This yields a distribution of temperature T, degree of cure X and glass transition temperature T_g over the part. Knowing these fields, the coefficients of chemical shrinkage β and thermal expansion α, as well as the mechanical properties can be determined. The latter will be used in the mechanical simulation.

The thermo-mechanical coupling can either be weak, staggered or strong. In the first case, the entire thermal simulation is performed and used as an input to the mechanical simulation. In the second case, this communication is performed at every time step. In the case of strong coupling, all the equations are solved simultaneously at each time step. The choice of the coupling method has almost no influence on the solution as the mechanical behavior has no influence on the thermal behavior, except for some second-order effects, e.g. distortions leading to a loss of thermal contact [2].

2.6 Mold Compensation Strategies

There are two types of strategies for a generic numerical compensation framework: CAD-based strategies and mesh-bashed strategies.

- CAD-based strategies consist in parametrizing a CAD model of the nominal geometry (target design) and using an optimizer, find the optimal value of the set of parameters $\mathcal{P}$ which reduces the cure-induced distortions as much as possible.

- Mesh-based strategies do not use an optimizer since they rely on the application of an appropriate correction to the mesh based on the distortions observed at a previous iteration.

The complexity of the computational chain (see Figure 2.9) depends on what must be automated or not. If the CAD geometry is changed, this geometry must be meshed automatically and then the input file for the simulation must be prepared automatically as well. From that standpoint, mesh-based strategies are simpler. Nevertheless, mesh-based strategies may require a time-consuming CAD reconstruction step after the final mesh is obtained.

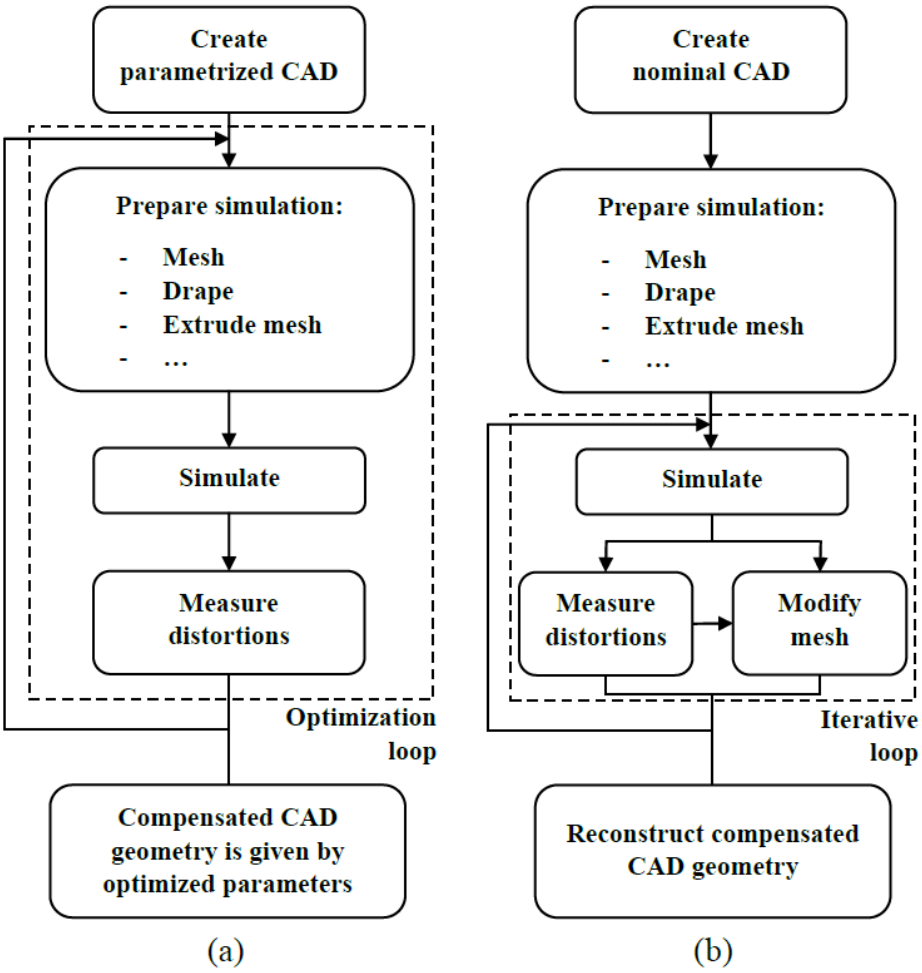

Figure 2.9: Flowchart of the different mold compensation techniques: (a) CAD-based (b) Mesh-based [2].

2.6.1 CAD-based Methods

CAD-based methods require an optimization loop to find the values of the set of parameters $\mathcal{P}$ that minimize the difference between the cured part and the nominal part. Thus, a quantitative indicator is necessary to measure the overall distortions: spring-in angle, twist angle, maximum deflection, or alternative approaches are used.

An alternative approach is selecting a set of points (control points) and measure the distance between each point in the distorted geometry and its counterpart on the

nominal geometry. The quantitative indicator is an averaged sum of all squared distances, proposed in [2], named D_{min}. The choice of the points remains subjective. They must be as representative of the main features of the geometry as possible.

It is necessary to implement an algorithm (optimization procedure) to find the optimal residual distance between the cured mesh and the nominal mesh. The algorithm must find the rigid body motion that minimizes D_{min}:

$$D_{min} = \frac{1}{N} \sum_{i=1}^{N} \| P_i(\lambda) P_i^0 \|^2 \tag{2.24}$$

where N is the number of control points (CPs), λ the applied rigid body mode, $P_i(\lambda)$ is the point to which λ is applied and P_i^0 is the point in the nominal geometry. If $D_{min} = 0$, then the two geometries (deformed and nominal) coincide perfectly.

Minimizing the spring-in angle or D_{min} for a chosen set of points may lead to different optimum layouts. In some cases the final results will match perfectly. That will strongly rely on the initial geometry and the amount of deformation variables involved in it.

2.6.1.1 Distortion Modes Method

One CAD-based technique is the Distortion Modes Method (DMM) [2]. In the DMM the compensation is based on the actual deformation mechanisms which give rise to the cure-induced distortions, e.g. spring-in or twist angles. The method is largely subjective as the deformation mechanisms to compensate, i.e. the optimization variables, are user-chosen. An optimization process is necessary to minimize the cure-induced mechanisms.

A schematic representation of the method is given in Figure 2.10 (a). In the present example, the set of parameters to compensate the composite part is $\mathcal{P} = \theta$, where θ is the spring-back angle – as the curved region tends to open.

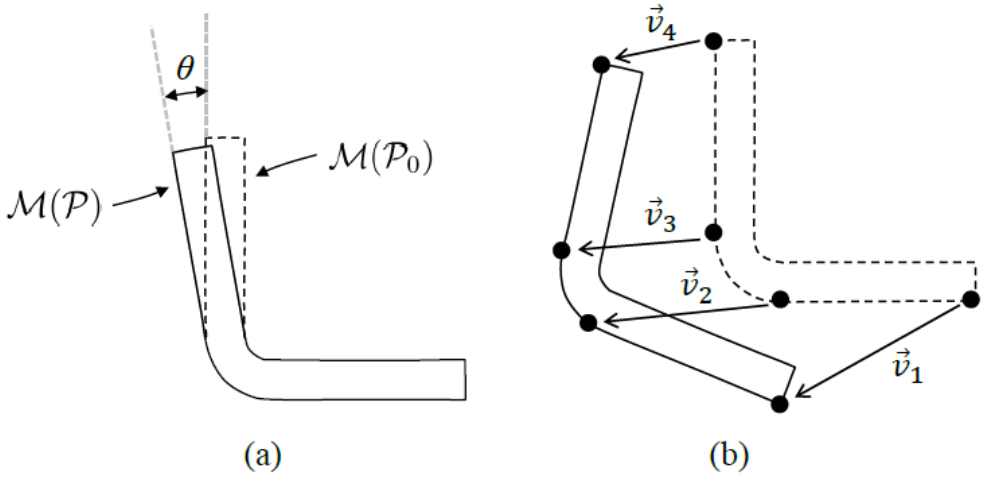

Figure 2.10: Schematic explanation (a) of the Distortion Modes Method; and (b) of the Control Points Method [2].

2.6.1.2 Control Points Method

Another CAD-based technique is the Control Points Method (CPM) [2]. The CPM requires the parametrization of the position of a certain set of points: the control points (CPs). The position of the control points, i.e. the displacement field with respect to the nominal geometry, is the set of variables to use in the optimization procedure. A schematic representation of the method is given in Figure 2.10 (b). In the present example, $\mathcal{P}$ is composed of the three components of each vector $\overrightarrow{v_i}$.

As aforementioned, the CPs must be as representative as possible of the geometry. This parametrization offers a richer design space (in comparison with DMM), since it leaves more freedom in terms of shapes to be tested by the optimizer. The parametrization does not need to be applied to the whole geometry, but still the CPM requires a higher number of parameters than the DMM.

2.6.1.3 Comparison: DMM and CPM

According to [2] both perform well, in different manners. If the objective of the compensation is to minimize the overall distance between a cured and nominal geometry for a given set of points, then the CPM is more efficient. On the other hand, the DMM is much faster and successful in minimizing several user-selected distortion values simultaneously. As the DMM is more subjective than the CPM, the latter seems more suitable for the perspective of developing a systematic mold compensation strategy for complex geometries.

2.6.1.4 Optimization Algorithms

Either in the DMM as in the CPM, the optimization problem in this thesis is an unconstrained optimization problem – i.e. neither the deformation modes nor the position of the CPs are theoretically constrained, despite, for instance, a spring-in angle being physically limited to be 360^o the most.

The objective function to be minimized is already determined for the CPM: D_{min} (see equation 2.24). On the other hand, the objective function for the DMM must be defined for every particular case. The latter requires a good understanding of the compensation problem (i.e. accurate prediction of the deformation modes), otherwise a poor-defined objective function may lead to a false optimum.

The optimization algorithm is greatly related to the objective function. In the literature there is a wide variety of algorithms at hand, which have their perks and downfalls depending on the optimization problem. The most relevant to mention for the present study are detailed below:

- **Gradient-based algorithms**: algorithms in which the search direction is defined by the gradient of the function at the current point. These algorithms, e.g. steepest descent or conjugate gradients, are globally convergent (finite number of iterations) to a *local* minimum with certain assumptions on the function: convexity and continuity of the gradient. There is no guarantee that they converge at all if the latter conditions are not satisfied. The most general way to detail such algorithms is detailed below. Let $f(x)$ be the objective function:

1. **Initialization**: choose $x^0 \in \mathbb{R}^n$ and set $k = 0$.
2. **Direction finding**: compute s^k such that $[s^k]^T \Delta f(x^k) < 0$.
3. **Line search**: find p^k such that $f(x^k + p^k s^k) = \min_{\alpha \geq 0} f(x^k + p^k s^k)$.
4. **Update**: set $x^{k+1} = x^k + p^k s^k$.
5. **Convergence check**: if satisfied, the optimum is $x^* \approx x^{k+1}$. Otherwise, set $k = k + 1$ and go back to step 2.

- **Second order algorithms**: besides gradient-based methods, second order methods, like the Newton Methods, could also be used. The main inconvenience of these methods is that first and second order derivatives must be computed for the update of the current iterate.

- **Surrogate-based algorithm**: it evaluates the objective function for a collection of individuals over a design space. Then, an interpolation function is fitted to these results – i.e. an approximation of the objective function, i.e. a surrogate model, is obtained. The fitting coefficient must be higher than a user-set threshold to have an approximation accurate enough, usually higher than 0.7. After, the minimum of the surrogate model is found, and the curing simulation of this optimum is computed and then fed into the data set for the next iteration. A new surrogate model is computed and the process is repeated until the optimum has not improved for a significant number of iterations, at the user's discretion. The use of this type of algorithm allows for a much faster global optimization process compared to gradient-based methods, which lack space exploration and convergence to a global minimum is not guaranteed.

All one-variable surrogate models of this thesis are polynomials of a certain user-chosen order fitted with `Excel`. All two-variable surrogate models of this thesis are polynomials of a certain user-chosen order fitted with `Matlab` using its built-in function *fit*. To find the minimum of the surrogate models a Wolfram|Alpha (the computational knowledge engine) widget has been used [8].

2.6.2 Mesh-based Methods

The mesh-based method proposed in [2] is called the Mirror Method (MM). It is based on the notion that cured-induced distortions may be considered as linear in a first approximation. Under this hypothesis, the compensated geometry should thus be close to the inverted cured geometry with respect to the nominal geometry. Correction of the geometry is performed based on the meshes as follows:

$$\mathcal{M}^{i+1} = \mathcal{M}^i + (\mathcal{M}^o - \mathcal{M}^i_c) \tag{2.25}$$

where $\mathcal{M}^i$ is the mesh of the mold geometry of part *before* curing at iteration i, $\mathcal{M}^o$ is the mesh of the nominal geometry and $\mathcal{M}^i_c$ is the mesh of the part geometry *after* curing at iteration i. An example of the process is depicted in Figure 2.11, where it can be seen that the update of the mold geometry following equation 2.25 tends to the inverted cured geometry with respect to the nominal geometry, as previously mentioned.

In the MM, the measurement of the distortions is the same as for CAD-based methods, except that the residual distance covers all the nodes, and not just the selected points as in the CPM.

This method converges towards a perfect compensation when the main distortion is spring-in, and in very little iterations (ranging from 1 to 4, normally) [2]. When warpage prevails, though, the method stagnates or diverges [2]. This is due to the radical change of behaviour between the nominal and reversed geometry. When warpage prevails the main hypothesis of the MM, that is *linear* cured-induced distortions, is not satisfied.

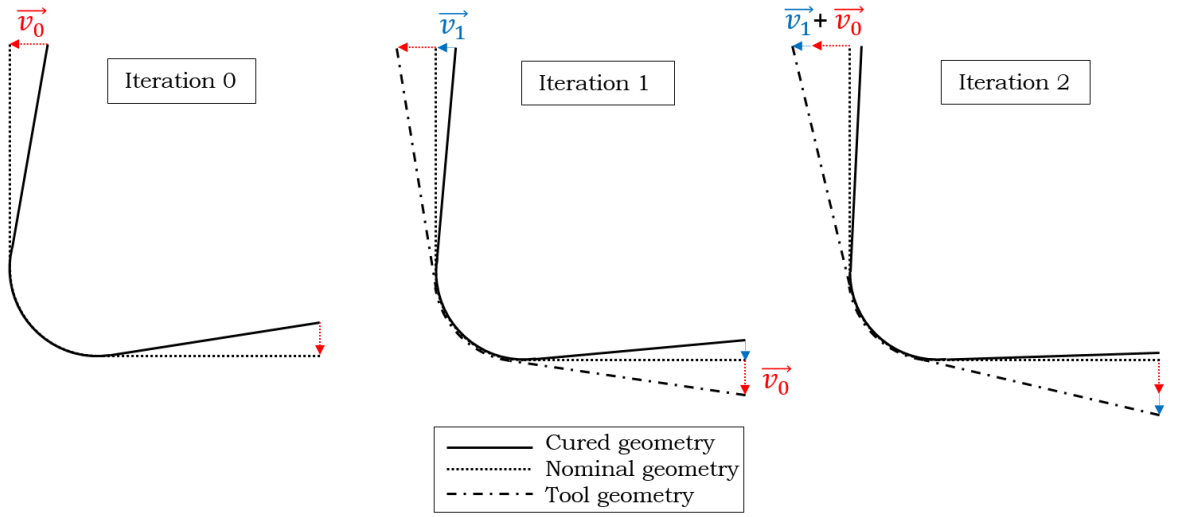

Figure 2.11: Schematic depiction of the Mirror Method. In iteration 0 the nominal geometry = mold geometry.

Numerical Model and Methodology

In this chapter, the numerical models employed to test the mold compensation techniques are presented. After, the methodology followed to implement each compensation method is detailed.

3.1 Numerical Model

3.1.1 Common Properties of All Models

The evolution of the mechanical properties of the composite material (parameter C_{ijkl} in equation 2.23), follows the default CHILE model implemented in `Samcef` − i.e. viscoelastic effects are neglected. The resin properties, E_m and ν_m, only have three discrete constant values each, one for every physical state that the resin undergoes throughout the curing process. Accordingly, C_{ijkl} will also be different at each physical state, using the resultant properties of the laminate that are computed with equations 2.16 to 2.22.

The name of the employed composite material on this thesis is not shared for confidentiality reasons. The mechanical, thermal and chemical properties of the used material are detailed in Table 3.1. Regarding the curing properties, the cure kinetics model $X(\dot{X}, T)$, the vitrification model $f_d(X)$ and the glass transition temperature $T_g(X)$ model are the ones described by equations 2.2, 2.3 and 2.4 in Section 2.5, respectively. The parameters of those models are detailed in Table 3.2.

The specific heat and the thermal conductivity, as well as the maximum curing heat released H_T of the employed composite are not defined. This is due to the thermal boundary conditions, which are defined below along with the mechanical boundary conditions.

- **Thermal boundary conditions**: prescribed temperature in all nodes. The temperature evolution during the curing cycle $T(t)$ (see Figure 3.1) is applied to all the nodes, thus not requiring the above mentioned properties − which are necessary in case of convection/conduction boundary conditions where the temperature field at each time step is an unknown. This boundary conditions are a good approximation as the thickness of the employed laminate is really small. Being so, assuming an homogeneous temperature field along the thickness is a good representation of reality [2]. Furthermore, this boundary conditions suppose a great reduction of CPU time.

- **Mechanical boundary conditions**: as the deformation caused by the cured-induced distortions are going to be studied, only the rigid body modes of the part are restricted.

The curing cycle applied has a total duration of 332 minutes starting at room temperature (21 °C) and a maximum curing temperature of 180 °C. That temperature is hold for 120 minutes. There is no dwell to reach that temperature, and the cooling and heating phases both last 106 minutes.

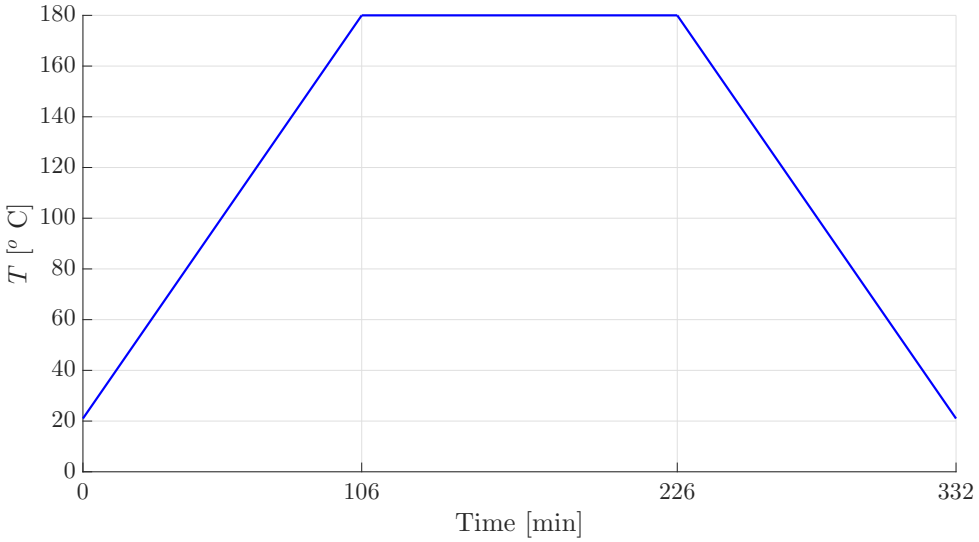

Figure 3.1: Evolution of the temperature during the curing process: curing cycle.

Regarding the laminate employed on every model has been changed depending on the deformation mode intended to be obtained on the part: a symmetrical laminate leads to pure spring-in deformation while unsymmetrical laminate produces out-of-plane deformations leading to warpage or spring-in plus warpage. The laminate used – number of plies, orientation and thickness of each ply and total thickness – is detailed at the beginning of each section of the Results chapter 4.

Finally, regarding the spatial and time discretizations, a remark must be made:

- The spatial discretization (mesh) has not been studied in-depth as the main goal of these models has been the proper implementation and test of the mold compensation techniques and not to obtain accurate results to machine or produce such mold. The main consideration to define the mesh has been obtaining a good trade-off between measuring a representative enough displacement field and the CPU time.

- The same must be mentioned for the time discretization: no accurate study has been performed to determine the best time step or time integration scheme. The time step has been chosen in order to properly capture all the physical phenomena that happens during the curing cycle, and the time integration scheme has been set to the default one.

The type of element used to model the composite material has been a 8 node solid element, with one element per ply.

Matrix			
Property	Glassy	Rubbery	Liquid
E_m [MPa]	4670	40.3	40.3
ν_m [-]	0.37	0.499	0.499
α_m [°C^{-1}]	4.89 E-5	1.5 E-4	0
β_m [-]	2.455 E-3	2.45592 E-3	0
X_{gel} [-]		0.31	
Fibers			
E_f [MPa]		228000	
G_f [MPa]		27600	
ν_f [-]		0.2	
α_{f1} [°C^{-1}]		-9 E-7	
α_{f2} [°C^{-1}]		7.2 E-6	
V_f [-]		0.5742	
UD ply			
ρ [kg/m^3]		1570	

Table 3.1: Mechanical, thermal and chemical properties of the material used in this thesis.

Cure kinetics model	
Property	Value
A_1 [Hz]	1 E-9
A_2 [Hz]	68229
S_1 [J]	0
S_2 [J]	64290
n_1 [-]	0
m [-]	0.492
n_2 [-]	1.75
Vitrification model	
X_{max} [-]	0.9051625
b_D [-]	0.03322
Glass transition temperature model	
T_{g0} [K]	275.82
T_{g1} [K]	491.42
λ [-]	0.5

Table 3.2: Parameters of the cure kinetics, vitrification and glass transition temperature models.

3.1.2 Z-Shaped Model

The implementation of the three main mold compensation techniques mentioned in Section 2.6 – the MM, the DMM and CPM – has been performed on a Z-shaped geometry with a symmetrical laminate. The geometrical features of the Z-shaped part are depicted in Figure 3.2. The out-of-plane dimension of the part is 150 mm.

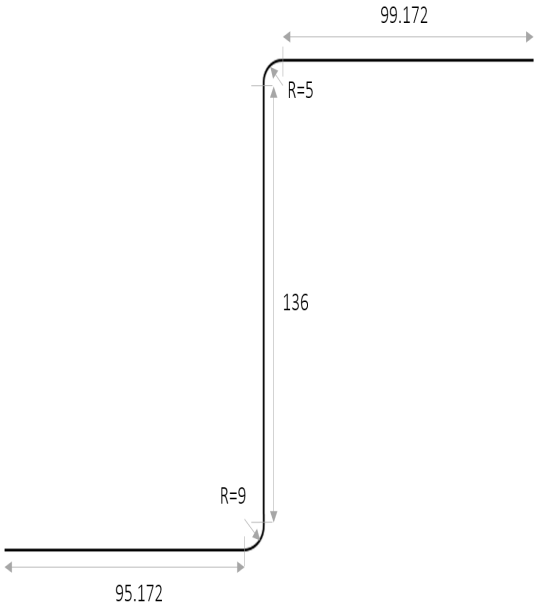

Figure 3.2: Z-shaped part geometric features (not scaled). All units in [mm].

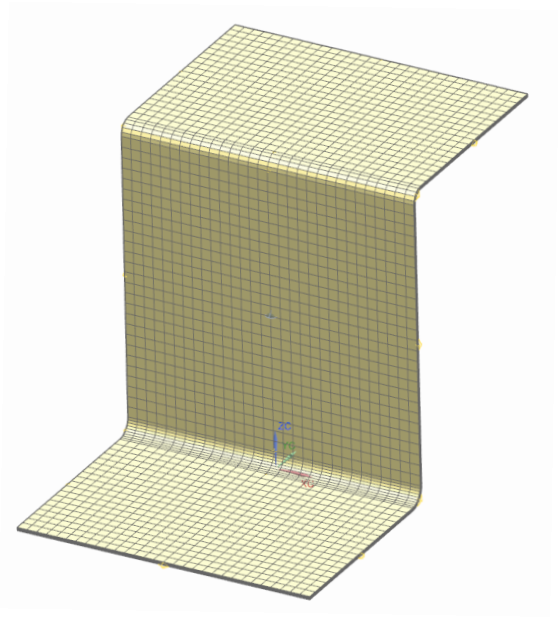

Figure 3.3: First mesh of the Z-shaped model.

3.1.2.1 Implementation and Optimization of the Z-Shaped Model

The initial numerical parameters of the model are detailed in Table 3.3. The mesh used is depicted in Figure 3.3.

Parameter	Value
Node density at curved regions [node/mm]	2/3
Node density at remaining regions [node/mm]	1/5
Elements per ply [-]	1
Total number of D.O.F [-]	240,591
Time step [min]	1

Table 3.3: Numerical parameters of the first Z-shaped model.

First Implementation

As mentioned in Section 2.5.5.1, there are two ways of modeling the thermo-mechanical coupling that occurs during the curing process: a two and one-model approach. In this first trial, a two-model approach has been followed. The latter implies creating and running a thermal model and then load the results to a mechanical model. To do so, identical meshes have been used for both models.

In the thermal model the archiving frequency [4] of $T(t)$, $X(t)$ and $T_g(t)$ is 1 min^{-1} (every time step). In the mechanical model, the displacement field is obtained at every time step. Thanks to this approach, a very accurate representation of $X(t)$ is obtained – see Figure 3.4.

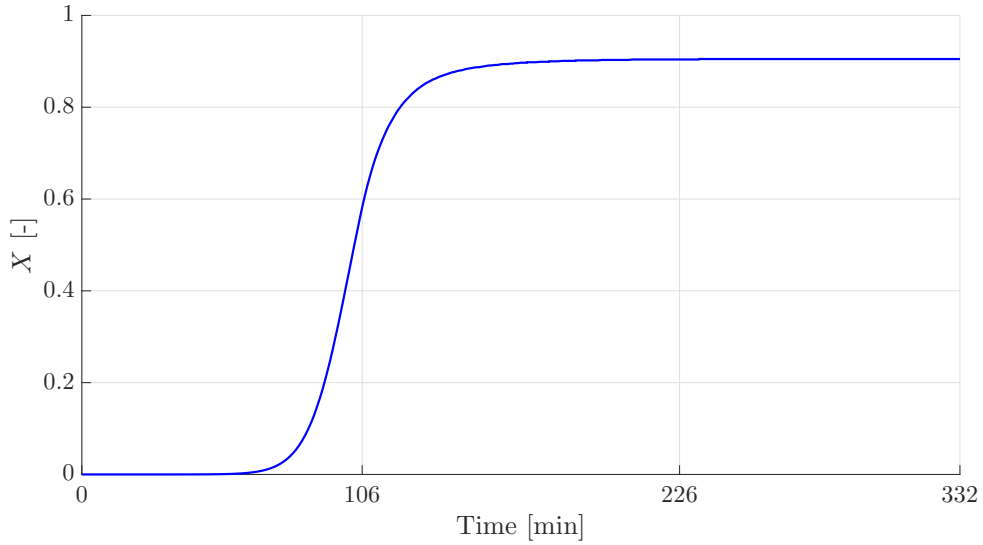

Figure 3.4: $X(t)$.

Model	**CPU time [min]**	**Archiving frequency [min^{-1}]**
Thermal	120	1
Mechanical	150	1

Table 3.4: CPU and archiving frequencies for both models in the first implementation of the Z-shaped model.

The CPU time required for both models is presented in Table 3.4. The total amount of time necessary to obtain the cured-induced distortions is 270 minutes (4.5 hours), which is excessively long. Checking the results file, it has been noticed that each iteration lasts about 2 to 4 seconds and that the highest number of iterations per time step is 5 to 6. But the CPU time for every time step can amount to more than 50 seconds because of the writing of results.

Analyzing $X(t)$ at Figure 3.4, the curing times at which the resin properties are going to change the most can be determined. Thus, different archiving frequencies at the thermal model must be set in accordance to that. Furthermore, by analyzing Figure 3.1, where the curing cycle is depicted, different archiving frequencies can be set in the mechanical model in order to capture the curing times at which the displacement field change is going to be more important.

[4] Frequency at which the variables are calculated and saved, i.e. number of time steps between every new value of the variables.

Second Implementation

The thermal and mechanical models archiving frequencies are modified, but the numerical parameters specified above are kept the same. The total curing time (simulation time) is divided in 4 regions in the thermal model and in 3 regions in the mechanical model.

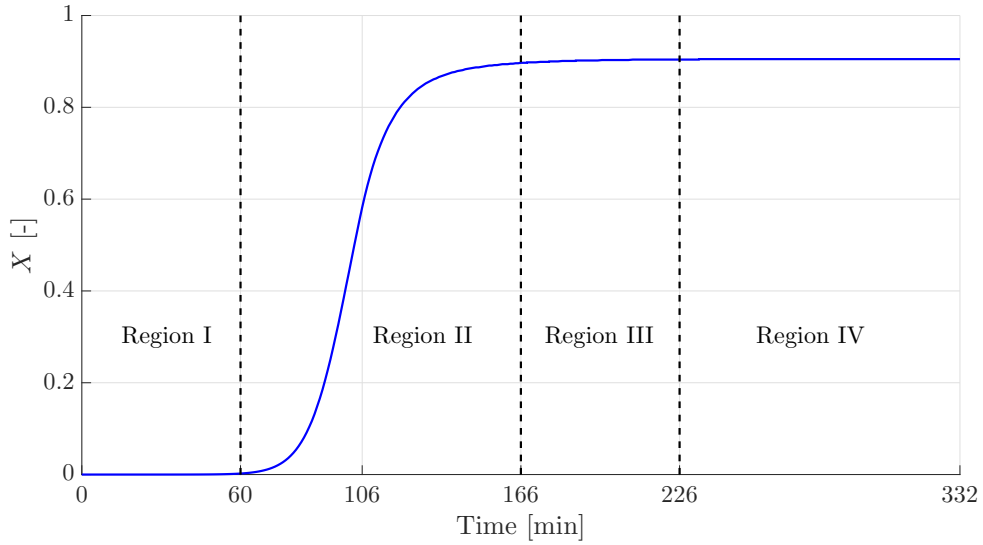

Figure 3.5: $X(t)$ divided in 4 regions.

Region	Comprised curing cycle [min]	Archiving frequency [min^{-1}]
I	0 - 60	0.2
II	60 - 166	1
III	166 - 226	0.1
IV	226 - 332	0.2

Table 3.5: Archiving frequencies modification to the Z-shaped thermal model.

As depicted in Figure 3.5, 4 regions have been defined. The archiving frequencies for each region are specified in Table 3.5. Region III has the lowest archiving frequency as at that part of the curing cycle, X does not vary much and the cycle temperature is constant. Regions I and IV have higher archiving frequencies as, despite X being almost constant in those regions, these regions represent the heating and cooling phases, respectively. Thus, thermal strains appear and they induce distortions. Finally, region II has the highest archiving frequency as X and, accordingly, the mechanical properties of the resin vary a lot.

Then, in Figure 3.6 3 regions have been defined. The archiving frequencies for each region are specified in Table 3.6. In the mechanical model the only interesting data is the last deformation field when $t = 332$ min. Despite that, the archiving frequencies of the heating and cooling phases of the curing cycle (region I and III) are set to 0.1 min^{-1} in order to have an evolution history of the displacement field – thus being able to detect any anomaly in the results.

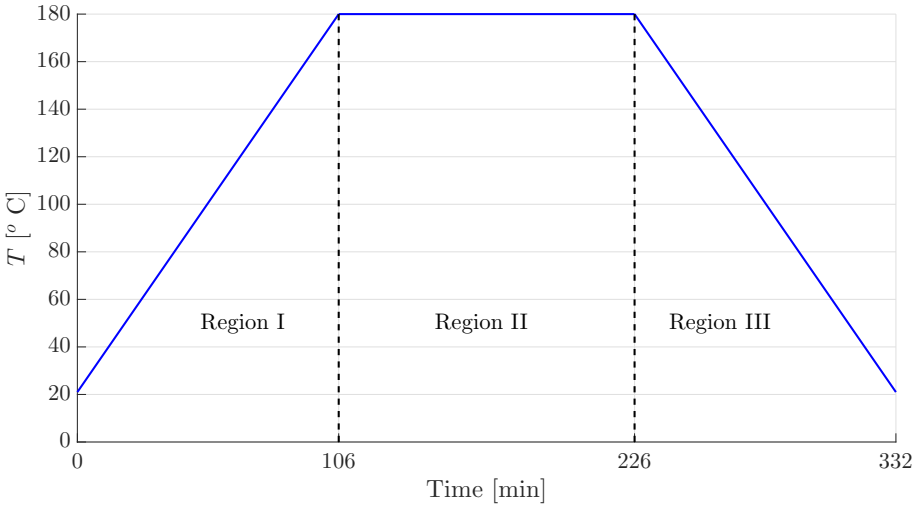

Figure 3.6: $T(t)$ divided in 3 regions.

Region	**Comprised curing cycle [min]**	**Archiving frequency [min^{-1}]**
I	0 - 106	0.1
II	106 - 226	1/120
III	226 - 332	0.1

Table 3.6: Archiving frequencies modification to the Z-shaped mechanical model.

After this simplifications, the total CPU time has been reduced to a total of 120 minutes to obtain the cured-induced distortions (50 and 70 minutes for the thermal model and mechanical model, respectively). Despite the reduction of the archiving frequencies, no accuracy has been lost – same results have been yielded.

Third Implementation

In the third implementation, the second option to define the thermo-mechanical coupling, stated in Section 2.5.5.1, has been chosen. A one-model approach has been followed. The model now is a mechanical model, for which $T(t)$, $X(t)$ and $T_g(t)$ have been introduced as input loads.

$X(t)$ and $T_g(t)$ have been discretized into 20 discrete values ($T(t)$ had already been defined for the thermal model), with which `Samcef` interpolates the curve by straight lines. The discretization of $X(t)$ and $T_g(t)$ is based on the results obtained for such variables in the thermal model. Doing so, the total CPU time is reduced to 40 minutes. But the introduction of the discretized data implies a difference in the maximum cured-induced distortion of 3% with respect to the two-model approach. That difference, though, is considered as acceptable regarding two aspects:

- It reduces the total CPU time from 120 to 40 minutes. That fact is really important as mold compensation techniques are based on iteration loops in which the curing process has to be simulated over and over – recall the flowcharts depicted in Figure 2.9.

- As explained at the beginning of this section, the accuracy of the measured displacements is not crucial for the accomplishment of this thesis objectives.

In conclusion, the one-model approach is considered as the most suitable option to implement the mold compensation techniques.

3.1.2.2 Spring-in/Spring-back Model

The initial implementation of the three mold compensation techniques (detailed in Section 2.6: the Mirror method, the DMM and CPM) has been done on the Z-shaped part with a pure spring-in/spring-back deformation mode. The latter is achieved using a symmetrical laminate.

The mechanical boundary conditions applied on the part – the suppression of the rigid body modes – are shown in Figure 3.7. The 6 degrees of freedom are suppressed by 6 displacement restrictions. After running the simulation, an uneven distribution of the total displacement can be noticed – see Figure 3.8 (a), which leads to a positive twist along the y axis (green axis of Figure 3.8).

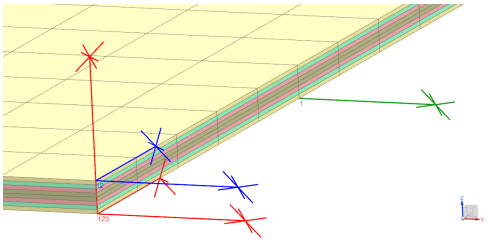

Figure 3.7: Boundary conditions to suppress the rigid body modes on the Z-shaped model.

The main cause of this phenomenon are the applied boundary conditions. Throughout the curing process, dilatational and compressive strains are developed in the 3 directions of each element. Due to the 3 nodes with applied x displacement restriction, an uneven x displacement field is generated along the Z-shaped part – see Figure 3.8 (b), which in turn creates the twist along the y axis.

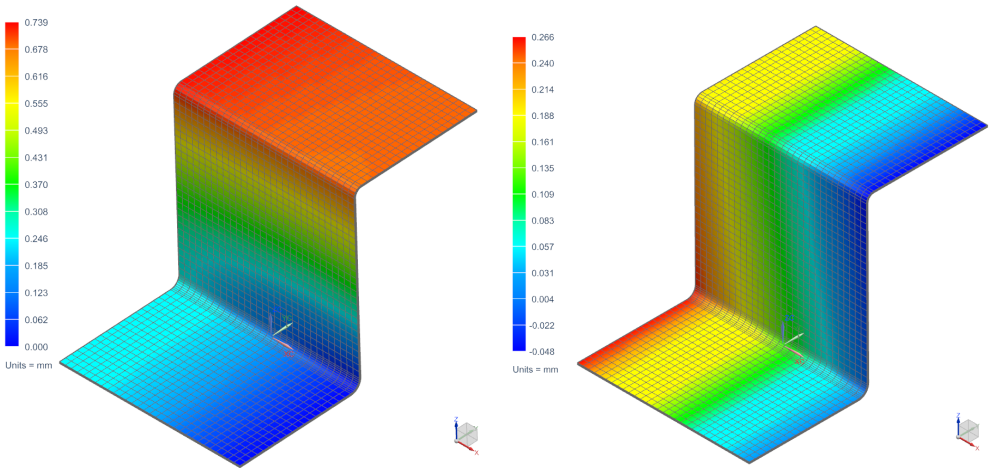

(a) Total displacement field. (b) x displacement field.

Figure 3.8: Uneven displacement field of the Z-shaped part after the curing process with a symmetric laminate.

In order to suppress such twist a simplification is made on the model. A section on the middle of the Z-Shaped part is modeled with only one element along x, with plain strain conditions – see Figure 3.9. The latter conditions simulate the presence of material at both (transverse) sides of the section and ensure no transverse displacement (x displacement), thus having only spring-in/spring-back deformations.

This model yields a different maximum displacement with respect to the fully modeled geometry one (around 10% difference). Nevertheless, the following reasons make this simplified model more convenient as:

- Thanks to the reduction of total elements, the density of elements along the curved regions has been increased – Appendix B proves that the number of circumferential elements is crucial to properly measure the change in spring-in angle. As seen in Table B.1, the most optimal number of elements along the circumference is 17. However, 15 elements has been the number chosen due to the inability of `NX` to extrude the volume elements when 17 is the chosen number of elements. This new model has a total number of D.O.F of 10,401 – check Table 3.7 for the rest of numerical parameters.

- The total CPU time of a full curing simulation is under 2 minutes, while with the full model is around 40 minutes. This fact allows this model to be the perfect model to implement the mold compensation techniques for the first time, as a lot of tests are required until a full working methodology is developed.

- A Z-shaped part with a symmetrical laminate and free deformation (only rigid body modes suppressed) is supposed to yield the same displacement field regardless of the transverse section. Thus, from a modeling point of view, this model accurately represents the reality of the problem and therefore, the difference in results with the previous model can be omitted.

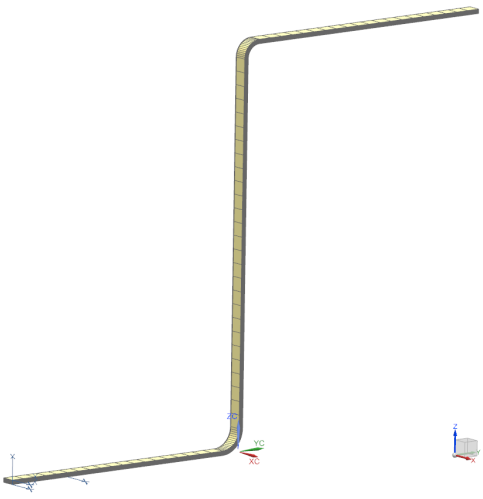

Figure 3.9: Simplified model of the Z-shaped part. A one-element section is modeled with plain strain conditions (the latter are not depicted).

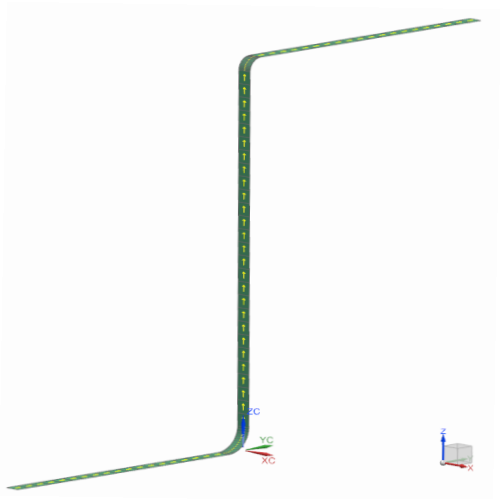

Figure 3.10: 0° element orientation of the Z-shaped spring-in/spring-back model.

Parameter	Value
Number of elements at curved regions [-]	15
Node density at remaining regions [node/mm]	1/5
Elements per ply [-]	1
Total number of D.O.F [-]	10,401
Time step [min]	1
CPU time [min]	2

Table 3.7: Numerical parameters of the Z-shaped spring-in/spring-back model.

3.1.2.3 Mixed Deformation Model

A model to study mixed deformation modes (warpage plus spring-in/spring-back) has been developed. As warpage occurs due to out-of-plane displacements, the whole section of the Z-shape part needs to be modeled – see Figure 3.11. The mixed deformation modes have been achieved by using different unsymmetrical laminates.

As in the spring-in/spring-back model, a one-model approach thermo-mechanical model has been followed ($T(t)$, $X(t)$ and $T_g(t)$ are introduced as input loads), the rigid body modes are also suppressed in the same way as in Figure 3.7, a 8 node solid type of element has been used and the number of elements along the curved part regions has also been 15. The rest of numerical parameters and relevant information are detailed in Table 3.8.

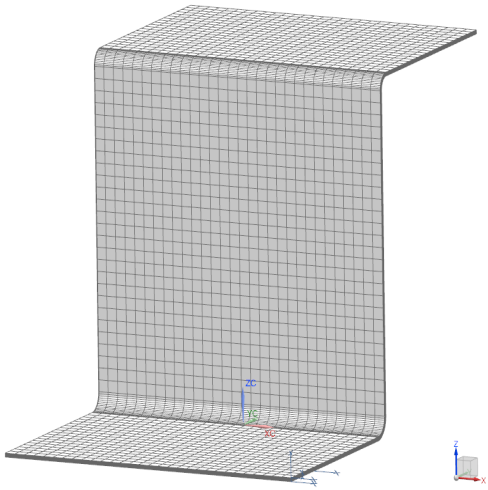

Figure 3.11: Z-shaped part mixed deformation model.

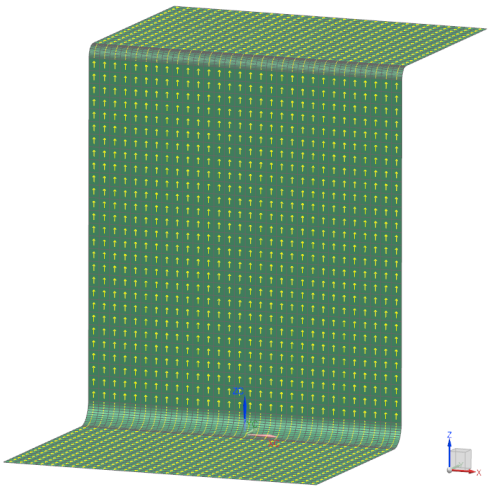

Figure 3.12: 0° element orientation of the Z-shaped mixed deformation model.

Parameter	Value
Number of elements at curved regions [-]	15
Node density at remaining regions [node/mm]	1/5
Elements per ply [-]	1
Total number of D.O.F [-]	282,549
Time step [min]	1
CPU time [min]	70

Table 3.8: Numerical parameters of the Z-shaped mixed deformation model.

3.1.3 Warpage Model

A model to study pure warpage deformation has been developed. To achieve such deformation mode different unsymmetrical laminates have been tried on a flat plate (see Figure 3.13) in order to study the different warpage or out-of-plane types of deformation – check Appendix's A Section A.4.2 for further details on those deformation modes. Details of each laminate tested are given at the beginning of each section of the Results chapter 4.

The geometrical dimensions of the plate are 200x150 mm. The suppression of rigid body modes has been applied at different locations depending on the warpage mode studied – they have been suppressed using 6 displacements restrictions. The three out-of-plane modes studied are: bending, torsion and mixed mode (bending + torsion). For the bending mode the boundary conditions have been applied at the center of the plate, while for the other two modes they have been applied at a corner, as depicted in Figure 3.7.

As in the Z-shaped model, a one-model approach thermo-mechanical model has been followed ($T(t)$, $X(t)$ and $T_g(t)$ are introduced as input loads), a 8 node solid type of element has been used and a time step of 1 min has been set. The rest of numerical parameters and relevant information are detailed in Table 3.9.

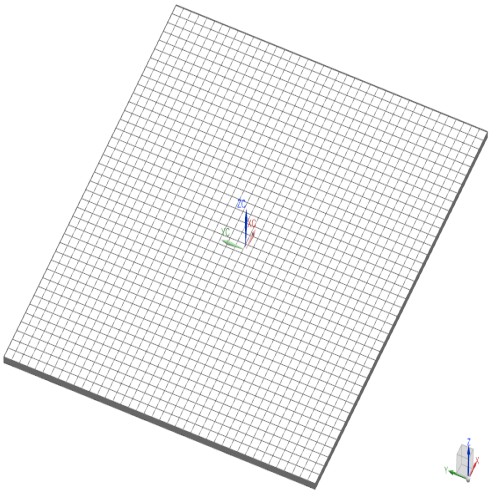

Figure 3.13: Warpage model.

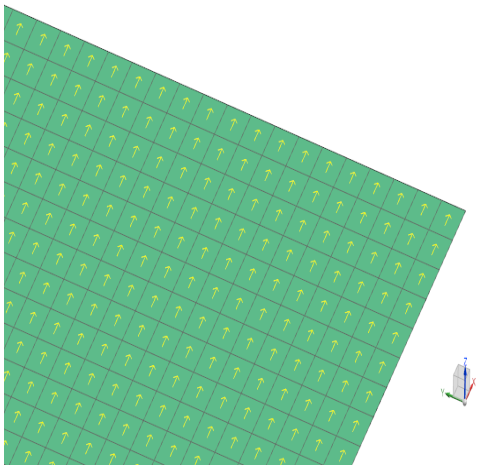

Figure 3.14: 0° element orientation of the warpage model.

Parameter	Value
Node density [node/mm]	1/5
Elements per ply [-]	1
Total number of D.O.F [-]	40,701
Time step [min]	1
CPU time [min]	11

Table 3.9: Numerical parameters of the flat plate model.

3.2 Methodology

In this section all the steps followed to implement the mold compensation techniques are detailed. The explanation of the latter must serve as the guidelines for anyone willing to develop such compensation strategies with its own means, i.e. CAD-modeling software, CAE software, optimization algorithm, etc. In the present thesis, the compensation methodology for CAD-based and mesh-based strategies is detailed in the frame of the employed software `NX`.

3.2.1 CAD-based Compensation Methodology

The key of both the DMM and CPM (see Section 2.6.1.1 and 2.6.1.2, respectively) is that the mold geometry is defined with a finite number of parameters, i.e. the mold geometry is parametrized. In the case of the DMM, that parameter(s) $\mathcal{P}$ is a distortion mode, e.g. a pring-in angle or a twist angle; and for the CPM those parameters $\mathcal{P}$ are the displacement field of one or more points of the mold geometry with respect to the nominal geometry. An example of the latter is depicted in Figure 3.15.

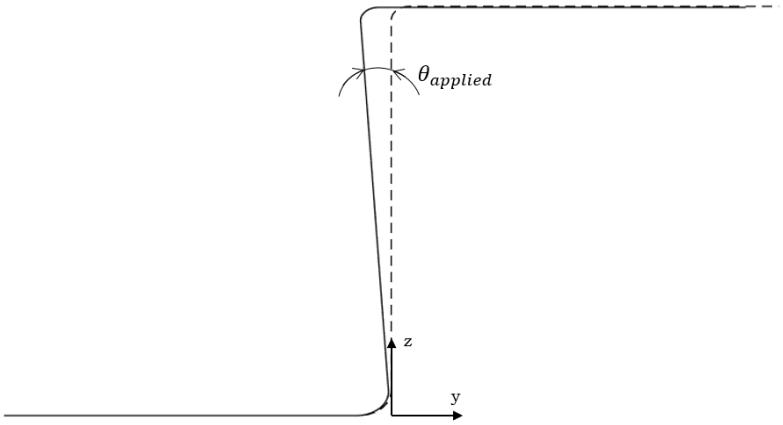

(a) $\mathcal{P} = \theta$ (spring-in angle).

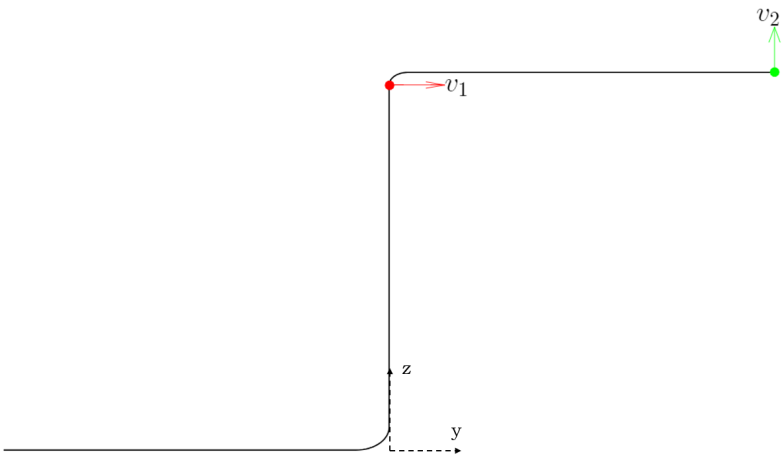

(b) $\mathcal{P} = \{v_1, v_2\}$.

Figure 3.15: Different parametrized models: (a) DMM and (b) CPM.

The CAD-based compensation methodology is detailed below. Figure 3.16 summarizes the process explained in a flowchart:

1. The first step of the method is to have the mold 2D geometry fully parametrized (.prt file). In the present thesis a 2D geometry approach has been followed as the composite laminate is then extruded in the FEM model.

2. With the geometry ready, a FEM model is created (.fem file). The steps necessary to have the model fully meshed and ready for the simulation are:

   i. An idealized part of the original geometry is created where the geometry can be partitioned in accordance with the desired mesh, e.g. partition the geometry so the curved regions can be have a higher density of elements than the rest.

   ii. With the geometry partitioned, the mesh density of the geometrical edges is defined.

   iii. Then the type of 2D element, i.e. 3-node triangular, 4-node rectangular or 8-node rectangular, is chosen. The general element size is defined for the edges where the node density was not specified. And the 2D mesh is generated.

   iv. The element orientation, directions 1 and 2, is defined in accordance with the problem of study, i.e. so it coincides with the laminate global axes. Then the laminate is defined and extruded (solid elements).

3. With the FEM model ready, the simulation model is created (.sim file). The required steps to launch the simulation are:

   i. Import $T(t)$, $X(t)$ and $T_g(t)$ and apply the three fields to all the nodes.

   ii. Apply the boundary conditions to suppress the rigid body modes – as explained in Section 3.1.2.2, 6 displacements restrictions have been used.

   iii. Then the integration limits, i.e. the curing cycle total duration, are defined in accordance to the archiving frequencies defined in Table 3.6: three subcases are created for the three archiving frequencies. Also the time step is defined.

   iv. With the above completed, the simulation can be launched.

4. Once the simulation is completed, the parameters $\mathcal{P}$ relevant for the optimization objective function are measured – the objective function must be preferably defined so that its minimum tends to 0. The objective function is evaluated in terms of the measured parameters $F_{obj}(\mathcal{P})$ and is compared to a chosen precision η.

   i. If $F_{obj}(\mathcal{P}) < \eta$, then the compensate geometry is obtained, which corresponds to the last parametrized CAD model.

   ii. If $F_{obj}(\mathcal{P}) > \eta$, then the process must be repeated from step 1 changing the mold geometry of the paramterized model in accordance to the optimization algorithm chosen.

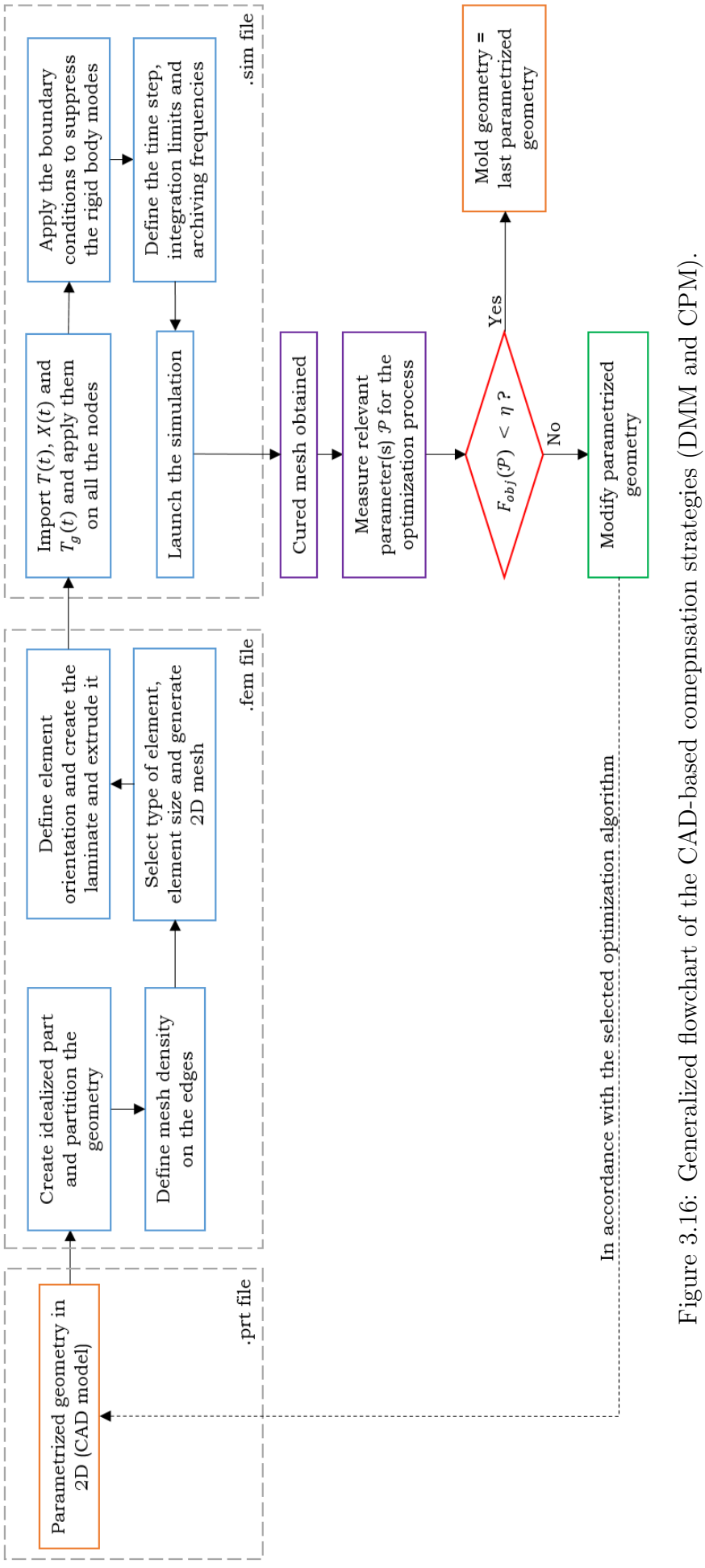

Figure 3.16: Generalized flowchart of the CAD-based comepnsation strategies (DMM and CPM).

3.2.2 Mesh-based Compensation Methodology

The key of the Mirror Method (see Section 2.6.2) is that the update of the mold shape from iteration to iteration is performed on the mesh – following equation 2.25. Thus, when the process is finished, a reconstruction is required to obtain a CAD file of the compensated mold geometry.

The Mirror Method methodology is detailed below. Figure 3.17 summarizes the process explained in a flowchart:

1. The first step of the method is to have the nominal 2D geometry modeled in a CAD model (.prt file). The MM is always initiated by modeling the mold geometry as the nominal geometry.

2. Same as in the CAD-based compensation methodology.

3. Same as in the CAD-based compensation methodology.

4. Once the simulation is completed, the residual distance δ_{res}, i.e. distance between cured mesh and nominal mesh, is measured for all mesh nodes. The maximum residual distance measured δ_{res}^{max} is compared to a chosen precision η.

- If $\delta_{res}^{max} < \eta$, then the compensate geometry is obtained. The latter corresponds to the last mold mesh.
- If $\delta_{res}^{max} > \eta$, then the process must be repeated from step 1 updating the mold mesh following equation 2.25. The updating of the mold mesh is explained below.

The update of the mold mesh consists in the following steps:

0. The nominal position of all nodes must be measured. The latter is saved to an `Excel` sheet, as `NX` allows to export results or model data to an `Excel` sheet.

1. At each iteration, the cured displacements of the mesh nodes are measured and exported to the `Excel` sheet.

2. Then, on the `Excel` sheet δ_{res} is computed in the three cartesian directions for all the mesh nodes. Afterwards, it is saved in a text file (.txt).

3. The new mold mesh is obtained by copying the FEM model (.fem) of the previous iteration mold mesh and rename it. Then, the displacement field of the residual distance δ_{res} (.txt file) is imported into the model and a `NX` *Field* is created. Finally, the `NX` option of *translate* is used, which allows to select all nodes of the mesh and apply the previously created *Field* with a user-chosen scale factor.

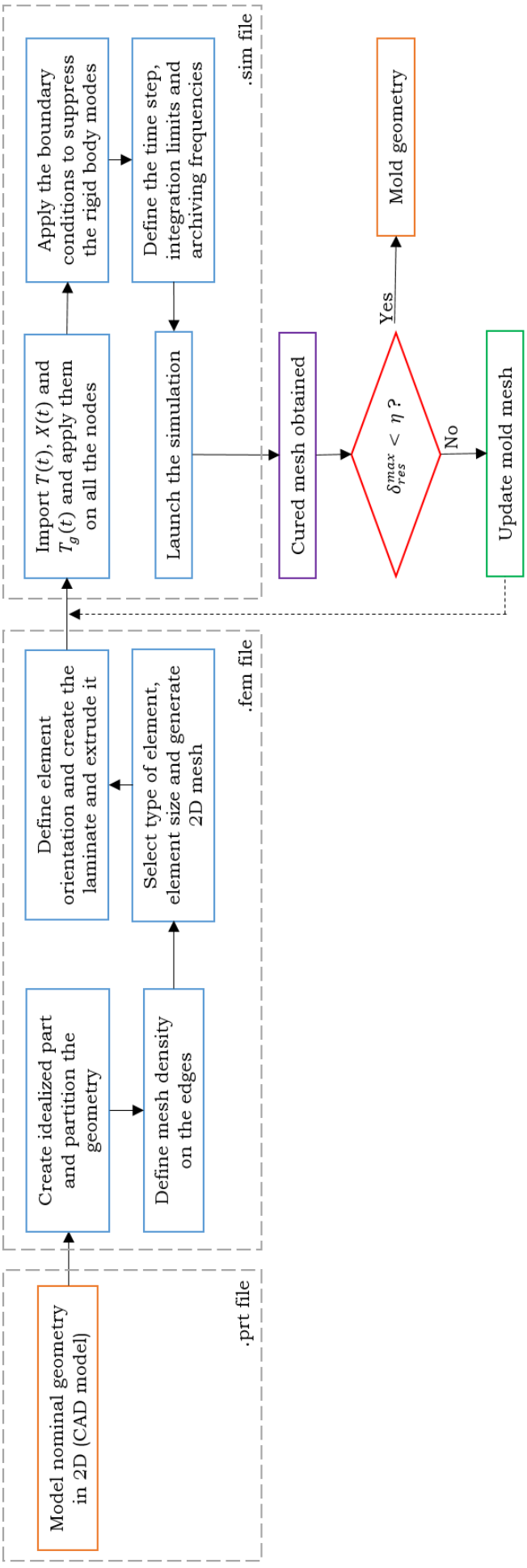

Figure 3.17: Flowchart of the Mirror Method.

Results

This chapter presents the results obtained with the three mold compensation techniques studied in this thesis: the MM, DMM and CPM. Three deformation modes have been studied: spring-in, warpage and a mixed mode; with two different geometries: a Z-shaped part and flat plate. The methods have been compared after analyzing the results of every deformation mode.

4.1 Z-shaped Part under Spring-in Deformation

In this section, the MM, the DMM and CPM have been implemented for the first time using `NX` – the methodology followed to do the latter is explained in Section 3.2 and depicted in Figures 3.16 and 3.17. The compensated geometry of the Z-shaped part is obtained with the three methods.

The laminate that has been used on the Z-shaped part in order to obtain spring-in deformations is the following: $[-45/0/\text{-}45/0]_s$, a symmetrical laminate, with plies of thickness $h = 0.205$ mm each ($h_{tot} = 1.64$ mm). The numerical model employed is the one detailed in Section 3.1.2.2, the spring-in/spring-back model. The element's reference vector (0° orientation) is aligned with the global axis y, but follows the Z-shape of the part – see Figure 3.10.

4.1.1 Compensation with the MM

Using the MM, the compensated geometry is obtained in 2 iterations. Figure 4.1 depicts the nominal geometry, the mold geometry and cured geometry at each iteration. At every iteration, the maximum residual distance between the cured and nominal geometries has been computed – see Table 4.1.

It is important to highlight the fact that in iteration 1 [5] the compensated geometry is already obtained: the maximum residual distance δ_{res}^{max} is 4.21 μm. Iteration 2 has been performed seeking higher accuracy, and being successful: δ_{res}^{max} is much less than a micron: 0.0239 μm. Another iteration (not shown in Table 4.1) has been performed but δ_{res}^{max} has increased a few hundreths of a micron. Therefore the process – if it's thought as a mathematical function – oscillates around the minimum from the third iteration and on.

[5] The actual first iteration is named 0 as it is a numerical simulation that must be performed, but is not after this iteration that the compensation process starts – i.e. the mold geometry is modified.

Iteration	δ_{res}^{max} [mm]
0	8.87 E-01
1	4.21 E-3
2	2.39 E-05

Table 4.1: δ_{res}^{max} between the nominal and cured mesh at each iteration using the MM for the Z-shaped part under spring-in deformation.

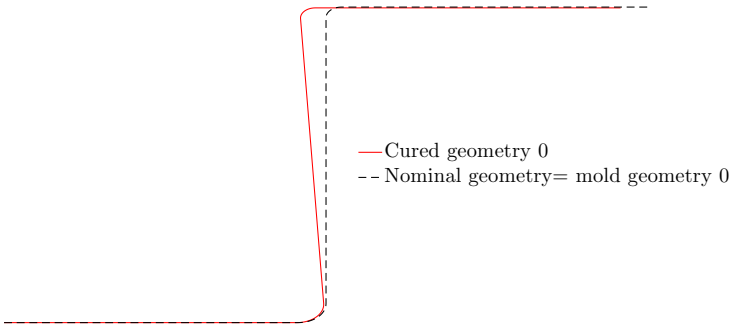

(a) Iteration 0.

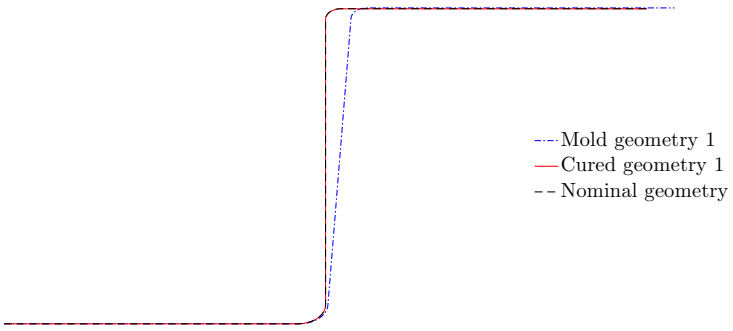

(b) Iteration 1.

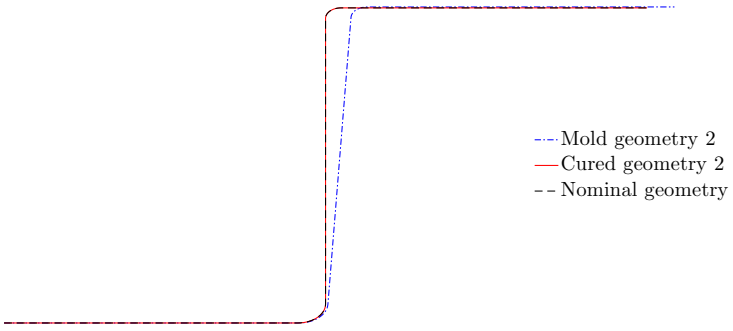

(c) Iteration 2.

Figure 4.1: Depiction of the iterative process followed to compensate the Z-shaped part under spring-in deformation with the MM. A deformation factor of 10 is applied.

4.1.2 Compensation with the DMM

Using the DMM, the only distortion mode in this specific case is spring-in deformation. Thus, the optimization process must seek to minimize the spring-in angle resulting from the curing process. Three optimization processes are proposed:

- **Optimization process 1**: the objective function is $F_{obj} = \frac{\theta_c^i - \theta_c^0}{\theta_c^0} \cdot 100$, where θ_c^i is the cured angle at iteration i and θ_c^0 is the cured angle at iteration 0. The process starts with $\theta_{applied}^0 = 0°$ and the update of the latter is $\theta_{applied}^{i+1} = \theta_{applied}^i - \theta_{cured}^i$ – see Figure 4.2. This is the same approach that is followed in the MM to modify the mold mesh. It has been carried out with `Excel`.

- **Optimization process 2**: the objective function is the same as in **optimization 1**. The update of the applied angle is $\theta_{applied}^{i+1} = -p^{i+1} \cdot \theta_{applied}^0$, which is a line search method in which the value of p that turns θ_c^i to 0 must be found. The first step is to find two values of p that yield $\theta_c > 0$ and $\theta_c < 0$. After, a bisection method has been followed in which the value of alpha is updated as follows: $p_{applied}^{i+1} = (p_{max}^i + p_{min}^i)/2$, where p_{max}^i and p_{min}^i are updated every iteration reducing the available range of values for p. It has been carried out with `Excel`.

- **Optimization process 3**: a surrogate-based algorithm (see Section 2.6.1.4) has been followed. The objective function selected has been $F_{obj} = \left(\theta_c^k/\theta_c^0\right)^2$, where θ_c^k is the cured angle for every configuration k. A set of 7 initial $\theta_{applied}$ have been tried and θ_c^k has been computed for each configuration: after, a surrogate model has been fitted into the data and the minimum has been sought. The minimum has been added to the set of individuals, by running a curing simulation, and a new surrogate model has been found until no improvement of F_{obj} has been shown.

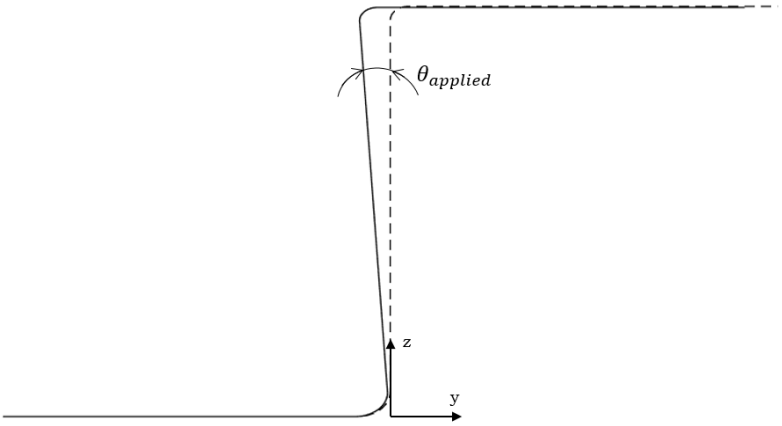

Figure 4.2: Schematic representation of the only deformation mode: spring-in. θ is the applied spring-back/spring-in angle to the mold geometry.

It is important to highlight that the variable update used in optimization processes 1 and 2 is a linear function. That is because the spring-in/spring-back deformation can be considered as linear: plain strain conditions and the thermal and chemical tractions (which evolve linearly with respect to ΔT and X, respectively) only appear in global directions y and z – see Figure 4.2. No bending nor torsion moments are generated due to the curing process: symmetrical laminate with homogeneous distribution of T and X – see Section A.3 of Appendix A. Therefore, the global deformation mode behaves linearly – the MM proves the latter by obtaining the compensated geometry in 1 iteration.

The first optimization process gets a compensated geometry in 2 iterations (compensated angle $\theta_{applied} = -0.32471°$) with a reduction of 99.938 % of the initial cured angle[6] – the followed convention is positive angle for an anticlockwise direction. Table 4.2 details the results of this process.

Iteration	$\boldsymbol{\theta_{applied}}$ [°]	$\boldsymbol{\theta_c}$ [°]	**Reduction** [°]	**Reduction** [%]
0	0.0000	0.325	-	-
1	-0.32500	-0.00025	0.0.32475	99.922
2	-0.32473	-0.00020	0.32480	99.938

Table 4.2: Results obtained with the first optimization process of the DMM.

Then, regarding the second optimization process, the number of iterations to obtain the final compensated geometry is larger – all the results are shown in Table 4.3. The line search procedure is really sensitive to the initial guesses, as it determines the initial interval of p values. If the guess is accurate, the number of iterations is highly reduced. Conversely, if the guess is not accurate the number of iterations gets increased as the initial interval is larger.

Iteration	$\boldsymbol{\theta_{applied}}$ [°]	$\boldsymbol{\theta_c}$ [°]	**Reduction** [°]	**Reduction** [%]	$\boldsymbol{p}$
0	0.0000	0.325000	-	-	-
1	-0.3250	-0.000254	0.32475	99.922	1
2	-0.2600	0.039900	0.28510	87.723	0.8
3	-0.2925	0.025800	0.29923	92.071	0.9
4	-0.3088	0.012885	0.31212	96.035	0.95
5	-0.3169	0.006442	0.31856	98.018	0.975
6	-0.3209	0.003221	0.32178	99.009	0.9875
7	-0.3230	0.001611	0.32339	99.504	0.99375
8	-0.3240	0.000805	-0.00055	99.752	0.996875
9	-0.3245	0.000403	0.03950	99.876	0.9984375
10	-0.3247	0.000201	0.02557	99.938	0.99921875

Table 4.3: Results obtained with the second optimization process of the DMM.

For last, optimization 3 has been executed. The initial 7 individuals tested to obtain the first surrogate model (see Figure 4.3) are detailed in Table 4.4 – individuals A to G. Additionally, the 2 minimums obtained of the 2 surrogate models (iterations) necessary for convergence are shown – individuals 1 and 2. All surrogate models are second order models and they have had a fitting parameter $R^2 = 1$, i.e. a perfect fit.

From Table 4.4, it can be deduced that the $\theta_{applied}$ that minimizes F_{obj} is individual 7: $\theta_{applied} = -0.3247°$. That is the optimum of the first surrogate model. That optimum has been added to the set of individuals in the next iteration, and a new surrogate model has been obtained. The optimum of the second surrogate model has turned to be the same value as the first, thus not improving F_{obj}. The process has been terminated there.

[6]The cured angle has been measured with the y and z position change of the geometrical point located at the upper part of the web of the Z-shaped part.

Conclusions

The same value of $\theta_{applied}$ is obtained using different optimization procedures. The latter was expected. However, success is highly dependent on proper formulation of the optimization algorithm. Otherwise, the optimum yielded may not be the real one – as mentioned in Section 2.6.1.4.

Individual	$\boldsymbol{\theta_{applied}}$ [°]	$\boldsymbol{\theta_{cured}}$ [°]	$\boldsymbol{F_{obj} = \left(\frac{\theta_c^k}{\theta_c^0}\right)^2}$ [-]
Initial set			
A	-1.0000	-0.6779	4.3511
B	-0.5000	-0.1758	0.2927
C	-0.3000	0.0249	0.0059
D	0.0000	0.325	1.0000
E	0.3000	0.6272	3.7248
F	0.5000	0.8281	6.4930
G	1.0000	1.3295	16.7346
Iterations			
1	-0.3247	0.0002	0.0000
2	-0.3247	0.0002	0.0000

Table 4.4: Tested configurations and F_{obj} obtained with the third optimization process of the DMM.

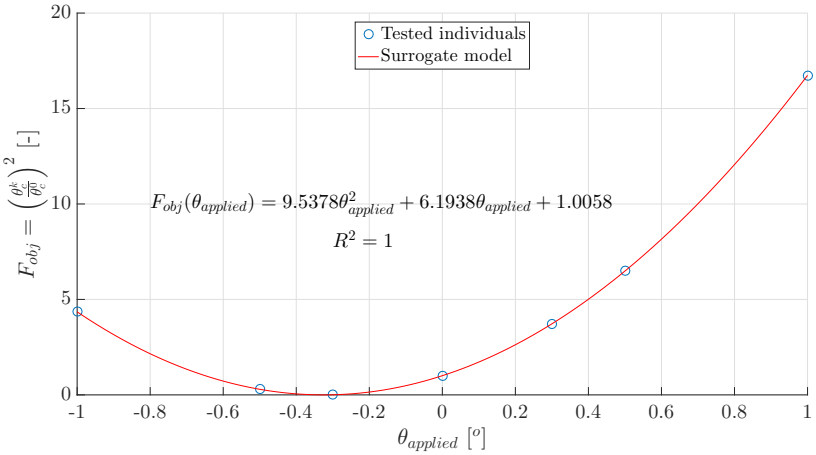

Figure 4.3: First surrogate model of the third optimization process of the DMM. It includes individuals 0 to 6.

Optimization process 3 algorithm is a surrogate-based approach. The use of such approach allows for a wide space exploration. However, surrogate-based algorithms rely on having enough representative tested configurations (i.e. if $\theta_{applied} \in [0, 1]$ then the surrogate model will be different and so will be the optimum) and on choosing the appropriate order of the surrogate model.

Optimization processes 1 and 2 use a fixed search direction throughout the process to update the current iterate: $s^k = -1$ (*constant* gradient algorithm). Gradient-based methods strongly depend on a proper iterate update method and on the initial iterate.

Then, regarding the objective function F_{obj}, it must represent accurately the deformation mode, i.e. the behaviour of the distortion variable θ_c for any $\theta_{applied}$. F_{obj} of optimization processes 1 and 2 are a function of θ_c, while F_{obj} of optimization process 3 is a function of θ_c^2. As the three processes yield the same $\theta_{applied}$ it can be assumed that both the objective function and the iterate update method are well formulated for each process.

Finally, the following conclusions can be deduced:

- The formulation of the objective function is key for the success of any optimization algorithm. Then, regarding the search direction, surrogate-based algorithms are more appealing as their implementation is less susceptible to errors: testing a wide range of possible values, despite more time-consuming, is safer than choosing the update of the the search direction and the initial guess.
- When using surrogate-based algorithms, the order of the surrogate model is as important as the definition of the objective function. If the objective function of the optimization process is formulated as $F_{obj} = \left|\frac{\theta_c^k}{\theta_c^0}\right|$, neither a first nor a second order surrogate model will yield the real optimum obtained above (see Figure 4.4). However, if $F_{obj} = \frac{\theta_c^k}{\theta_c^0}$, thus now taking into account the sign, a first order surrogate model will make $F_{obj} = 0$ when $\theta_{applied} = -0.3247°$ (see Figure 4.5).

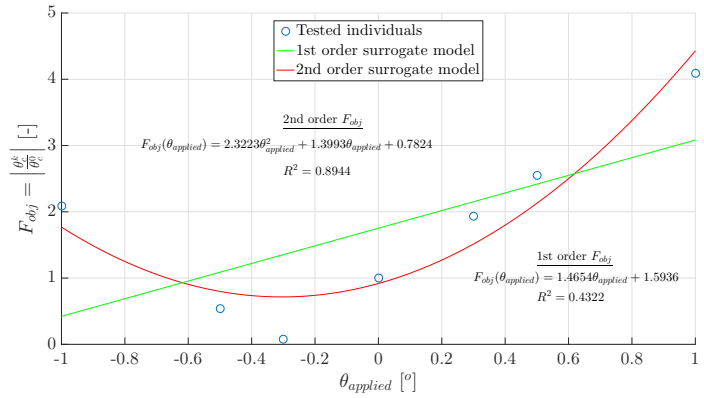

Figure 4.4: $F_{obj} = \left|\frac{\theta_c^k}{\theta_c^0}\right|$. Bad objective function as neither a second nor first order surrogate model fits it.

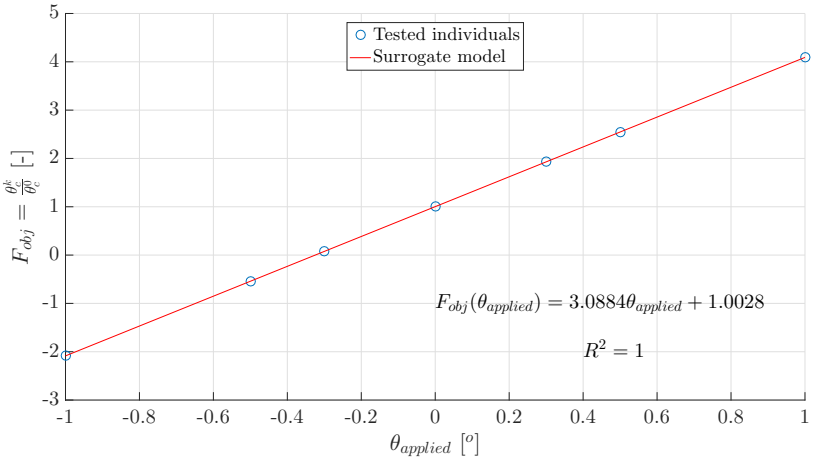

Figure 4.5: $F_{obj} = \frac{\theta_c^k}{\theta_c^0}$ and first order surrogate model. Good choice.

4.1.3 Compensation with the CPM

Using the CPM, the CPs position (x, y, z) are the optimization variables. D_{min} (see equation 2.24) is the objective function to minimize, i.e. the averaged sum of the squared distances – residual distance of the CPs. The studied case can be considered 2-dimensional as plain strain conditions are imposed. So, a CP can only have a maximum of two variables.

The CAD model of the mold geometry is parametrized with the variables of the chosen CPs. The rest of geometrical features will accordingly move when any of these variables are modified. If the CPM is executed with a number of CPs equal to the number of meshed nodes, the method resembles the MM but using a CAD-based strategy. Using the CPM with a high number of CPs requires a high automation of the process, otherwise it is very difficult to be executed manually. For the latter reason, this method has only been implemented for 1 and 2 variables – no automation has been developed in this thesis.

For the one-variable case (see Figure 4.6 and 4.7), the chosen CP (CP1) is at the geometrical point at the end of the web before the upper radial part starts. Both radial parts have tangential constrains with the web, and the upper flange is constrained to remain horizontal (parallel to the lower flange). Variable v_1 is the y-position of CP1.

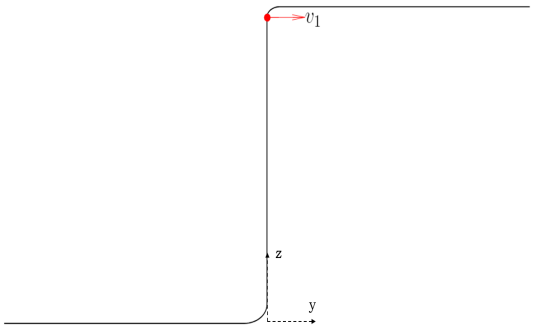

Figure 4.6: CP1 and v_1 of the one-variable application of the CPM.

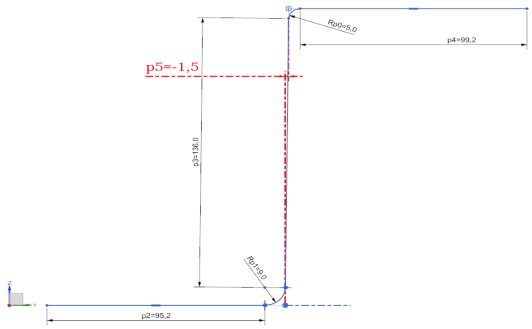

Figure 4.7: Parametrized model of the one-variable application of the CPM on NX. v_1 = p5 = −1.5 mm.

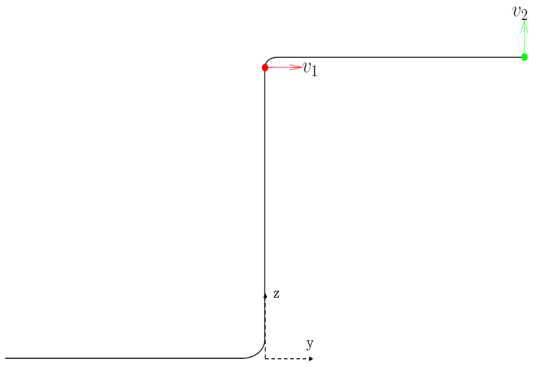

Figure 4.8: CP1 (red, v_1) and CP2 (green, v_2) of the two-variable application of the CPM.

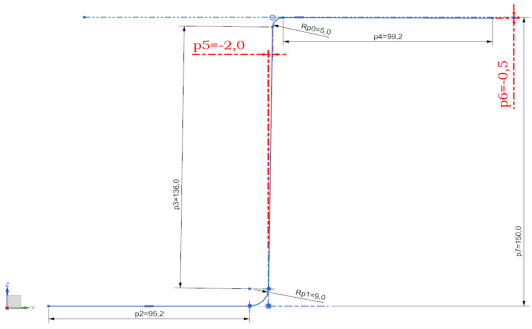

Figure 4.9: Parametrized model of the two-variable application of the CPM on NX. v_1 = p5 = −2 mm and v_2 = p6 = −0.5 mm.

For the two-variable case (see Figure 4.8 and 4.9), two CPs are chosen: the same as in the one-variable case (CP1) and another one at the free edge of the upper flange (CP2). Both radial parts have tangential constrains with the web, and the upper flange is not constrained anymore to remain horizontal. Variable v_1 is the y-position of CP1 and variable v_2 is the z-position of CP2.

To solve the two cases, a surrogate-based algorithm has been chosen. The tested individuals of the one-variable problem are detailed in Table 4.5. The first surrogate model has been obtained with individuals 1 to 9 – see Figure 4.10. The minimum of the first surrogate model (individual 10) is fitted to the set of individuals and the second surrogate model is obtained. The same minimum is yielded again (individual 11), finishing the optimization process: $v_1 = -0.81663$ mm. Both surrogate models are second order models and have a fitting parameter of $R^2 = 1$, i.e. a perfect fit.

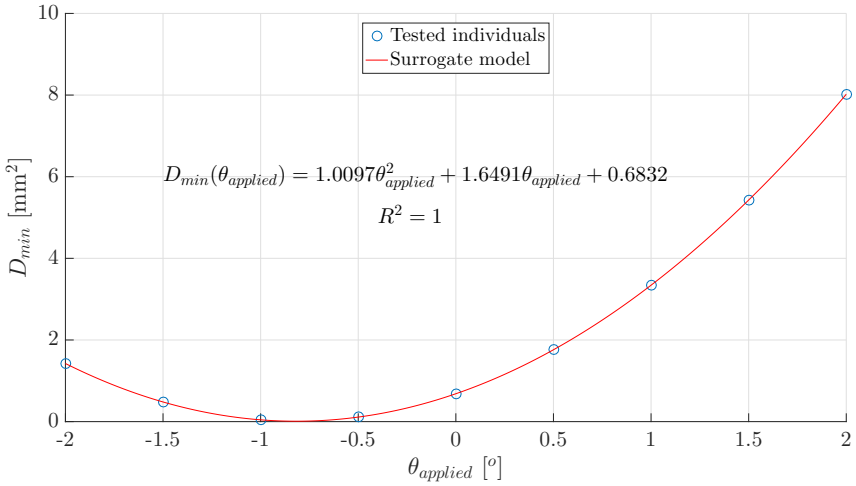

Figure 4.10: First surrogate model of the one-variable case of the CPM. It includes individuals 0 to 9.

Individual	v_1 [mm]	D_{min} [mm^2]
Initial set		
A	-2.0	1.424860
B	-1.5	0.480950
C	-1.0	0.042861
D	-0.5	0.110284
E	0.0	0.682911
F	0.5	1.761049
G	1.0	3.343546
H	1.5	5.429010
I	2.0	8.019067
Iterations		
1	-0.81663	0.008904
2	-0.81663	0.008904

Table 4.5: Tested configurations and D_{min} obtained for the one-variable application of the CPM.

The first set of tested individuals of the two-variable problem are detailed in Table 4.6. Then the optimums of the 4 iterations performed are shown in Table 4.7 (Figure 4.11 shows the first fitted surrogate model). As D_{min} does not improve in 4 iterations, the process is stopped. The solution found is $v_1 = -0.856132$ mm and $v_2 = 0.03088$ mm. All surrogate models are in the second order in both variables and have a fitting parameter of $R^2 = 0.95$.

D_{min} [mm^2]					
v_1/v_2 [mm]	**-0.5**	**-0.25**	**0**	**0.25**	**0.5**
-2	1.495796	1.380387	1.249745	1.338713	1.412426
-1	0.174149	0.069219	0.028176	0.050175	0.135224
0	0.85765	0.764906	0.73522	0.768563	0.864944
1	3.549187	3.469542	3.449438	3.494137	3.601873
2	8.248266	8.178242	8.227333	8.227333	8.346385

Table 4.6: Initial tested cases for the two-variable case of the CPM.

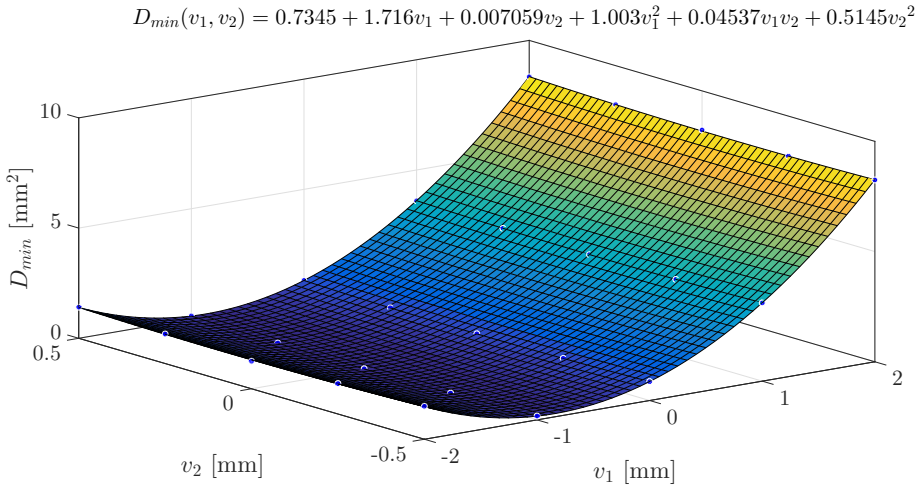

Figure 4.11: First surrogate model of the two-variable case of the CPM.

Iteration	v_1 [mm]	v_2 [mm]	D_{min} [mm^2]
1	-0.856132	0.03088	0.007748253
2	-0.856134	0.03099	0.007755155
3	-0.856135	0.03107	0.007759916
4	-0.856136	0.03111	0.007763585

Table 4.7: Optimums of the surrogate models of the two-variable case of the CPM.

As it was expected, different solutions are found in the two applications of the CPM. The optimization result depends on the number of variables considered. As mentioned above, in order to achieve an accurate result resembling the one obtained with the MM is necessary to increase the number of variables. It is not necessary, though, to have as much CPs as meshed nodes, but there must be a set of CPs representative of the geometry.

Checking the two values of v_1 yielded by the two cases, -0.81663 and -0.856132 mm, the corresponding $\theta_{applied}$ are -0.3228 and -0.3384°, for the one and two-variable cases, respectively. The value obtained in Section 4.1.2 with the DMM $\theta^{DMM}_{applied} = -0.3261°$ lies in between the two values, but is closer to the one obtained by the one-variable case.The latter is due to the fact that D_{min} is an *averaged* quantity and thus, when minimizing two variables the optimization aims to reduce the residual distance of CP1 and CP2 at the same time. On the other hand, when only one variable is minimized, the residual distance of CP1 is being reduced more than when two are used.

Finally, is important to remark that the one-variable yielded $\theta_{applied}$ resembles more $\theta^{DMM}_{applied}$ baceuse in the DMM the cured angle is measured with the y and z displacements of the geometrical point where CP1 is located.

4.1.4 First Comparison of the Three Methods

The three compensation methods are compared in this section for the first time. With the implementation of every strategy, valuable information has bee retrieved: number of iterations, easiness of execution, total compensation time, etc. But to compare the effectiveness of the compensation process with every method, a common variable must be measured as every method uses different indicators, e.g. maximum residual distance, spring-back angle or a cartesian component of the displacement vector. The common variable chosen has been D_{min} with a set of 7 representative CPs (see Figure 4.12). The latter has been computed on the last cured geometry yielded by every method – see Table 4.8.

Method	$\boldsymbol{D_{min}}$ **[mm²]**
MM	2.33 E-10
DMM	5.95 E-3
CPM1	8.21 E-3
CPM2	6.94 E-3

Table 4.8: D_{min} (7 CPs) at the last iteration for the three methods. CPM1 and CPM2 stands for one or two-variable application of the CPM.

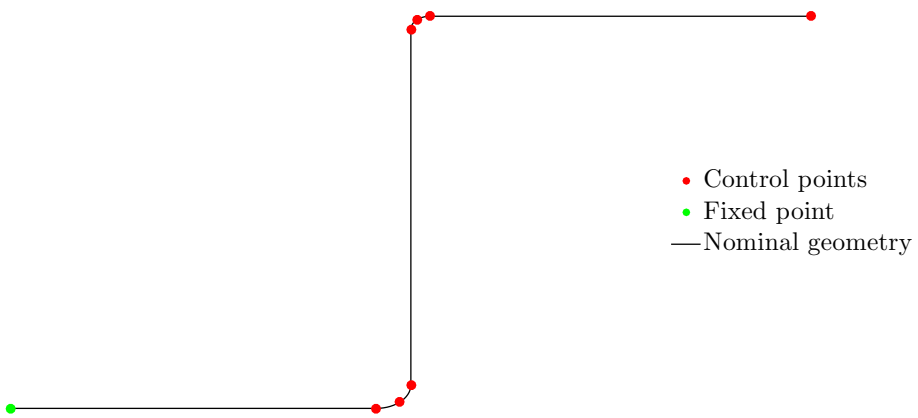

Figure 4.12: Chosen CPs to compare the effectiveness of compensation methods.

Below, a few common features of the three methods are discussed and compared with the acquired experience up to now, which is exclusively related to the studied deformation mode in this section: spring-in deformation.

- **Complexity of the computational chain**: CAD-based methods (DMM and CPM) require a greater number of steps to perform a single iteration of the compensation process. While mesh-based methods (MM) only require an initial CAD model plus an initial FEM model that is then modified after every iteration, the DMM and CPM require a new CAD model and FEM model every iteration. The latter implies modifying the parametrized CAD model, seeding the geometry to obtain the desired mesh, modify the orientation of the elements, create the laminate and extrude it, assign boundary conditions, loads, set the different archiving frequencies and launch the simulation. After that procedure, the optimization process must be applied. And also the post-processing, which is required by the three methods. Mesh-based methods, on the other hand, just require an update of the mesh following equation 2.25, plus applying the loads, boundary conditions and the archiving frequencies. Thus, the MM is simpler than the DMM and CPM, i.e. is easier to be automated.

- **Compensation iterations**: in a spring-in dominated geometry, the MM converges in very few iterations: 1 or 2 (depending on the desired accuracy). The DMM also performs really well as the deformation mode is well-known, but it can take more iterations to optimize the spring-in angle than the MM, i.e. it is very sensitive to the chosen optimization process. If DMM optimization processes 2 or 3 are chosen the amount of simulations/iterations required is higher than with the MM. On the other hand, the CPM is very sensitive to the amount of CPs chosen for the optimization. The greater the number of CPs, the higher the number of iterations. In conclusion, with a spring-in deformation mode, the MM requires the least number of iterations.

- **Compensation time**: considering the last two characteristics, complexity and iterations of the methods, the MM is the one that requires less time for the compensation to be obtained: less time to complete a whole iteration and less iterations to achieve the optimum than the DMM and CPM.

- **Compensation accuracy**: the accuracy of the MM is greater than the DMM and CPM – check Table 4.8. The cause of the difference in D_{min} between methods is due to the fact that in the MM the optimization of the geometry is applied to the totality of the nodes of the model. Thus, the accuracy achieved is very high. In the DMM only one variable is minimized, $\theta_{applied}$, which despite driving the main displacement mode is less precise than taking into account each and every geometrical point. For last, the CPM is really dependent on the amount of CPs. A larger amount of CPs will lead to a higher accuracy, resembling the MM – the latter is proved in Table 4.8, where the two-variable application of the CPM yields a lower value of D_{min} than the one-variable application.

- **CAD model of the compensated mold**: the DMM and CPM are better than the MM as they are CAD-based methods. Once the compensation process is finished, the CAD model of the last iteration is the CAD model of the mold. The MM, on the other hand, requires the conversion of the final mold mesh to a CAD model – which can actually be done using `NX` (see Figure 4.13).

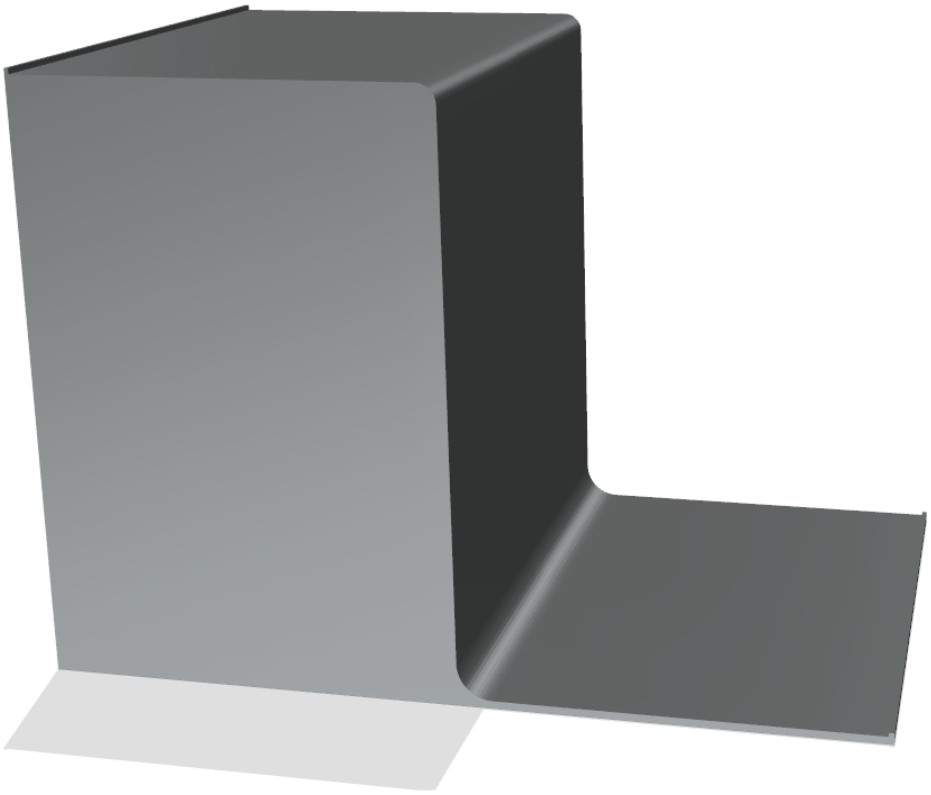

Figure 4.13: CAD model of the mold obtained using the MM for the Z-shaped part under spring-in deformation.

4.2 Flat Plate under Warpage Deformation

In this section, compensation when warpage is the main (and only) deformation mode is studied. Warpage occurs if a non-symmetrical laminate is used, as the use of a symmetrical laminate leads to null moments – inspection of equations A.22 and A.23, taking into account that there is a homogeneous distribution of T and X, leads to $M^T = M^{CH} = 0$. Besides, lack of symmetry in the laminate causes in-plane/out-of-plane couplings (see Section A.4.2), i.e. an in-plane traction generates a change in curvature.

There are three types of warpage deformation: pure bending, pure torsion and mixed warpage (bending + torsion). Accordingly, three laminates have been used:

- **Pure bending**: $[90/0]_4$, an anti-symmetrical cross-ply laminate.
- **Pure torsion**: $[-45/45]_4$, an anti-symmetrical angle-ply laminate.
- **Mixed warpage**: $[-45/0/45/0/0/-45/0/45]$, an unsymmetrical laminate.

The three laminates plies have thickness of $h = 0.205$ mm each ($h_{tot} = 1.64$ mm). The numerical model employed is the one detailed in Section 3.1.3, the warpage model. The element's reference vector (0° orientation) is aligned with the global axis x – see Figure 3.14.

4.2.1 Flat Plate under Pure Bending

In this section the compensation of a flat plate under pure bending is obtained with two of the three methods studied in this thesis: the MM and the DMM. Despite not solving this case with the CPM, its approach is evaluated and discussed. The laminate $[90/0]_4$ is used.

4.2.1.1 Compensation with the MM

The MM has been applied for 8 iterations with a δ_{res}^{max} of 0.0421 μm yielded in the last iteration – see Table 4.9. The process oscillates at iterations 3 and 4 and finally starts converging from iteration 5.

Iteration	$\boldsymbol{\delta_{res}^{max}}$ **[mm]**
0	1.54
1	0.14
2	1.71 E-02
3	1.01 E-01
4	1.15 E-01
5	1.77 E-02
6	2.25 E-03
7	2.91 E-04
8	4.21 E-05

Table 4.9: δ_{res}^{max} between the nominal and cured mesh at each iteration using the MM for the flat plate under pure bending.

Below, two figures show the initial and final iterations of the process. Figure 4.14 depicts iteration 0: the mold geometry (shaded) is the nominal geometry; and the cured geometry takes an expected saddle shape, as the contraction of the 0° plies competes with that of the 90° plies. Figure 4.15 depicts iteration 8: (a) the cured geometry which has a extremely small δ_{res}^{max}; and (b) the mold geometry is close to the inverse shape of the first cured geometry, with curvatures along x and y, κ_x and κ_y, of opposite sign. The compensated mold's CAD model is depicted in Figure C.1.

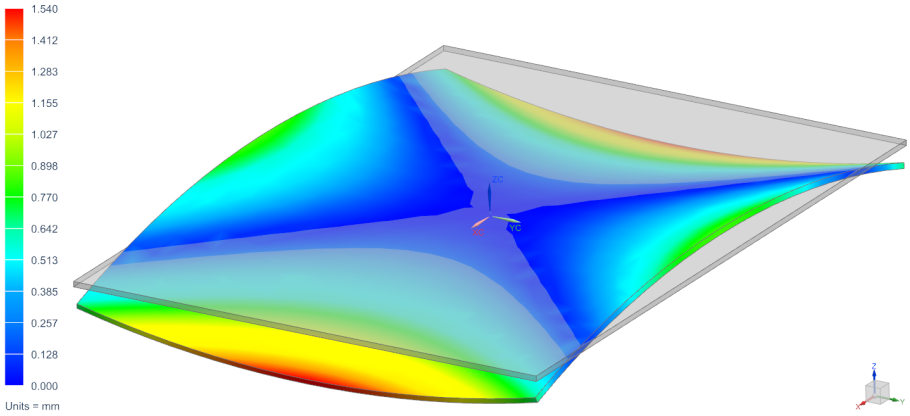

Figure 4.14: Cured geometry and mold geometry = nominal geometry (shaded) at iteration 0 of the MM for the flat plate under pure bending. A deformation factor of 10 is applied.

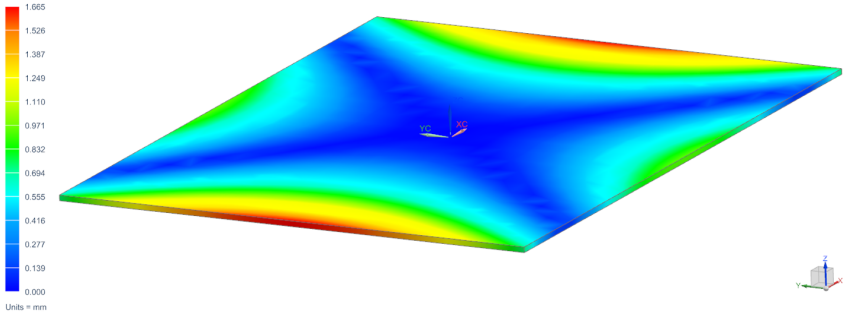

(a) The flat plate is recovered after curing.

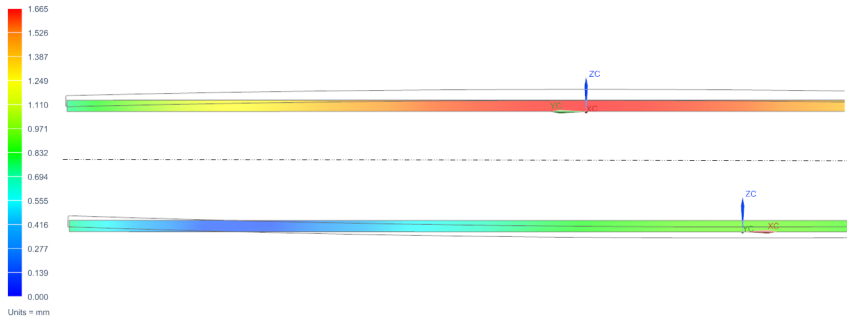

(b) The mold shape (feature lines) is close to the inverse cured shape of iteration 0. Up: short edge (yz plane); Down: long edge (xz plane).

Figure 4.15: Cured geometry at iteration 8 of the MM for the flat plate under pure bending.

4.2.1.2 Compensation with the DMM

The distortion mode that must be minimized is the curvature of the edges caused by the bending of the plate. As the plate bends along x and y, both curvatures κ_x and κ_y must be considered. In the parametrized model of the plate, the edges have been defined as parabolas – see Figure 4.16. The vertices of the parabolas are forced to stay on the xy plane, and thus the equations to define them and the curvatures are:

$$\begin{cases} z(x) = px^2 + b \\ \kappa_x = z''(x) = 2p \end{cases} \quad (4.1) \qquad \begin{cases} z(-100) = 0 \\ z(+100) = 0 \end{cases} \quad (4.2) \qquad \begin{cases} p = -\frac{b}{100^2} \\ \kappa_x = -\frac{2b}{100^2} \end{cases} \quad (4.3)$$

$$\begin{cases} z(y) = my^2 + a \\ \kappa_y = z''(y) = 2m \end{cases} \quad (4.4) \qquad \begin{cases} z(-75) = 0 \\ z(+75) = 0 \end{cases} \quad (4.5) \qquad \begin{cases} m = -\frac{a}{75^2} \\ \kappa_y = -\frac{2a}{75^2} \end{cases} \quad (4.6)$$

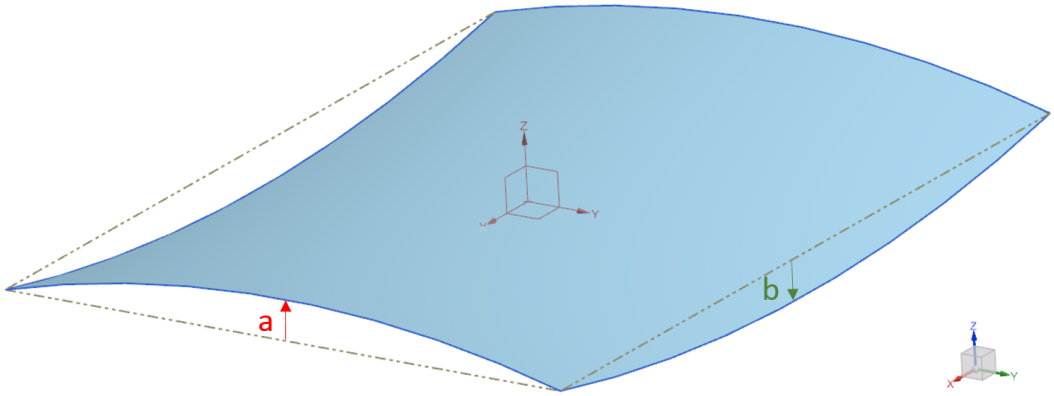

Figure 4.16: Parametrized model of the plate in which the curvatures κ_x and κ_y are modelled with the parameters a and b.

The proposed objective function for the optimization of the mold geometry is $F_{obj} = \left(\kappa^k_{cx}/\kappa^0_{cx}\right)^2 + \left(\kappa^k_{cy}/\kappa^0_{cy}\right)^2$, where κ^k_{cx} and κ^k_{cy} are the cured curvatures measured for each configuration k, and κ^0_{cx} and κ^0_{cy} are the reference cured curvatures, i.e. obtained when the mold geometry is equal to the nominal geometry (flat plate).

The reference cured curvatures are: $\kappa^0_{cx} = 0.0003$ and $\kappa^0_{cy} = -0.0003$ ($\kappa^0_{cx} = -\kappa^0_{cy}$). The curvatures are measured as follows: export from `NX` the cured displacements of the plate edges to an `Excel` sheet; then, fit a second order curve to the deformed edges, $y = ex^2 + q$, and find the curvature $\kappa_i = 2e$ ($i = x$, y).

A surrogate-based algorithm has been chosen to solve the compensation problem. A set of 16 different mold geometries have been tried following the parametrized model described in Figure 4.16 and equations 4.3 and 4.6. Four values of a and b each have been tried, i.e. different values of initial κ_x and κ_y. Those are: $\{a, b\} = -2$, -1, 1 and 2.

The set of initial curvatures and the yielded values of the F_{obj} for each configuration are presented in Table 4.10. The first surrogate model obtained with the initial set of cases is presented in Figure 4.17 – all surrogate models used are in the second order in both variables and have a fitting parameter of $R^2 = 0.95$.

$F_{obj} = \left(\frac{\kappa^k_{cx}}{\kappa^0_{cx}}\right)^2 + \left(\frac{\kappa^k_{cy}}{\kappa^0_{cy}}\right)^2$ [-]				
κ_x/κ_y (x 10^{-4}) [-]	**-4**	**-2**	**2**	**4**
-7.11	7.63	4.66	1.82	2.16
-3.55	5.86	3.13	0.21	0.07
3.55	7.77	6.02	4.90	5.24
7.11	12.44	11.28	11.12	11.83

Table 4.10: Initial tested cases for the DMM of the flat plate under pure bending.

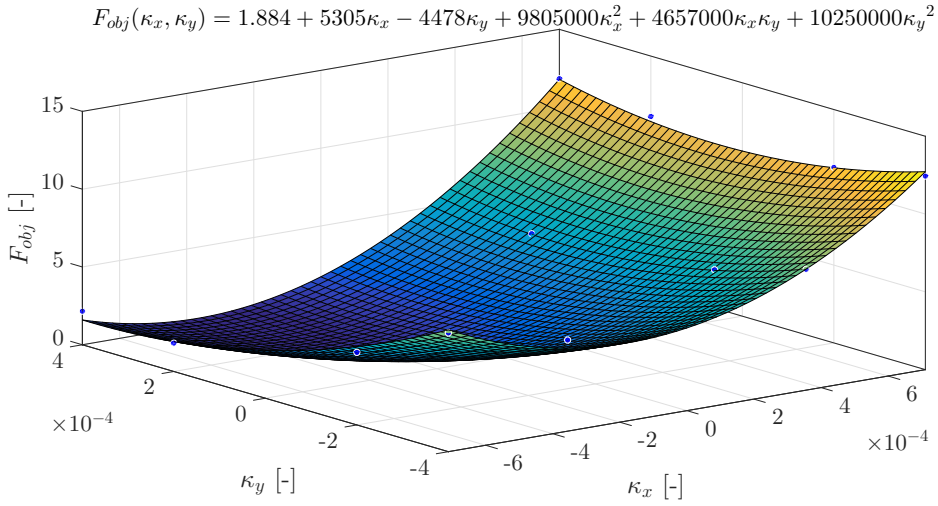

Figure 4.17: First surrogate model of the DMM for a flat plate under pure bending.

The optimum of the first surrogate model is $\kappa_x = -3.408$ E-4 and $\kappa_y = 2.958$ E-4, detailed along the other optimums of each iteration in Table 4.11. As it can be seen after 5 iterations, the tendency of κ_x is to decrease and κ_y is to increase, while F_{obj} is being reduced. This iterative process has been carried through manually (as any iterative process in this thesis), taking around 30 minutes per each tested configuration (16+5), which amounts to 10.5 hours to obtain the results shown up to now.

For the latter reason, the compensated geometry of the mold yielded by the MM in Section 4.2.1.1 has been examined. The curvatures of the mold's edges have been measured and are $\kappa_x^{MM} = -3.3158$ E-4 and $\kappa_y^{MM} = 3.3168$ E-4 ($\kappa_x^{MM} \simeq -\kappa_y^{MM}$). With the MM, though, the vertices of the plate do not stay on the xy plane – see Figure 4.18. Despite that difference, the same curvatures have been applied to the parametrized model and the curing simulation has been executed. With the obtained cured curvatures, the corresponding objective function value has been computed, being $F_{obj} = 1.213$ E-5 – i.e. the optimum has been found.

In conclusion, the optimization process would have reached $\kappa_x = -3.3158$ E-4 and $\kappa_y = 3.3168$ E-4. Due to the slow change of the iterates, as long as the limited time to achieve all the objectives of the thesis, the process has been terminated earlier and the MM solution has been tested. The latter has been proved to be the optimum of the DMM despite having boundary conditions that are not satisfied in the MM.

Iteration	κ_x (x 10^{-4}) [-]	κ_y (x 10^{-4}) [-]	κ_{cx} (x 10^{-4}) [-]	κ_{cy} (x 10^{-4}) [-]	$F_{obj} = \left(\frac{\kappa^k_{cx}}{\kappa^0_{cx}}\right)^2 + \left(\frac{\kappa^k_{cy}}{\kappa^0_{cy}}\right)^2$ [-]
1	-3.4078	2.9585	-0.0302	-0.1905	4.134 E-3
2	-3.3970	2.9701	-0.0249	-0.185	3.872 E-3
3	-3.3887	2.9782	-0.0208	-0.1811	3.692 E-3
4	-3.3842	2.9868	-0.0187	-0.1768	3.512 E-3
5	-3.3805	2.9919	-0.0176	-0.1742	3.406 E-3

Table 4.11: Optimums of the surrogate models of the DMM for a flat plate under pure bending.

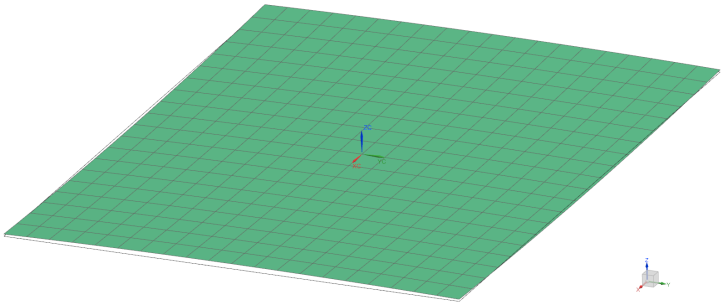

Figure 4.18: Compensated mold mesh of the flat plate under pure bending.

4.2.1.3 Compensation with the CPM

The CPM has not been applied to this particular case for two reasons:

- The optimization process carried with the DMM might as well be thought as a CPM. The curvatures (distortion modes) are modified by changing the z-component of 2 points (CPs).
- As previously discussed in the implementation of the CPM in Section 4.1.3, if higher accuracy is sought, a high number of CPs is necessary to be used (resemblance to the MM) – see Figure 4.19. A richer design space would be available and a different solution, where for instance the vertices do not have to be in xy plane, can be found. A high number of CPs implies a multi-variable optimization, which is very time-consuming and hard to execute manually. As the CPM has already been executed twice in this thesis, for this case it has been discarded.

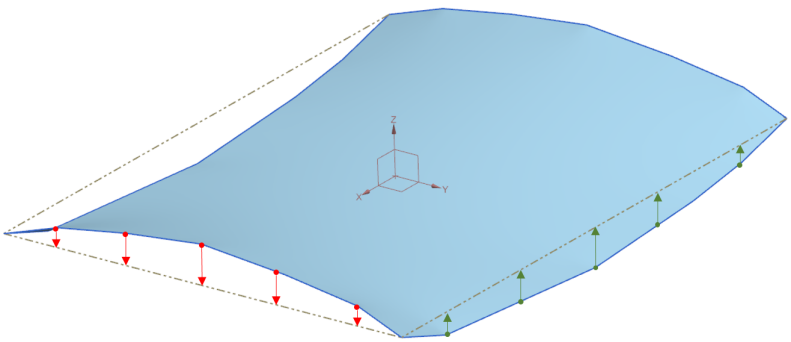

Figure 4.19: Example of the parametrized model to compensate the flat plate under bending. Points in red and green are the CPs and their z-component are the optimization variables.

4.2.1.4 MM Convergence with Warpage Deformation

The main hypothesis of the MM is that the cured-induced distortions are consider as linear, and thus, the compensated mold geometry should be close to the inverted cured geometry with respect to the nominal geometry. The only deformation mode studied in this section is bending and there is a consequent change in curvature of the plate's edges. And curvature is a second order phenomena, e.g. $\kappa_x = \frac{\partial^2 w}{\partial x^2}$, where w is the z-oriented displacement. Therefore, it must be analyzed whether the MM will always converge or not under this type of deformation.

In [2] the MM is used to compensate several geometries with different laminates. A small mention is made to the compensation of a flat plate with an unsymmetrical laminate: $[0_6/90_6]$. It is claimed that the method will diverge or stagnate when warpage is the only deformation mode. It is also mentioned that a modification of equation 2.25, the mesh update method, has been tried without success: a relaxation factor has been introduced to try to adjust the non-linearities, i.e. $\mathcal{M}^{i+1} = \mathcal{M}^i + \boldsymbol{\xi}(\mathcal{M}^o - \mathcal{M}_c^i)$, where ξ is the relaxation factor.

The flat plate with $[0_6/90_6]$ laminate has been simulated with the MM adapting it to the curing model and information of this thesis (as no information on that matter is given in [2] for this case). The results obtained are the same as in [2]: the cured geometry oscillates between saddle shapes across iterations – see Figure 4.20.

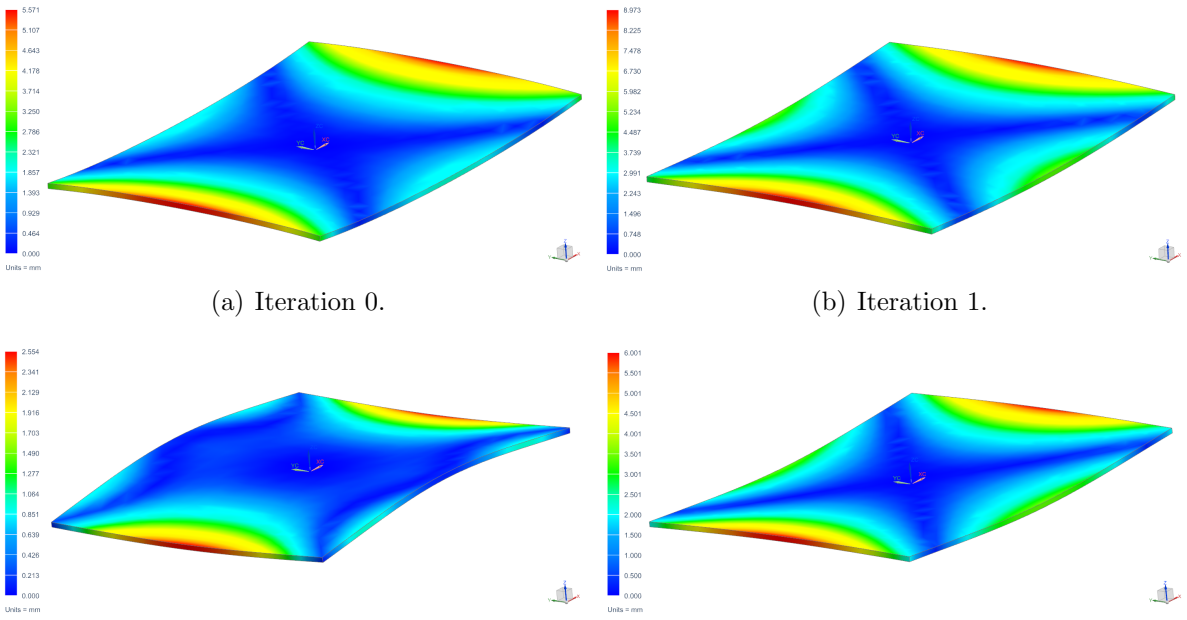

(a) Iteration 0. (b) Iteration 1.

(c) Iteration 2. (d) Iteration 3.

Figure 4.20: Divergence of the MM on a flat plate with an anti-symmetrical cross laminate: $[0_6/90_6]$.

So far, then, the MM is successful in compensating a flat plate with $[90/0]_4$ but fails when the employed laminate is $[0_6/90_6]$. Matrix $\mathcal{B}$ is the one that accounts for the coupling between in-plane/out-of-plane phenomena (see Appendix A). The main source of non-linearities comes from that coupling, as the moments generated in the laminate are

going to be less important than the tractions because the employed laminates are very thin − moments are related with the thickness (see equations A.22 and A.23).

By inspection of equation A.13, it can be stated that the amplitude of $\mathcal{B}$ will be greater in the $[0_6/90_6]$ laminate rather in than the other. Therefore, the non-linearities are more important when $[0_6/90_6]$ is used and thus, the MM does not succeed. A relaxation factor of $\xi = 0.8$ has been tried obtaining the same oscillation between saddle shapes.

No more ξ have been tried as the only purpose of this section is to determine the effectiveness of the MM when warpage prevails. The conclusion that can be extracted is: when the non-linearities are such that the MM fails to succeed, it is more convenient to use a CAD-based method rather than reformulating the MM strategy − introducing a relaxation factor, for instance, is really case-dependent: the geometry, laminate, and thermo-mechanical conditions will influence the value of ξ that adjusts the non-linearities.

4.2.2 Flat Plate under Pure Torsion

In this section the compensation of a flat plate under pure torsion is obtained with two of the three methods studied in this thesis: the MM and the DMM. Despite not solving this case with the CPM, its approach is evaluated and discussed. The laminate $[-45/45]_4$ is used.

4.2.2.1 Compensation with the MM

The MM has been applied for 8 iterations with a δ_{res}^{max} of 5.4 μm yielded in the last iteration − see Table 4.12. The latter is two orders of magnitude bigger than the one achieved for the flat plate under pure bending. As it happened with the pure bending deformation case, the process oscillates: at iteration 3, δ_{res}^{max} increases with respect to iteration 2; but then, from iteration 4 the process starts converging.

Iteration	$\boldsymbol{\delta_{res}^{max}}$ **[mm]**
0	9.80
1	0.43
2	5.49 E-02
3	1.85 E-01
4	2.21 E-02
5	1.46 E-02
6	1.05 E-02
7	7.52 E-03
8	5.40 E-03

Table 4.12: δ_{res}^{max} between the nominal and cured mesh at each iteration using the MM for the flat plate under pure torsion.

Below, two figures show the initial and final iterations of the process. Figure 4.21 depicts iteration 0: the mold geometry (shaded) is the nominal geometry, i.e. the flat plate; and the cured geometry suffers a torsional deformation around the x axis. Figure 4.22 depicts iteration 8: the cured geometry is now flat and the mold geometry (shaded) has a

torsional angle of opposite sign to the one of the first cured geometry. The compensated mold's CAD model is depicted in Figure C.2.

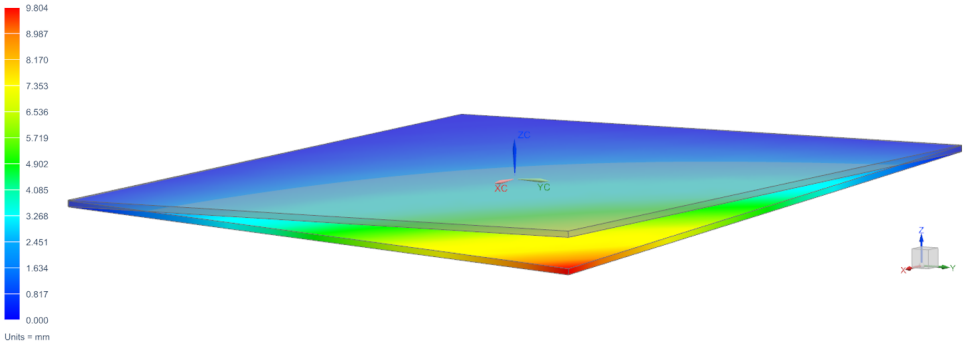

Figure 4.21: Iteration 0 of the MM for the flat plate under pure torsion. The cured geometry and mold geometry = nominal geometry (shaded) are depicted.

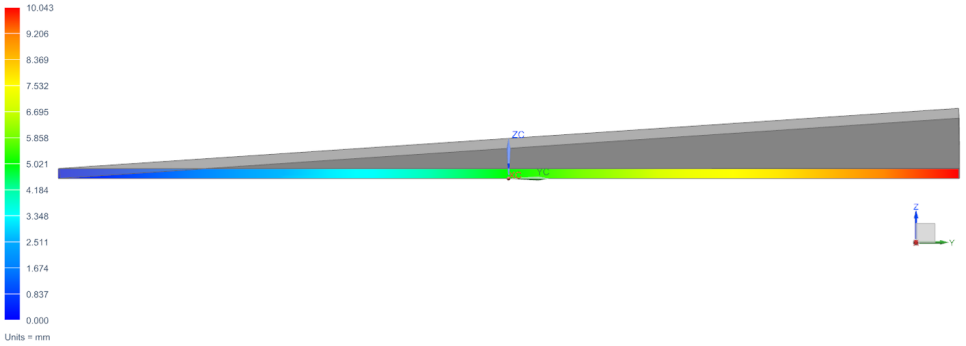

Figure 4.22: Iteration 8 of the MM for the flat plate under pure torsion. The cured geometry and mold geometry (shaded) are depicted.

4.2.2.2 Compensation with the DMM

The distortion mode that must be minimized is the torsional angle ϕ caused by the torsion moment generated in the plate. In the parametrized model of the plate, one of the short edges of the plate has been given an initial torsional angle – see Figure 4.16. One of the vertex of that edge is forced to stay on the xy plane, and thus the relation to define the edge on the parametrized model (parameter c) according to the desired applied torsional angle $\phi_{applied}$ is deduced from simple trigonometry:

$$c = 150 \cdot tan(\phi_{applied}) \tag{4.7}$$

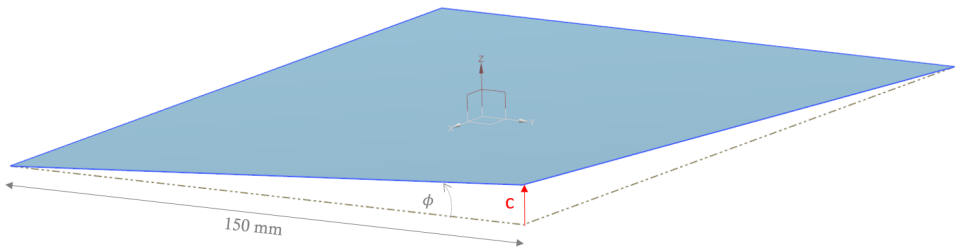

Figure 4.23: Parametrized model of the plate in which the torsional angle ϕ is modeled parameter c.

The proposed objective function for the optimization of the mold geometry is $F_{obj} = \left(\phi_c^k/\phi_c^0\right)^2$ where ϕ_c^k is the cured torsional angle measured for each configuration k, and ϕ_c^0 is the reference torsional angle, i.e. obtained when the mold geometry is equal to the nominal geometry (flat plate). The reference torsional angle is $\phi_c^0 = -3.68$. The torsional angle ϕ is measured as follows: export from `NX` the cured displacements of the plate edge to an `Excel` sheet; then, fit a first order curve to the deformed edges, $y = ex + q$, and find the torsional angle $\phi = tan^{-1}(e)$.

A surrogate-based algorithm has been chosen to solve the compensation problem. A set of 11 different mold geometries have been tried following the parametrized model described in Figure 4.16, i.e. 11 values of ϕ_0 have been tried, which have been obtained by setting the parameter c (see equation 4.7).

The set of initial torsional angles ($\phi > 0$ when there is a counterclockwise change in torsional angle) and the yielded values of the F_{obj} for each configuration are presented in Table 4.13. The first surrogate model obtained with the initial set of cases is presented in Figure 4.24 – all surrogate models are second order models of ϕ with a fitting parameter of at least $R^2 = 0.9992$.

The optimum of the first surrogate model is $\phi_{applied} = 3.8512°$, detailed along the other optimums of each iteration in Table 4.10. The optimums found after the first surrogate model are all worst than the first optimum. Thus, the process is terminated and $\phi_{applied} = 3.8512°$ is taken as the initial torsional angle that the mold geometry must have to obtain the flat plate geometry after the curing process.

Individual	$\boldsymbol{\phi_{applied}}$ [°]	$\boldsymbol{\phi_c}$ [°]	$\boldsymbol{F_{obj} = \left(\frac{\phi_c^k}{\phi_c^0}\right)^2}$ [-]
Initial set			
A	-5.0000	-7.9865	4.7099
B	-4.0000	-7.1306	3.7546
C	-3.0000	-6.2716	2.9045
D	-2.0000	-5.415	2.1656
E	-1.0000	-4.5568	1.5333
F	1.0000	-2.7823	0.5717
G	2.0000	-1.8500	0.2527
H	3.0000	-0.8708	0.0550
I	4.0000	0.1604	0.0019
J	5.0000	1.5523	0.1779
K	6.0000	2.3421	0.4050
Iterations			
1	3.8512	0.0051	1.9635 E-06
2	3.8581	0.0114	9.6964 E-06
3	3.8673	0.0229	3.8786 E-05
4	3.8683	0.0229	3.8786 E-05
5	3.8742	0.0286	6.0602 E-05

Table 4.13: Tested configurations and F_{obj} of the DMM for a flat plate under pure torsion.

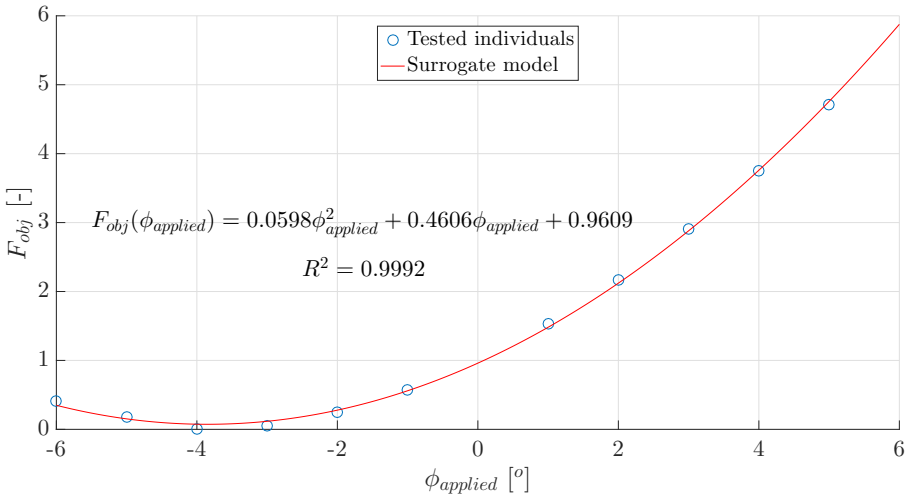

Figure 4.24: First surrogate model of the DMM for a flat plate under pure torsion.

4.2.2.3 Compensation with the CPM

The CPM has not been applied to this particular case for the same two reasons as with the pure bending case:

- The optimization process carried with the DMM might as well be thought as a CPM. The torsional angle $\phi_{applied}$ is modified by changing the z-component of 1 point (CP).
- Ideally, multiple CPs should be used and a multi-variable optimization is then required. In that way, a higher accuracy can be reached. But that is very time-consuming and hard to execute manually, and it has been avoided as the CPM has already been implemented in this thesis. A proposal of CPM is depicted in Figure 4.25.

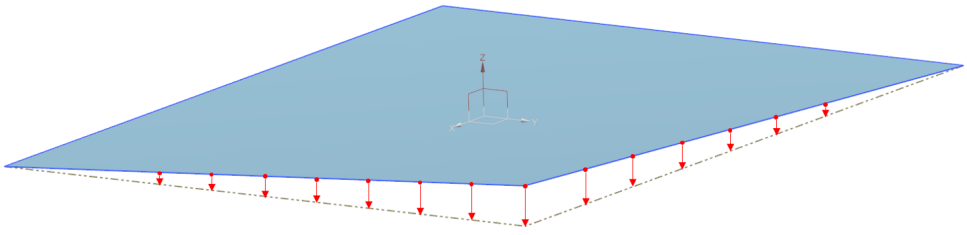

Figure 4.25: Example of the parametrized model to compensate the flat plate under torsion. Points in red and green are the CPs and their z-component are the optimization variables.

4.2.3 Flat Plate under Mixed Warpage

In this section the compensation of a flat plate under mixed warpage (bending + torsion) is analysed with one of the three methods studied in this thesis: the MM. Despite not solving this case with the DMM and CPM, their approaches are evaluated and discussed. The laminate [−45/0/45/0/0/-45/0/45] is used.

4.2.3.1 Compensation with the MM

The MM has been applied and it has failed to find the compensated mold geometry. As detailed in Section 4.2.1.4, when the non-linear terms have a big amplitude, the hypothesis of the MM does not apply anymore and the method diverges or stagnates.

In the present case, the in-plane/out-of-plane coupling is higher than in the pure bending and torsion cases. Now, bending and torsion occur at the same time, i.e. they are coupled. As a result, when applying the MM, the cured geometry oscillates between saddle shapes every iteration. A relaxation factor $\xi = 0.8$ has been tried in order to adjust the correction performed to the mesh with the non-linearities. The latter has not solved the convergence issues. As aforementioned, in such situation it is better to try a CAD-based strategy to solve the compensation problem.

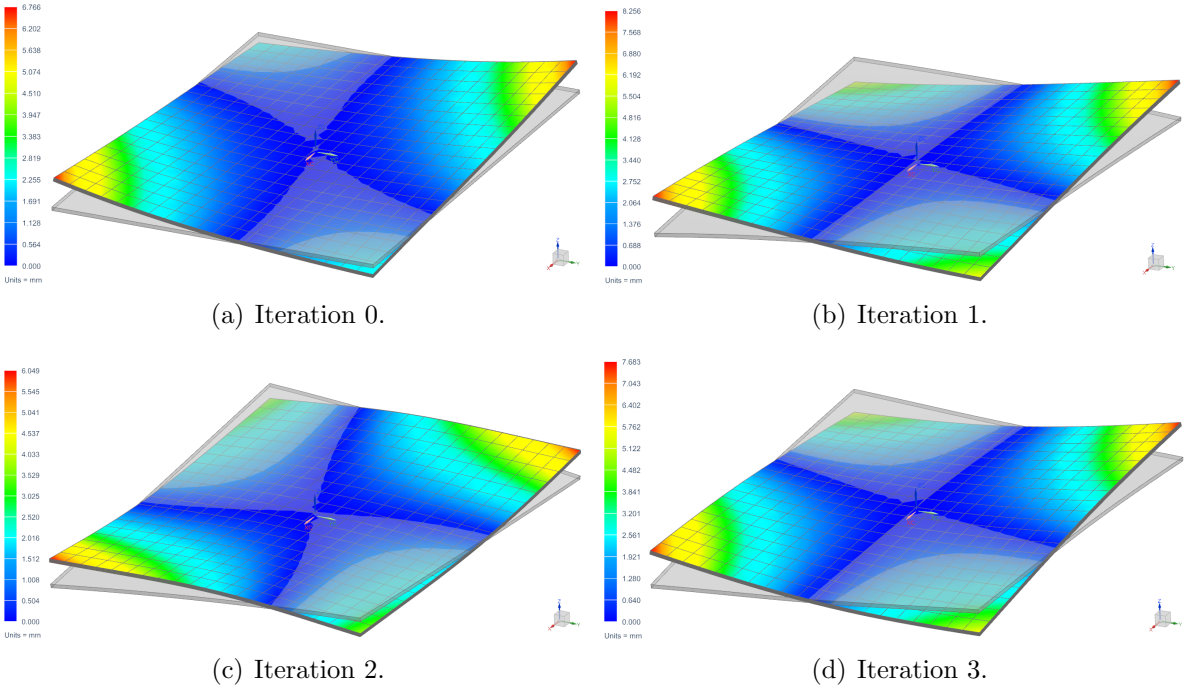

(a) Iteration 0. (b) Iteration 1.

(c) Iteration 2. (d) Iteration 3.

Figure 4.26: Divergence of the MM on a flat plate under mixed warpage.The shaded shapes represent the mold geometry.

4.2.3.2 Compensation with the DMM

Compensation with the DMM has not been performed in this section. In this particular case there are three distortion modes: two curvatures and one torsional angle, supposing that parallel edges have same curvatures; or on the contrary, four curvatures and one torsional angle. That implies a multi-variable optimization process, which is very time-consuming and hard to execute manually.

The latter two factors have limited the amount of compensation problems tried in this thesis. Despite that, the DMM has already been implemented for warpage-dominated geometries. A proposal of a parametrized model to solve this problem with the DMM is depicted in Figure 4.27: parameters a, b and c used in the un-coupled problems would

be used in the same way to produce intial torsional angles and initial curvatures. The proposed objective function to minimize the three distortion modes at the same time is $F_{obj}^{mixed} = \left(\frac{\kappa_{cx}^k}{\kappa_{cx}^0}\right)^2 + \left(\frac{\kappa_{cy}^k}{\kappa_{cy}^0}\right)^2 + \left(\frac{\phi_c^k}{\phi_c^0}\right)^2 = F_{obj}^{bending} + F_{obj}^{torsion}$.

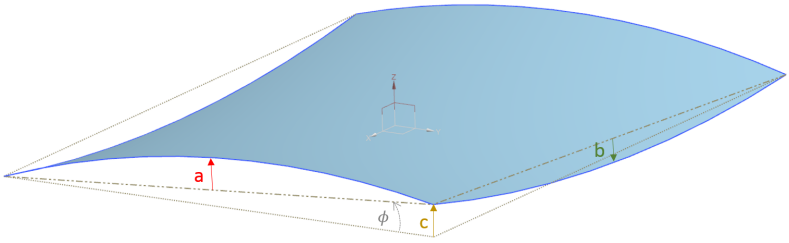

Figure 4.27: Example of the parametrized model to compensate the flat plate under mixed warpage with the DMM.

4.2.3.3 Compensation with the CPM

Compensation with the CPM has not been performed in this section. Several CPs are necessary to capture both the bending and the torsion of the plate. As previously mentioned, a multi-variable optimization has not been considered to be solved as the whole execution of the method is done manually. Lack of automation has been a huge limiting factor in this thesis.

4.2.4 Applicability of the Methods when Warpage Dominates

A comparison of the three methods on general terms like accuracy, number of iterations, compensation time, complexity of the computational change or the CAD model of the compensated mold, was discussed on Section 4.1.4. In this section, the advantages and downfalls of compensating a geometry where warpage prevails are discussed for each method. Also, some comments in regard to spring-in/spring-back deformation prevailing geometries are added for completeness.

- **Mirror Method**
  - The accuracy order reached with the MM when warpage is caused by pure bending is the same as in the spring-back case: 10^{-2} μm. But it takes 8 iterations while in the spring-back case it only takes 2. Then, regarding warpage caused by pure torsion, with 8 iterations the accuracy order reached is lower: 10^{0} μm.
  - Convergence is not guaranteed when warpage dominates. The MM's main hypothesis is to assume cure-induced distortions as linear. When the non-linearities associated with warpage are not too important, the method still converges; on the contrary, when second order effects dominate the displacement field, the method stagnates and oscillates between saddle shapes.
- **Distortion Modes Method**
  - If the distortion modes, i.e. curvatures and torsional angles, are well identified, the process is effective and the compensated geometry is obtained.

- Complexity of the method increases as the distortion modes are second-order phenomena: good identification of the distortion modes and a representative enough first set to start iterating is necessary. For instance, when using the DMM for the pure bending case (Section 4.2.1.2), the set of tested individuals has been more representative for κ_x than for κ_y, as its optimum value on the first surrogate model has lied closer to the final optimum of the process.
- Furthermore, warpage deformation implies optimization of multiple variables at the same time, in comparison with spring-in/spring-back deformation. In a flat plate, three deformation modes can be identified for the mixed warpage mode (two curvatures and one torsional angle). Therefore, more complex geometries will require a higher number of variables (distortion modes) to be solved in the compensation process – a good selection of the optimization algorithm is necessary.

- **Control Points Method**
  - Despite not being executed in this section, the CPM with a deformation mode such as warpage requires a higher number of CPs than in a spring-in/spring-back deformation mode. The second-order phenomena requires a higher number of variables to be precise in the proper characterization of the deformation of the geometry. A higher amount of CPs directly implies a higher complexity in the optimization process of the problem, i.e. multi-variable optimization.

4.3 Z-shaped Part under Mixed Deformation

In this section, compensation when mixed deformation occurs (spring-in/spring-back + warpage) is studied. As previously detailed in Section 4.2, there are different types of warpage depending on the type of laminate used. Regarding spring-in/spring-back, it is a geometrical phenomenon that occurs due to the anisotropical expansion/contraction of the material throughout the curing process. The same three laminates as in Section 4.2 have been used: $[90/0]_4$, for which it can be expected global spring-back deformation and bending (**mixed deformation 1**); $[-45/45]_4$, for which it can be expected global spring-back and torsional deformation (**mixed deformation 2**); and $[-45/0/45/0/0/-45/0/45]$, whose deformation is expected to be a combination of the latter two laminates (**mixed deformation 3**).

The three laminates are composed of plies of thickness $h = 0.205$ mm each ($h_{tot} = 1.64$ mm). The numerical model employed is the one detailed in Section 3.1.2.3, the mixed deformation model. The element's reference vector (0° orientation) is aligned with the global axis y, but follows the Z-shape of the part– see Figure 3.12.

Finally, it is important to mention that only the MM has been employed to compensate the Z-shaped part under mixed deformation. The latter is in accordance with what has been discussed in Section 4.2.4: the amount of distortion modes (DMM) or CPs (CPM) is very high in this present case, as the global deformation is a composition of several deformation modes. Therefore, the compensation of this case with the DMM and CPM has been unapproachable in this thesis. As mentioned early in the text, multi-variable optimization without automation is very time consuming and complex. Despite not applying the two methods, a brief discussion on how they should be applied to the present problem is given.

4.3.1 Compensation of Mixed Deformation 1 the with the MM

The MM has been applied for 8 iterations with a δ_{res}^{max} of 0.0242 μm yielded in the last iteration (see Table 4.14). The achieved accuracy is the same order of magnitude as the one yielded in the spring-in deformation case. In the latter case it takes just two iterations to achieve such accuracy, 10^{-5} mm, while in the present case it has taken 6 iterations as warpage (non-linearities) slow down the compensation process.

Iteration	$\boldsymbol{\delta_{res}^{max}}$ **[mm]**
0	11.56
1	1.044
2	1.08 E-1
3	1.07 E-2
4	1.18 E-3
5	1.27 E-4
6	3.30 E-5
7	2.89 E-5
8	2.42 E-5

Table 4.14: δ_{res}^{max} between the nominal and cured mesh at each iteration using the MM for the Z-shaped part under mixed deformation 1.

Two figures depicting the initial and last iterations of the process are shown below. Figure 4.28 depicts the cured geometry of iteration 0 of the mixed deformation 1, which has experienced spring-back and warpage (due to bending) deformation. Note that the bending of the part makes the upper and lower flanges experience a spring-in/spring-back deformation while in the pure spring-back deformation case of Section 4.1 they barely change its horizontal shape.

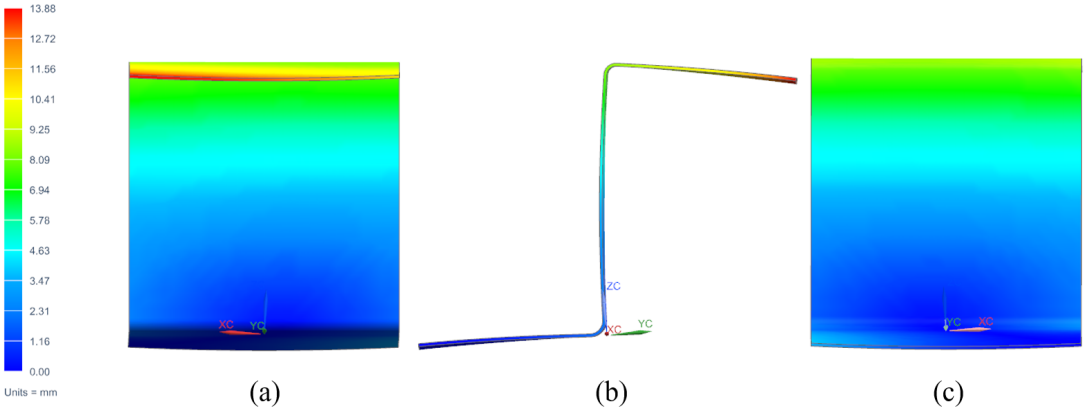

Figure 4.28: Initial cured geometry of the Z-shape part under mixed deformation 1: (a) curvature of upper flange; (b) curvature and spring-back of the web; and (c) curvature of the lower flange. A deformation factor of 2 is applied.

Then, in Figure 4.29 (a) the cured geometry at iteration 8 is depicted, which is very close to the nominal geometry. The mold geometry is also shown (shaded). Figure 4.29 (b) is added to explain why there is a twist on the mold geometry. It is caused by the applied boundary conditions to restrict the rigid body modes. The latter are applied on one side of the Z-shaped part, and thus, the expansion/contraction of the material induces an uneven displacement field along x. That twist is purely numerical and the only geometrical features that are necessary to account for in the final mold geometry are the spring-back angle and the curvatures of the flanges and web. To remove that twist the boundary conditions (see Figure 3.7) should be applied on the same fashion but on the plane of symmetry of the part.

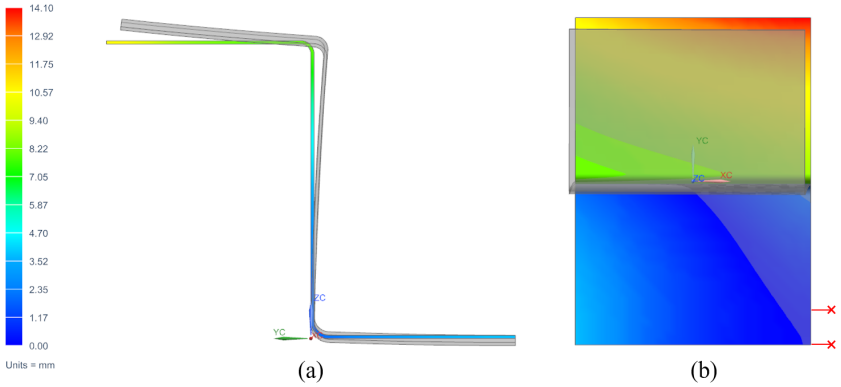

Figure 4.29: Last cured geometry and mold geometry of the Z-shape part under mixed deformation 1: (a) the nominal geometry is recovered; (b) twist of the mold induced by the boundary conditions.

4.3.2 Compensation of Mixed Deformation 2 the with the MM

The MM has been applied for 8 iterations with a δ_{res}^{max} of 0.0257 μm yielded in the last iteration (see Table 4.15). In the present case, it takes 5 iterations to achieve an order of magnitude of 10^{-5} mm. The highest accuracy is achieved in iteration 6. In iteration 7, δ_{res}^{max} increases and in iteration 8 it decreases again. The latter behaviour can be understood as an accuracy threshold of the method – the same behaviour was observed when applying the MM to the Z-shaped part under spring-in deformation.

Iteration	$\boldsymbol{\delta_{res}^{max}}$ **[mm]**
0	10.57
1	5.64 E-1
2	5.63 E-2
3	5.99 E-3
4	5.58 E-4
5	4.01 E-5
6	2.24 E-5
7	2.91 E-5
8	2.57 E-5

Table 4.15: δ_{res}^{max} between the nominal and cured mesh at each iteration using the MM for the Z-shaped part under mixed deformation 2.

Two figures depicting the initial and last iterations of the process are shown below. Figure 4.30 depicts the cured geometry of iteration 0 of the mixed deformation 2, which has experienced spring-back and torsion deformation. Note that there is a torsional angle in both flanges and on the web.

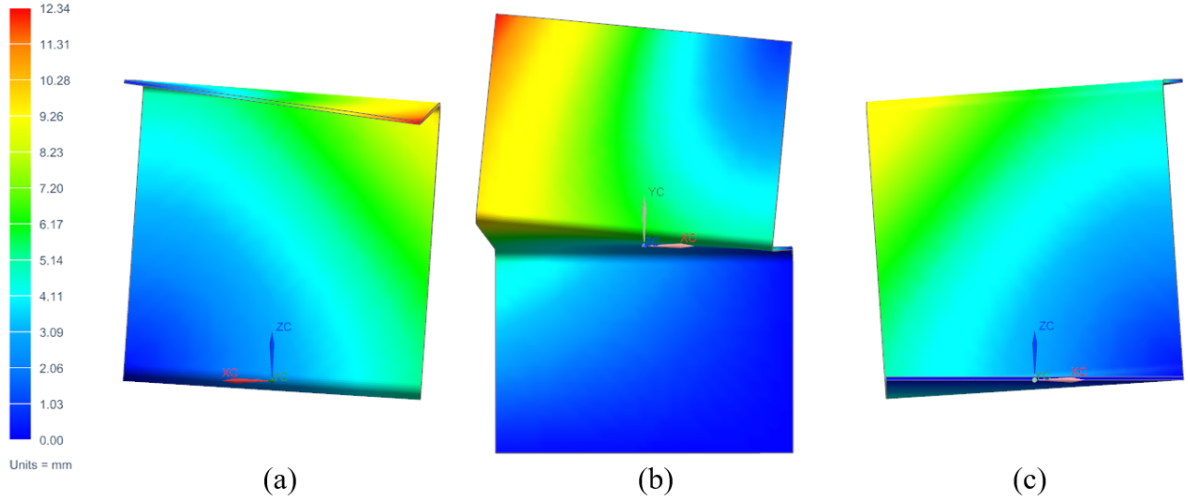

Figure 4.30: Initial cured geometry of the Z-shape part under mixed deformation 2: (a) torsion of upper flange; (b) torsion and spring-back of the web; and (c) torsion of the lower flange. A deformation factor of 2 is applied.

Then, in Figure 4.31 the cured geometry at iteration iteration 8 is depicted, which is very close to the nominal geometry. Figure 4.31 also depicts the mold geometry (shaded), which is close to the the inverse of the first cured geometry (depicted in Figure 4.30) with respect to the nominal geometry.

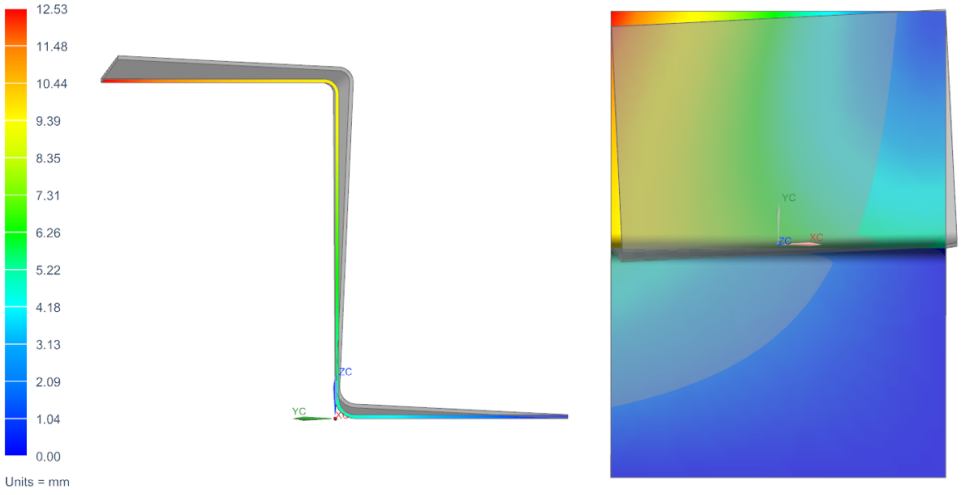

(a) (b)

Figure 4.31: Last cured geometry and mold geometry of the Z-shape part under mixed deformation 2: (a) the nominal geometry is recovered; (b) twist of the mold geometry along the web of the part.

4.3.3 Compensation of Mixed Deformation 3 the with the MM

The MM has been applied for 8 iterations with a δ_{res}^{max} of 0.118 mm yielded in the last iteration (see Table 4.16). The achieved accuracy is way less than the one yielded with mixed deformations 1 and 2. Three extra iterations have been performed seeking higher accuracy: δ_{res}^{max} has only been reduced to 0.0415 mm. The main cause behind this slow reduction of the residual distance is a higher dominance of the non-linear effects on the cured-induced distortions – the main hypothesis of the MM is less satisfied. Warpage now couples bending and torsion, which in contrast with mixed deformation modes 1 and 2, where they are uncoupled, makes the compensation process reduce the residual distance field less per iteration.

Iteration	$\boldsymbol{\delta_{res}^{max}}$ **[mm]**
0	19.31
1	3.16
2	1.27
3	8.11 E-1
4	4.79 E-1
5	3.42 E-1
6	2.36 E-1
7	1.68 E-1
8	1.18 E-1

Table 4.16: δ_{res}^{max} between the nominal and cured mesh at each iteration using the MM for the Z-shaped part under mixed deformation 3.

Two figures depicting the initial and last iterations of the process are shown below. Figure 4.32 depicts the cured geometry of iteration 0 of the mixed deformation 3, which has experienced spring-back and warpage (bending + torsion) deformation. Torsion dominates more as the employed laminate has ±45° plies (responsible for the torsion of the part) while there are not 90° plies for the 0° plies: 90/0° ply groups are responsible for the change in curvature. Nonetheless, as the laminate is unsymmetrical, the coupling terms responsible for curvature changes are non-zero ($\mathcal{B}_{11}$ and $\mathcal{B}_{22}$) – see Section A.4.

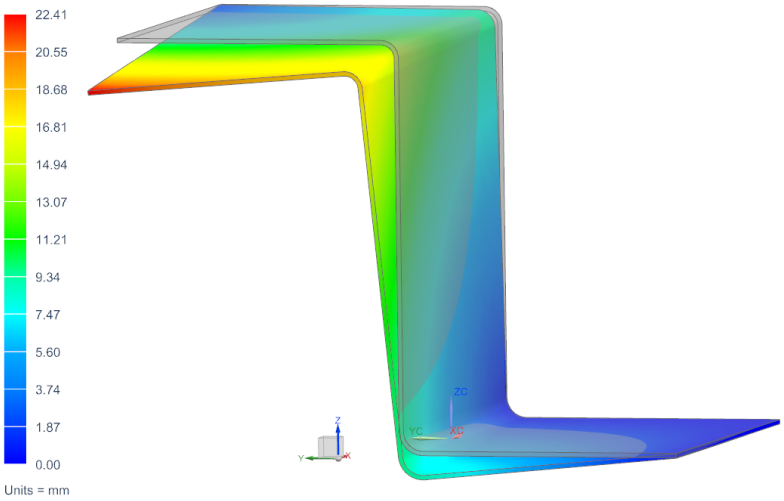

Figure 4.32: Initial cured geometry of the Z-shape part under mixed deformation 3: spring-back + warpage (torsion and bending).

Then, in Figure 4.33 the cured geometry at iteration 8 is depicted, which is close to the nominal geometry. However, as δ_{res}^{max} is only a tenth of a millimeter, there are some areas where some curvature can be subtly sensed: curved region of the upper flange. The latter calls for an extension of the compensation process to achieve higher accuracy. The mold geometry is also shown (shaded).

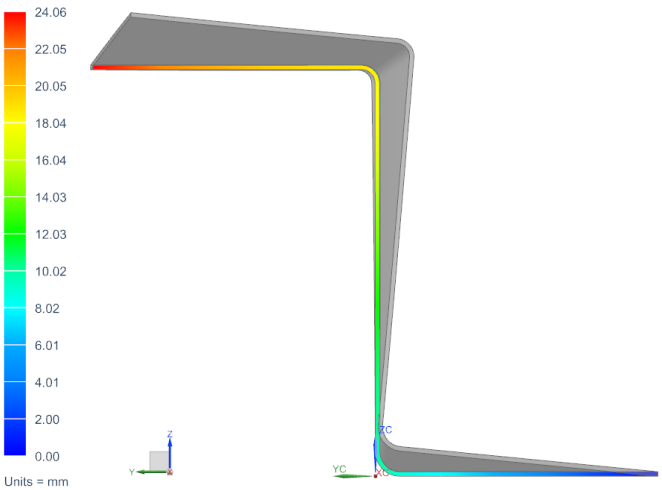

Figure 4.33: Last cured geometry and mold geometry of the Z-shape part under mixed deformation 3: the nominal geometry is recovered; the compensated mold (shaded) is depicted .

4.3.4 MM Convergence with Mixed Deformation

In this section, some conclusions are deduced about the convergence of the MM when mixed deformation occurs. The last three sections, where the MM has been applied with different laminates that induce different warpage deformations, serve as a basis to the discussion of the subject.

In [2], several geometries and laminates have been compensated with the MM. It is stated that when mixed deformation occurs in the curing process, the MM converges if the spring-in/spring-back deformation is more dominant than warpage on the global cure-induced displacement field. The earlier presented results yielded on the Z-shaped part under mixed deformation prove the latter. In the three cases the method converges, and thus it can be assumed that spring-in/spring-back dominates over warpage.

In the mixed deformation modes 1 and 2 (bending and torsion uncoupled) an accuracy order of 10^{-5} mm is achieved in 6 and 5 iterations, respectively. When mixed deformation 3 laminate is applied (bending and torsion coupled), the accuracy order achieved in 8 iterations is 10^{-2} mm. When bending and torsion are coupled the non-linear effects are higher and thus, spring-in/spring-back deformation dominates less over warpage.

As it was done in Section 4.2.1.4, a $[90_6/0_6]$ laminate has been applied to the the present geometry: the Z-shaped part. With such laminate, the non-linearities are more present in its displacement field due to the in-plane/out-of-plane coupling. This test has been performed in order to prove that if warpage dominates over spring-in/spring-back deformation, i.e. the displacement field is dominated by non-linear phenomena, then the MM should not converge as its main hypothesis is that cured-induced distortions are linear.

Effectively, as it happened in Section 4.2.1.4 with the flat plate when this laminate was used, the method does not converge. In Figure 4.34, the first 4 iterations of the method are depicted. And the latter divergence is shown: iterations 0 and 1 depict spring-back and bending of the flanges and web; then, in iteration 2 and 3, a torsional moment starts appearing on the whole structure; and in iteration 4 that torsional angle seems to be reducing. No more iterations have performed, but the cured geometry of iteration 4 seems to be recovering the shape of cured geometry 1 – showing a similar behaviour as the flat plate oscillating between saddle shapes.

From the results of the above mentioned test, plus the 3 mixed deformation modes studied, it can be stated that the conclusions deduced in [2] are confirmed: the MM will converge only if the spring-in/spring-back deformations prevail over warpage deformations. In such circumstances, the MM hypothesis of linear cure-induced distortions still has some validity, and despite taking more iterations, the method is able to yield a compensated mold mesh. Conversely, if warpage prevails the method does not converge.

4.3.5 Compensation with the DMM and CPM

As earlier mentioned, the compensated mold geometry of the Z-shaped part has not been found using the DMM and CPM. However, for the sake of completeness, some brief comments on how to approach the problem with these methods are detailed below:

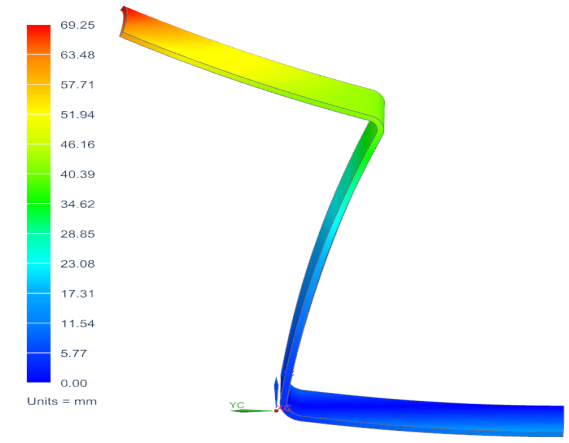

(a) Iteration 0.

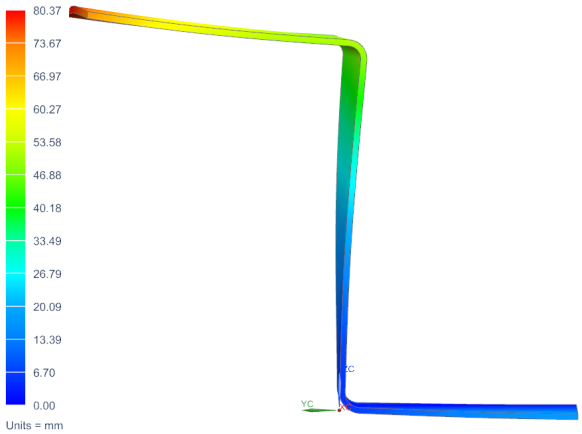

(b) Iteration 1.

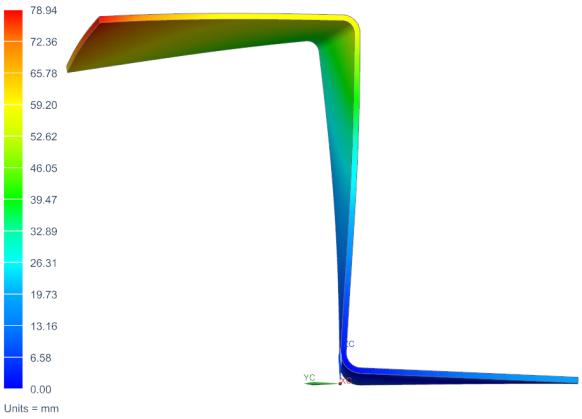

(c) Iteration 2.

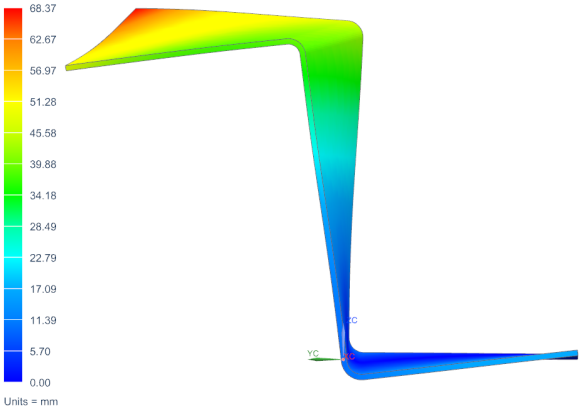

(d) Iteration 3.

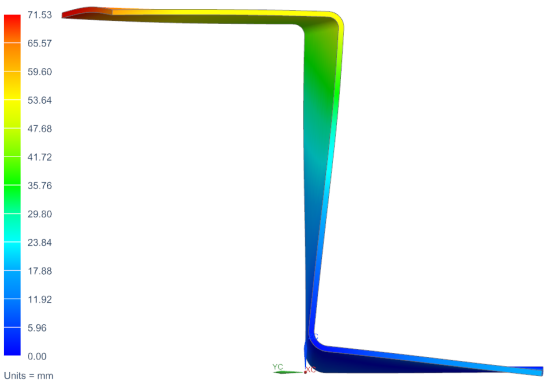

(e) Iteration 4.

Figure 4.34: Divergence of the MM on a flat plate under mixed warpage. A $[90_6/0_6]$ laminate has been used.

- **DMM**: the distortion modes that can be identified in this geometry under mixed deformation are: three spring-in/spring-back and twist/torsional angles, θ_i and ϕ_i (upper and lower flanges, and web); and 8 curvatures κ_i corresponding to the 8 edges. The total amounts to 14 parameters. A proposal of objective function is the following: $F_{obj} = \sum_{k=1}^{3} \left(\left| \frac{\theta_k}{\theta_0} \right| + \left| \frac{\phi_k}{\phi 0} \right| \right) + \sum_{i=1}^{8} \left| \frac{\kappa_i}{\kappa_0} \right|$. A similar one is used in [2], where a C-shaped curved spar is compensated and 7 distortion modes are identified.

- **CPM**: accounting for the mixed deformation, a prediction of how many CPs and how many variables are necessary is detailed next. The curvatures of the 8 edges require at least 3 CPs per edge. That amounts to 24 CPs. With such number of CPs on the edges, the twist and spring-in/spring-back angles can also be measured. As the deformation mode is mixed, 3 variables are required per CP (x, y and z components of each CP). Therefore, the total minimum amount of variables to solve this problem with the CPM is $24 \,\mathrm{x}\, 3 = 72$.

4.3.6 Applicability of the Methods under Mixed Deformation

Finally, a few comments on the three methods when the geometry to be compensated is under mixed deformation are detailed below:

- **Mirror Method**
  - The rate of reduction of residual distance per iteration is directly related with the intensity of the warpage deformation. The more warpage dominates the deformation field, the less residual distance is reduced per iteration.
  - Convergence is not guaranteed: if warpage (non-linear phenomenon) prevails over spring-in/spring-back deformation, the method diverges.
- **Distortion Modes Method**
  - The number of distortion modes increases a lot. In the spring-in/spring-back case there was only 1 distortion mode; in the warpage case there were 2 distortion modes; and in this case there are 14 distortion modes.
  - Complexity of the method increases: optimization of multiple variables at the same time. However, if the distortion modes are well identified and the optimization algorithm is well chosen and executed, the method will succeed [2].
- **Control Points Method**
  - The number of CPs and number of variables per CP increases drastically. A higher amount of total variables directly implies a higher complexity of the optimization process.
  - If the CPs are representative enough of the geometry, and the right variables are chosen, the method will succeed [2].

Conclusions

This chapter presents the final conclusions of the main subject of the thesis, mold compensation techniques. Besides from that, some proposals on how the achieved knowledge can be continued and expanded are discussed. Finally, a project overview is done in where a general valuation of the thesis is given.

5.1 Compensation Methods

This section presents a thorough comparison of the three compensation methods implemented and tested in this thesis. The characteristics to discuss the strengths and weaknesses of every method have been the ones chosen in [2], as they encompass all that can be compared from the results obtained in this thesis. Some of these characteristics have already been visited earlier in the text, but will be explained more in-depth.

Complexity of the computational chain: CAD-based methods (DMM and CPM) require a greater number of steps to perform a single iteration of the compensation process than the MM – see Figure 3.16 and 3.17. While the MM only requires an initial CAD model plus an initial FEM model that is then modified after every iteration, the DMM and CPM require a new CAD model and a FEM model every iteration.

The latter implies modifying the parametrized CAD model, seeding the geometry to obtain the desired mesh, modify the orientation of the elements, create the laminate and extrude it, assign boundary conditions, loads, set the different archiving frequencies and launch the simulation. After those steps, the optimization process must be applied. And finally, the post-processing must be done to obtain the final results, which is required by the three methods. The MM, on the other hand, just require an update of the mesh following equation 2.25, plus applying the loads, boundary conditions and the archiving frequencies. The above process to prepare the mesh is just performed once.

In terms of automating the process, the MM has less steps/tasks to be automated than the CAD-based methods. Thus, the MM is simpler than the DMM and CPM.

Compensation time: most of the compensation time is spent on the curing simulations (if the whole process is automated). CAD-based methods update the current iterate based on an optimization algorithm, which leads to a high number of total simulations. With the most employed algorithm in this thesis, the surrogate-based algorithm, there is a minimum of simulations required to create the first surrogate model, plus then the optimization iterations. This initial set of simulations and the total optimization iterations grow with the number of parameters, as mentioned in [2]. The latter is also proved in this thesis in the Results chapter, where 1 and 2 variable problems have been solved using the DMM or

the CPM and the latter tendency is observed.

On the other hand, the MM follows a fixed update of the mesh every iteration and converges quickly, if it converges. The tested cases in which the MM has converged have always required less simulations than the total simulations required by CAD-based methods (initial set + optimization). Therefore, when the method converges, the MM needs less time to obtain the compensated mold geometry.

In the case of a non-automated process, the mesh update must be done manually for the MM, and for CAD-based strategies a new CAD and FEM model must be created for every iteration. From those tasks, CAD-based strategies are the ones take more time.

Current robustness: CAD-based methods show a better robustness than the MM. The MM diverges when warpage prevails on the global cured-induced displacement field. The introduction of a relaxation factor to correct the non-linearities has been tried, being unsuccessful. On the other hand, CAD-based methods always lead to convergence if they are well formulated. The CPM, although it has only been tested twice in this thesis, is theoretically very effective. If choosing representative enough CPs, the method must yield the compensated position of such parametrized points. The DMM, as it is based on the knowledge of the distortion modes, has an excellent robustness if the modes are well identified.

Compensation success (accuracy): in terms of reduction of the distortions, the most efficient method is the MM, when it converges. The residual distance reduction is of almost 100 %, with δ_{res}^{max} achieved of the order of 10^{-5} mm. Recall that the compensation process on the MM is performed on all the geometrical points at the same time – geometrical points are represented by the mesh. Then, regarding the DMM and CPM, their success depends on the richness of the parametrization.

When the Z-shaped part was tested under spring-in deformation, the 3 methods' accuracy was compared. The DMM had a better accuracy than the CPM, which was only applied with 1 and 2 variables. The only distortion mode, i.e. the spring-in angle, was well identified and thus the process was effective. Regarding the CPM, the accuracy achieved with 2 variables was higher than with 1, proving that its accuracy depends on the number of variables used – as earlier mentioned in the thesis. Summing up, the MM (mesh-based) is more accurate than CAD-based methods.

Universality: the MM is the most generic method among the three presented in this thesis. It always starts by running one curing simulation where the mold geometry is the nominal geometry, and then the latter is updated iteratively until convergence is reached. The same cannot be said about CAD-based methods, which require adaptations from one geometry to another. They involve geometry-dependent tasks: parametrization of the geometry using different number of variables, definition of objective function in accordance with the geometry, etc.

Finally, as stated in [2], the principles of the CAD-based methods are generic: it is always possible to parametrize a geometry with control points or distortion modes. But by doing so, CAD-based methods remain subjective as these parameters are user-chosen. In

that respect, the CPM is more objective than the DMM: it is easier to choose the control points than the distortion modes, specially in complex geometries.

Control of the final shape: some shape constraints must be necessary to be introduced to the compensation process for manufacturing reasons: the vertices of a surface must remain on the same plane or two edges must remain parallel. The latter cannot be introduced in the MM as it is currently defined, whereas they are inherently part of the design process in CAD-based methods. In both the CPM and DMM, the user controls the parametrization and, therefore, controls the shape that the mold can take during the optimization.

CAD model of the compensated mold: the DMM and CPM are better than the MM in this aspect as they are CAD-based methods. Once the compensation process is finished, the CAD model of the last iteration is the CAD model of the compensated mold. The MM, on the other hand, requires the conversion of the final mold mesh to a CAD model.

It can be concluded that the choice of compensation method is not straightforward and it will be driven by considering each and every above exposed factor to the particular case: the complexity of the geometry and deformation mode – if warpage dominates the MM must be avoided, and if the deformation mode is too complex the CPM is more appealing than the DMM; the requirements in terms of manufacturing tolerances (compensation quality) – in which the MM achieves the lowest residual distance; the manufacturing constraints – if any, the only option is to use CAD-based methods; and so forth.

From an industrial point of view, the MM is the most appealing method: it is the easiest to be executed, it is generic and the achieved accuracy is very high. The key for this method to outrun CAD-based strategies is to improve its robustness: if some easy-ruled correction is found for the method to converge also when warpage prevails, then it is, by far, the best compensation technique. In respect to the inability of applying manufacturing constraints, [2] proposes a hybrid method where first an unconstrained mold shape is found with the MM and then with a CAD-based approach, the shape is tried to be reproduced introducing the constraints. Finally, regarding the CAD model of the mold, `NX` allows the conversion from mesh to volume CAD model following simple steps – thus, not being an important weakness of the method.

Regarding CAD-based methods, they are more difficult to be executed and its subjectivity (choice of the distortion modes and/or of the control points) should be improved. Even with the latter improved, they are less interesting as automation of the process would be very difficult to implement in a commercial software as `NX` – user-selection of optimization parameters, modification of the parametrized model after every iteration, proper meshing of the new geometry, etc. On the contrary, the MM formulation would allow it to be automated with less effort.

5.2 Future Work

The three compensation methods have been implemented and tested on different geometries and laminates in this thesis. From this basis, the next steps that may be interesting to investigate are the following:

- Model the mold on the numerical model instead of representing it as a surface of the part to be compensated. Modeling both the laminate and the mold, different subjects could be studied:
  - Mold/part interaction. Simulate the curing process taking into account the friction force between the mold and the part and how that affects the final shape.
  - Control the cycle temperature of the part by heating the mold and study the conduction between mold and part. An uneven distribution of temperature and its uneven displacement field could be studied.
  - Model the unmolding procedure: study the effect of suddenly releasing the part from the mold and how the residual stress converts into a residual displacement field once the part is free to move.
- Study the viability of introducing a correction into the MM to ensure its convergence when warpage deformation prevails over spring-back deformation.
- Automation of any of the three methods.
- Include the effect of viscosity in the curing process and study if its effect deviates the new mold geometry from the mold geometry obtained with a pure elastic formulation.
- Take a known composite part and design and manufacture a mold to produce it. Then produce the part and check the obtained tolerances. To achieve such goal, a painstaking numerical study should be performed: the final shape of the mold depend on how accurately the numerical model represents reality. A space discretization should be performed, i.e. refinement of the mesh on the curved regions or areas where large displacements happen; and study of the time step is crucial to capture the expansion/contraction of the part during the curing process.

The above proposed topics are just a few examples that could be undertaken as a new project from the level of know-how achieved in this thesis.

5.3 Project Overview

Overall, the scope and objectives set at the beginning of the document have been fully satisfied. However, and as in any project, more goals could have been tackled. But there have been two limiting factors: time, and lack of automation of the employed methods. The former has been taken into account to stop the investigation at a certain point, and the latter has limited the amount of tested geometries and laminates with the DMM and CPM.

The making of this thesis in a professional environment in collaboration with Samtech has been a truly enriching experience. Working with Siemens `NX` software for 4 months has allowed me to become skillful with it.

Finally, it is worth mentioning that this thesis has encouraged me to keep up with my education. The project and the internship in Samtech have been a good experience to realize that my student background is a good basis which allows me to work in a professional environment. But at the same time, it has shown me that I have still a lot new things to learn and discover.

Appendices

Classical Laminate Theory

The Classical Laminate Theory (CLT) is a direct extension of the classical plate theory for isotropic and homogeneous material as proposed by Kirchhoff – Love. However, the extension of this theory to laminates requires some modifications to take into account the inhomogeneity in the thickness direction, i.e. the stiffness variation through plies is considered. Below the assumptions made in this theory along with the assumptions made for classical plate theory are detailed.

A.1 Assumptions of the Classical Laminate Theory

1. The laminate consists of perfectly bonded plies. There is no slip between the adjacent plies. In other words, it is equivalent to saying that the displacement components are continuous through the thickness.

2. Each ply is considered to be a homogeneous layer such that its effective properties are known.

3. Each ply is in a state of plane stress.

4. The strain in the direction perpendicular to the ply due to the Poisson effect is ignored.

5. The individual ply can be isotropic, orthotropic or transversely isotropic.

6. The laminate deforms according to the Kirchhoff - Love assumptions for bending and stretching of thin plates (as assumed in classical plate theory). The assumptions are:

   (a) The normals to the midplane remain straight and normal to the midplane even after deformation.

   (b) The normals to the midplane do not change their lengths.

A.2 Development of the Classical Laminate Theory

The the tractions $\mathbf{N}$ and moments $\mathbf{M}$ applied to the plate at a position x,y are assumed to be known – see Figure A.1. These tractions and moments are normalized by the width of the plate, having units of N/m and N-m/m, or simply N, respectively. Coordinates x and y are the directions in the plane of the plate, and z is customarily taken as positive downward.

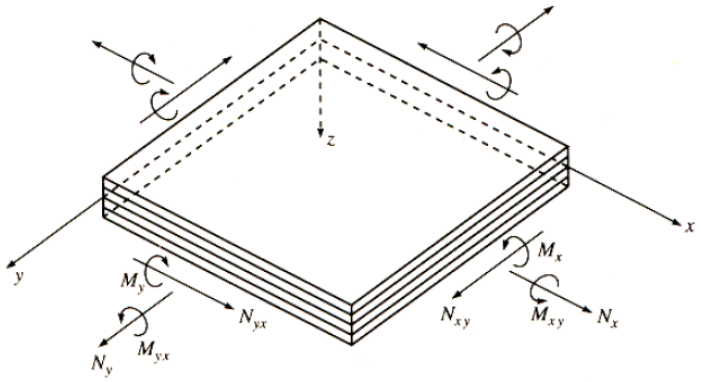

Figure A.1: Applied tractions and moments in a plate [9]

$$N = \begin{Bmatrix} N_x \\ N_y \\ N_{xy} \end{Bmatrix} \qquad M = \begin{Bmatrix} M_x \\ M_y \\ M_{xy} \end{Bmatrix} \tag{A.1}$$

When these tractions and moments are applied, a displacement field is generated in the plate. The plate bends (see Figure A.2) and the different in-plane displacements follow the relations described below:

$$u(x,y,z) = u_0 - z\frac{\partial w}{\partial x}, \qquad v(x,y,z) = v_0 - z\frac{\partial w}{\partial y}, \qquad w(x,y,z) = w_0(x,y) \tag{A.2}$$

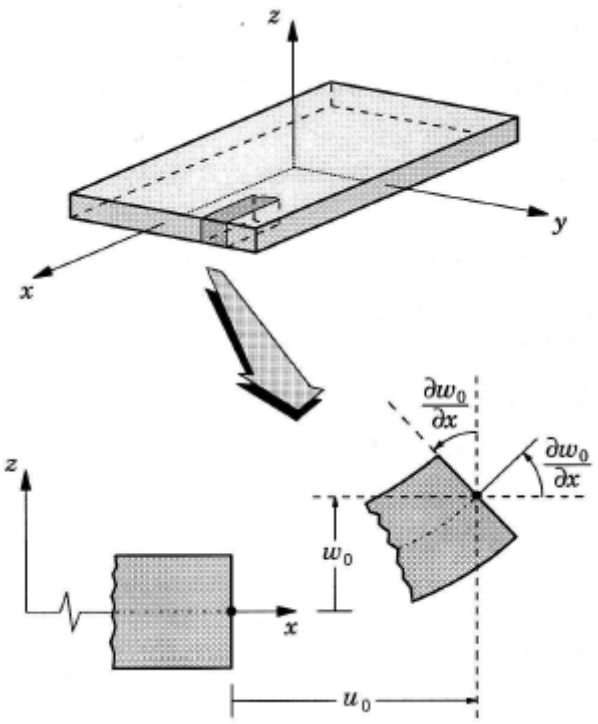

Figure A.2: Undeformed and deformed geometries of an edge of a plate under the CLT assumptions [10].

Displacement u corresponds to the x direction, v to the y direction and w to the z direction, while u_0, v_0 and w_0 are displacements of the midplane in x, y and z directions, respectively. It is important to recall that w is constant as it was stated on assumption 4, i.e. the strain in z direction due to Poissson effects is neglected. Being so, equation A.2 can be rewritten as

$$u(x,y,z) = u_0 - z\frac{\partial w_0}{\partial x}, \qquad v(x,y,z) = v_0 - z\frac{\partial w_0}{\partial y} \tag{A.3}$$

Based on the displacement field above, the strain field is defined as follows:

$$\begin{aligned} \varepsilon = \begin{Bmatrix} \varepsilon_x \\ \varepsilon_y \\ \gamma_{xy} \end{Bmatrix} = \begin{bmatrix} \frac{\partial}{\partial x} & 0 \\ 0 & \frac{\partial}{\partial y} \\ \frac{\partial}{\partial y} & \frac{\partial}{\partial x} \end{bmatrix} \begin{Bmatrix} u \\ v \end{Bmatrix} = \begin{Bmatrix} \frac{\partial u_0}{\partial x} \\ \frac{\partial v_0}{\partial y} \\ \frac{\partial u_0}{\partial y} + \frac{\partial v_0}{\partial x} \end{Bmatrix} + z \begin{Bmatrix} -\frac{\partial^2 w_0}{\partial x^2} \\ -\frac{\partial^2 w_0}{\partial y^2} \\ -2\frac{\partial^2 w_0}{\partial x \partial y} \end{Bmatrix} = \\ = \begin{Bmatrix} {\varepsilon_x}^0 \\ {\varepsilon_y}^0 \\ {\gamma_{xy}}^0 \end{Bmatrix} + z \begin{Bmatrix} \kappa_x \\ \kappa_y \\ \kappa_{xy} \end{Bmatrix} = \varepsilon^0 + z\kappa \end{aligned} \tag{A.4}$$

where ε^0 is the midplane strain and κ is the vector of second derivatives of the displacement, i.e. the *curvature*. The component k_{xy} is a twisting curvature, stating how the x-direction midplane slope changes with y (or equivalently how the y-direction slope changes with x).

The stresses relative to the x-y axes are now determined from the strains, and it must be consider that each ply will (usually) have a different stiffness – depending on its own mechanical properties and also its orientation with respect to the x-y axes. This is accounted for by computing the transformed stiffness matrix $\overline{D}$, which is the same matrix D as in Hooke's law $\sigma = D \cdot \varepsilon$, but multiplied by the transformation matrix $\mathcal{T}$.

$$\mathcal{T} = \begin{bmatrix} c^2 & s^2 & 2sc \\ s^2 & c^2 & -2sc \\ -sc & sc & c^2 - s^2 \end{bmatrix} \tag{A.5}$$

where $c = \cos\theta$ and $s = \sin\theta$. The angle θ is the angle that that the fibers form with the x-axis. The properties of each ply must be transformed to a common x-y axes, chosen arbitrarily for the entire laminate. The stresses at any vertical position are then:

$$\sigma = \overline{D}\varepsilon = \overline{D}\varepsilon^0 + z\overline{D}\kappa \tag{A.6}$$

where here $\overline{D}$ is the transformed stiffness of the ply at which the stresses are being computed. Each of these ply stresses must add to balance the traction per unit width $\mathbf{N}$:

$$N = \int_{-\frac{h}{2}}^{+\frac{h}{2}} \sigma dz = \sum_{k=1}^{N} \int_{z_k}^{z_{k+1}} \sigma_k dz \tag{A.7}$$

where σ_k is the stress in the *kth* ply and z_k is the distance from the laminate midplane to the bottom of the *kth* ply. Using equation A.6 to write the stresses in terms of the midplane strains and curvatures, it yields:

$$N = \sum_{k=1}^{N} \left(\int_{z_k}^{z_{k+1}} \overline{D}^k \varepsilon^0 dz + \int_{z_k}^{z_{k+1}} \overline{D}^k \kappa z dz \right) \tag{A.8}$$

The curvature κ and midplane strain ε^0 are constant throughout z, and the transformed stiffness $\overline{D}^k$ does not change within a given ply. Removing these quantities from the integrals, the expression is rearranged:

$$N = \sum_{k=1}^{N} \left(\overline{D}^k \varepsilon^0 \int_{z_k}^{z_{k+1}} dz + \overline{D}^k \kappa \int_{z_k}^{z_{k+1}} z dz \right) \tag{A.9}$$

After evaluating the integrals, this expression can be written in the compact form

$$N = \mathcal{A}\varepsilon^0 + \mathcal{B}\kappa, \tag{A.10}$$

where $\mathcal{A}$ is an *extensional* stiffness matrix defined as:

$$\mathcal{A} = \sum_{k=1}^{N} \overline{D}^k (z_{k+1} - z_k) \tag{A.11}$$

And $\mathcal{B}$ is a *coupling* stiffness matrix defined as:

$$\mathcal{B} = \frac{1}{2} \sum_{k=1}^{N} \overline{D}^k ({z_{k+1}}^2 - {z_k}^2) \tag{A.12}$$

The $\mathcal{A}$ matrix gives the influence of an *extensional* midplane strain (ε^0) on the in-plane traction $\mathbf{N}$, and the $\mathcal{B}$ matrix gives the contribution of a curvature (κ) to the traction (*coupling*). "It may not be obvious why bending the plate will require an in-plane traction, or conversely why pulling the plate in its plane will cause it to bend. But visualize the plate containing plies all of the same stiffness, except for some very low-modulus plies somewhere above its midplane. When the plate is pulled, the more compliant plies above the midplane will tend to stretch more than the stiffer plies below the midplane. The top half of the laminate stretches more than the bottom half, so it takes on a concave-downward curvature." [11, page 9]

Similarly, the resultant moments per unit width must be balanced by the moments contributed by the internal stresses. Following the same procedure as with the tractions:

$$M = \int_{-\frac{h}{2}}^{+\frac{h}{2}} \sigma z dz = \sum_{k=1}^{N} \int_{z_k}^{z_{k+1}} \sigma_k z dz \tag{A.13}$$

$$\begin{aligned} M &= \sum_{k=1}^{N} \left(\int_{z_k}^{z_{k+1}} \overline{D}^k \varepsilon^0 z dz + \int_{z_k}^{z_{k+1}} \overline{D}^k \kappa z^2 dz \right) = \\ &= \sum_{k=1}^{N} \left(\overline{D}^k \varepsilon^0 \int_{z_k}^{z_{k+1}} z dz + \overline{D}^k \kappa \int_{z_k}^{z_{k+1}} z^2 dz \right) \end{aligned} \tag{A.14}$$

$$M = \mathcal{B}\varepsilon^0 + \mathcal{D}\kappa \tag{A.15}$$

where $\mathcal{D}$ is a *bending* stiffness matrix defined as:

$$\mathcal{D} = \frac{1}{3} \sum_{k=1}^{N} \overline{D}^k ({z_{k+1}}^3 - {z_k}^3) \tag{A.16}$$

The complete set of relations between applied forces and moments, and the resulting midplane strains and curvatures, can be summarized as a single matrix equation:

$$\begin{Bmatrix} N \\ M \end{Bmatrix} = \begin{bmatrix} \mathcal{A} & \mathcal{B} \\ \mathcal{B} & \mathcal{D} \end{bmatrix} \begin{Bmatrix} \varepsilon^0 \\ \kappa \end{Bmatrix} \tag{A.17}$$

The $\mathcal{A}/\mathcal{B}/\mathcal{B}/\mathcal{D}$ matrix in brackets is the *laminate stiffness matrix*, and its inverse will be the *laminate compliance matrix*.

The above relations provide a straightforward – although tedious to solve unless a computer is used – means of determining stresses and displacements in laminated composites subjected to in-plane traction or bending loads.

A.3 Thermal and Chemical Effects in Laminates

If thermal and chemical effects are considered, the tractions and moments originated by these phenomena have to be computed. As $N = \mathcal{A}\varepsilon^0 + \mathcal{B}\kappa$, the thermal and chemical strains must be included. The total strain is the sum of the mechanical, thermal and chemical strain $\varepsilon_{tot} = \overline{S}^k\sigma + \varepsilon_{th} + \varepsilon_{ch}$, where $\overline{S}^k = \left(\overline{D}^k\right)^{-1}$. Therefore $\sigma = (\overline{D}^k(\varepsilon_{tot} - \varepsilon_{th} - \varepsilon_{ch})$, where $\varepsilon_{th} = \alpha\Delta T$ and $\varepsilon_{ch} = -\beta_m\Delta X$. Following equation A.7 it can be deduced:

$$N = \mathcal{A}\varepsilon^0 + \mathcal{B}\kappa - N^T + N^{CH} \tag{A.18}$$

Similarly for the moments, it can be deduced:

$$M = \mathcal{B}\varepsilon^0 + \mathcal{D}\kappa - M^T + M^{CH} \tag{A.19}$$

The thermal and chemical tractions and moments are described as follows:

$$N^T = \sum_{k=1}^{N} \left(\int_{z_k}^{z_{k+1}} \overline{D}^k \alpha^k \Delta T^k dz \right) \tag{A.20}$$

$$N^{CH} = \sum_{k=1}^{N} \left(\int_{z_k}^{z_{k+1}} \overline{D}^k \beta_m^k \Delta X^k dz \right) \tag{A.21}$$

$$M^T = \sum_{k=1}^{N} \left(\int_{z_k}^{z_{k+1}} \overline{D}^k \alpha^k \Delta T^k z dz \right) \tag{A.22}$$

$$M^{CH} = \sum_{k=1}^{N} \left(\int_{z_k}^{z_{k+1}} \overline{D}^k \beta_m^k \Delta X^k z dz \right) \tag{A.23}$$

where $\alpha^k = \begin{Bmatrix} \alpha_1 \\ \alpha_2 \\ \alpha_6 \end{Bmatrix}_k$ and $\beta_m^k = \begin{Bmatrix} \alpha_1 \\ \alpha_2 \\ \alpha_6 \end{Bmatrix}_k$ are the thermal expansion coefficient and chemical shrinkage coefficient, respectively, at the *kth* ply.

A.4 Types of Coupling

Equation A.17 can be expanded, detailing every component of matrices $\mathcal{A}$, $\mathcal{B}$ and $\mathcal{D}$ – see equation A.24.

$$\begin{Bmatrix} N_x \\ N_y \\ N_{xy} \\ M_x \\ M_y \\ M_{xy} \end{Bmatrix} = \left[\begin{array}{ccc:ccc} A_{11} & A_{12} & A_{16} & B_{11} & B_{12} & B_{16} \\ A_{12} & A_{22} & A_{26} & B_{12} & B_{22} & B_{26} \\ A_{16} & A_{26} & A_{66} & B_{16} & B_{26} & B_{66} \\ \hdashline B_{11} & B_{12} & B_{16} & D_{11} & D_{12} & D_{16} \\ B_{12} & B_{22} & B_{26} & D_{12} & D_{22} & D_{26} \\ B_{16} & B_{26} & B_{66} & D_{16} & D_{26} & D_{66} \end{array}\right] \begin{Bmatrix} {\varepsilon_x}^0 \\ {\varepsilon_y}^0 \\ {\gamma_{xy}}^0 \\ \kappa_x \\ \kappa_y \\ \kappa_{xy} \end{Bmatrix} \tag{A.24}$$

The coupling terms of this equation are A_{16} and A_{26}, the shear-extension coupling; the whole matrix $\mathcal{B}$, the in-plane/out-of-plane coupling; and D_{16} and D_{26}, the bending/torsion coupling.

A.4.1 Shear/Extension Coupling

The terms A_{16} and A_{26} imply the following: an in-plane traction oriented with any of the plate axis (x,y) will induce a shear deformation, and conversely, an in-plane shear traction will induce a x or y deformation. These terms will be zero if these type of laminates are used:

- Cross-py laminates (symmetrical or unsymmetrical): only made by 0 and 90°plies.
- Balanced angle-ply laminates (symmetrical or unsymmetrical): only made by $+\theta$ and -θ plies and in order to be *balanced* there must be the same amount of $+\theta$ and -θ plies.

A.4.2 In-plane/Out-of-plane Coupling

The presence of nonzero elements in the coupling matrix $\mathcal{B}$ indicates that the application of an in-plane traction will lead to a curvature or warping of the plate, or that an applied bending moment will also generate an extensional strain. However, this coupling can be avoided by making the laminate symmetrical about the midplane, as examination of equation A.12 can reveal.

The terms of the $\mathcal{B}$ matrix will be zero or nonzero depending on the type of laminate employed:

- symmetrical laminate: $[\mathcal{B}] = 0$.
- Unsymmetrical laminate: $[\mathcal{B}] \neq 0$.
- Anti-symmetrical cross-ply laminate: only made by 0 and 90°plies and anti-symmetry with respect to the midplane. $B_{11} \neq 0$ and $B_{22} \neq 0$ and the remaining terms are 0.
- Anti-symmetrical angle-ply laminate: only made by $+\theta$ and -θ plies and anti-symmetry with respect to the midplane. $B_{16} \neq 0$ and $B_{26} \neq 0$ and the remaining terms are 0.

A.4.3 Bending/Torsion Coupling

The terms D_{16} and D_{26} imply the following: a bending moment traction will induce a twist or warpage deformation, and conversely, a torsional moment induce a bending deformation. These terms will be zero if these type of laminates are used:

- Symmetrical and anti-symmetrical cross-ply laminates.
- Anti-symmetrical angle-ply laminates.

The latter can be deduced by proper examination of equation A.16. The terms $\overline{D}_{16}$ and $\overline{D}_{26}$ are zero for 0 and 90°plies. And regarding angle plies, $\overline{D}_{16}$ and $\overline{D}_{26}$ are nonzero but they have opposite signs and thus, they cancel out only when the laminate is anti-symmetrical.

A.4.4 Summary of Couplings

A summary of the couplings is depicted in Figure A.3, and Table A.1 groups together all the laminates described above and their respective $\mathcal{A}$, $\mathcal{B}$ and $\mathcal{D}$ matrices.

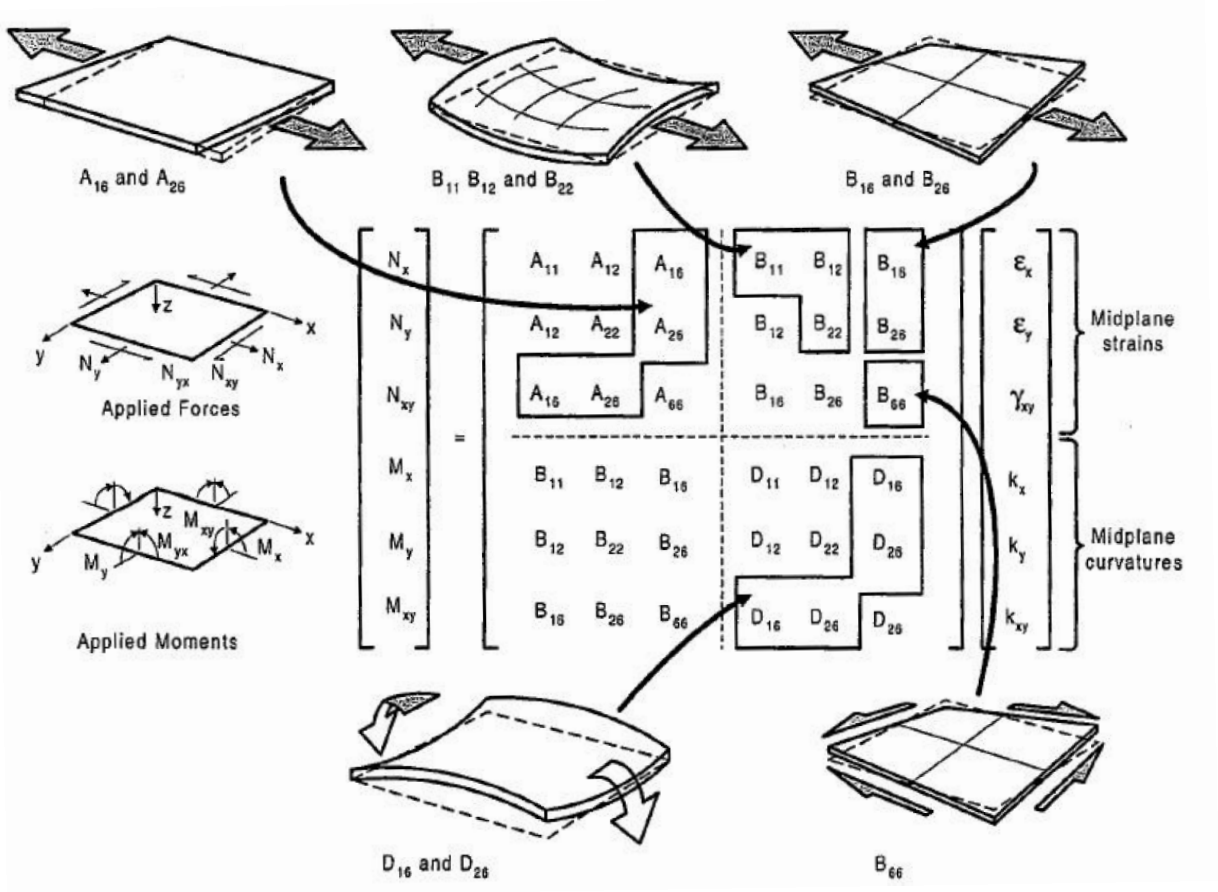

Figure A.3: Possible couplings in laminates [12].

Laminate	$\mathcal{A}$	$\mathcal{B}$	$\mathcal{D}$
Symmetrical cross-ply	$\begin{bmatrix} x & x & 0 \\ x & x & 0 \\ 0 & 0 & x \end{bmatrix}$	$\begin{bmatrix} 0 & 0 & 0 \\ 0 & 0 & 0 \\ 0 & 0 & 0 \end{bmatrix}$	$\begin{bmatrix} x & x & 0 \\ x & x & 0 \\ 0 & 0 & x \end{bmatrix}$
Anti-symmetrical cross-ply	$\begin{bmatrix} x & x & 0 \\ x & x & 0 \\ 0 & 0 & x \end{bmatrix}$	$\begin{bmatrix} x & 0 & 0 \\ 0 & x & 0 \\ 0 & 0 & 0 \end{bmatrix}$	$\begin{bmatrix} x & x & 0 \\ x & x & 0 \\ 0 & 0 & x \end{bmatrix}$
Symmetrical angle-ply	$\begin{bmatrix} x & x & 0 \\ x & x & 0 \\ 0 & 0 & x \end{bmatrix}$	$\begin{bmatrix} 0 & 0 & 0 \\ 0 & 0 & 0 \\ 0 & 0 & 0 \end{bmatrix}$	$\begin{bmatrix} x & x & x \\ x & x & x \\ x & x & x \end{bmatrix}$
Anti-symmetrical angle-ply	$\begin{bmatrix} x & x & 0 \\ x & x & 0 \\ 0 & 0 & x \end{bmatrix}$	$\begin{bmatrix} 0 & 0 & x \\ 0 & 0 & x \\ x & x & 0 \end{bmatrix}$	$\begin{bmatrix} x & x & 0 \\ x & x & 0 \\ 0 & 0 & x \end{bmatrix}$

Table A.1: Different types of laminates and its $\mathcal{A}$, $\mathcal{B}$ and $\mathcal{D}$ matrices.

Analytical Verification

`Samcef` capabilities have been tested on a simple geometry as performed in [13]. The main goal of the test is to compare the numerical measured spring-back angle – one of the main deformation modes in the curing of thermoset composites – with the analytical value. The test is performed in a 90° angle shape part made of a material with anisotropic thermal expansion coefficients.

The part geometry and boundary conditions are depicted in Figure B.1. Material '1' direction is parallel to the inner surface, direction '3' is perpendicular to the latter and direction '2' is perpendicular to the plane of interest.

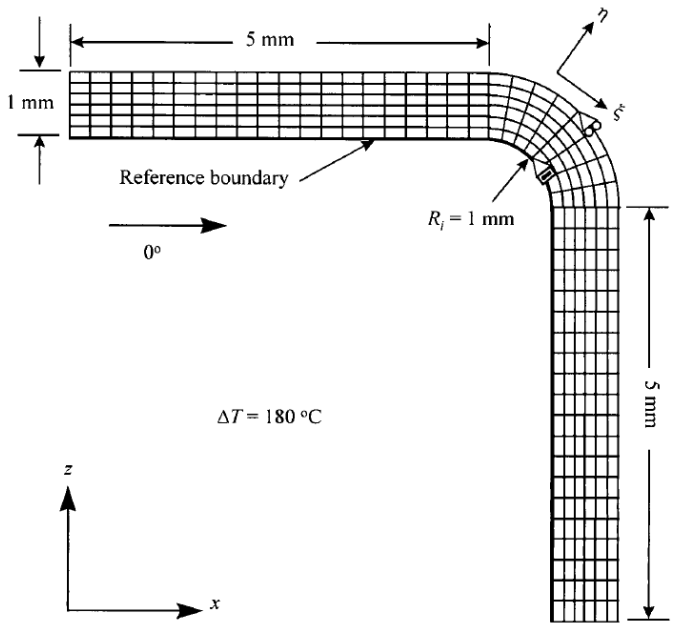

Figure B.1: Geometry employed for the thermal anisotropy spring-back test [13].

The material thermal expansion coefficients are $\alpha_1 = \alpha_2 = 0$ and $\alpha_3 = 100 \cdot 10^{-6}$ °C^{-1}. A total temperature difference of 180 °C is applied. The change in spring-back angle for this case can be calculated with the first-order approximation given in [13]:

$$\Delta\theta = \theta \left[\frac{(\alpha_\theta - \alpha_r)\Delta T}{1 + \alpha_r \Delta T} \right] \tag{B.1}$$

where θ is the initial angle (in this case 90°), $\alpha_\theta = \alpha_1$ and $\alpha_r = \alpha_3$. For a $\Delta T = 180$°C, equation B.1 yields an analytical spring-back angle of -1.591°. The convention used is that a positive spring-back angle induces a decrease on the original angle – see Figure B.2.

The effect of mesh density on predicted spring-back has been examined by varying the number of corner elements in the radial and circumferential directions. The type of elements used are 8-node solid elements. Additionally, all possible non-linearities have not been taken into account as equation B.1 is a first-order approximation.

The tested combinations of corner elements are presented in Table B.1:

Circumferential elements [−]	**Radial elements [−]**	**Predicted spring-back angle [º]**	**Prediction error [%]**
1	3	-0.3937	75.253
2	3	-1.3708	13.839
2	4	-1.3711	13.820
2	5	-1.3712	13.812
2	6	-1.3713	13.807
3	6	-1.5153	4.759
5	6	-1.5675	1.475
8	6	-1.5821	0.558
15	6	-1.5872	0.239
16	6	-1.5877	0.209
17	6	-1.5881	0.184
18	6	-1.5817	0.583
19	6	-1.5796	0.718
20	6	-1.5805	0.657
20	10	-1.5805	0.657

Table B.1: Tested corner elements and deviation with respect to the analytical solution.

For the above simulations, different boundary conditions have been used so that an odd number of elements along the circumference can be used – see Figure B.3. With the boundary conditions proposed in Figure B.1, just an even number of elements along the circumference can be used as the displacement constraints are applied on a 45^o tilted line with respect to the global axis z. Both boundary conditions have been implemented and tested with 8 and 6 elements along the circumference and radius, respectively. There is only a 0.01% difference in the measurements with each boundary conditions.

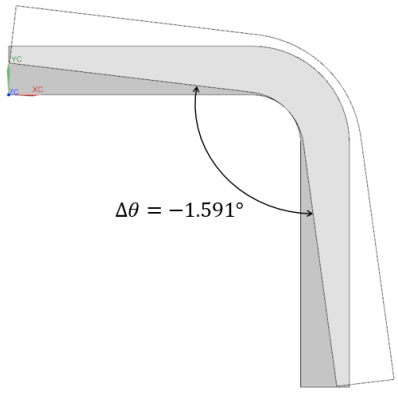

Figure B.2: Analytical spring-back of a 90^o angle shape with a $\Delta T = 180°$C.

As seen in the Table B.1, the influence of the number of radial elements can be neglected – when using 2 elements along the circumference, the number of radial elements does not modify the measured spring-back angle. Regarding the number of circumferential elements, a point is reached when increasing the number of elements does not reduce the prediction error but it increases it again. That point is

reached with 17 elements along the circumference. The same divergence is observed in [13] – where the software COMPRO is used, but at a different number of elements along the circumference.

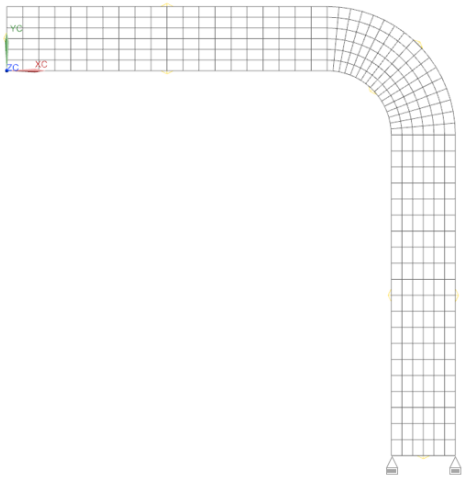

Figure B.3: Alternative boundary conditions so that odd number of elements along the circumference can be tested.

The reasons behind this divergence must have a relation with:

- The way of measuring the spring-back angle change. $\Delta\theta$ has been measured on the upper 1 mm edge with respect to the vertical z axis. The latter angle may not be the actual $\Delta\theta$.
- The assumptions made in [13] to deduce equation B.1, which are not detailed. If there is some additional condition that was taken to deduce such equation that what can be inferred by Figure B.1, the latter has not been taken into account.

The numerical divergence requires an in-depth study for it to have a detailed and clear explanation. In regards with `Samcef`, the test performed prove that it is completely capable of measuring spring-back angles when anitostropical thermal conditions are applied on a curved shape – accordance with analytical solution of more than 99 % when more than 8 elements along the circumference are used.

Compensated Molds with the Mirror Method

The MM final solution of the compensated mold is a mesh, but for the manufacturing purposes a CAD model with the mold's geometry needs to be created. This appendix's main purpose is briefly explain the procedure followed to convert a mesh into a CAD model with `NX`. The procedure is in fact very straightforward:

1. Open the FEM model (.fem) with the last mesh of the iterative process.
2. Then, in *Face operations*, there is an option called *Face from Mesh*. Then choose *2D element* as the type of mesh and next, select the final 2D mesh: a surface is created.
3. Once the surface is obtained it must be added to a CAD model. To do so in a FEM model environment, only one way has been found: create an empty CAD model, and assign it as the idealized part of the FEM model – the idealized part is the CAD model used to partition the geometry for meshing purposes. The latter is done using the option *Replace Ideal/ Master Part*. Once that is done, the surface can be added to the CAD-model by using the command *Insert>Model Preparation>Surface>From Polygon Face*.
4. The last step to perform is to open the CAD model with the surface and create the mold geometry by adding a surrounding structure to the surface.

Some examples of CAD models of compensated molds obtained in this thesis with the MM are depicted next:

- **Flat plate under pure bending (warpage)**

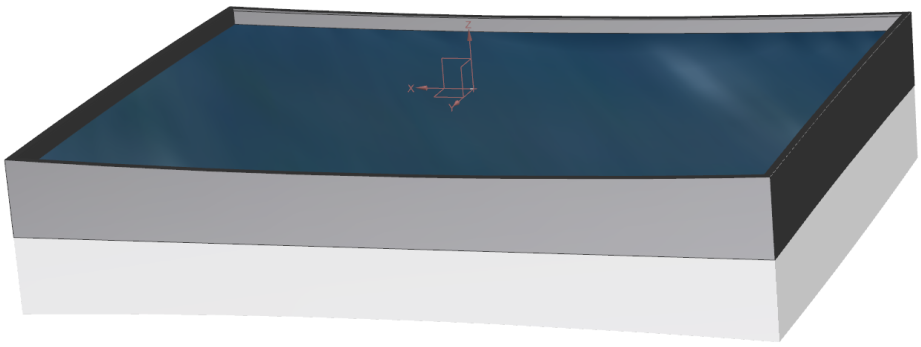

Figure C.1: CAD model of the mold obtained using the MM for the flat plate under pure bending.

- **Flat plate under pure torsion (warpage)**

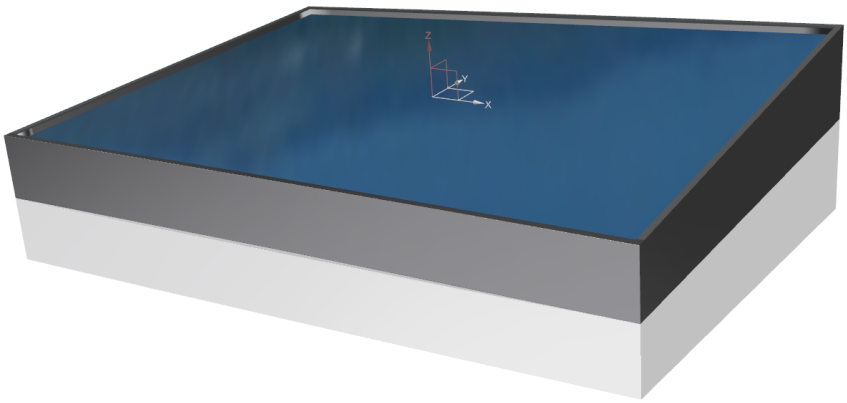

(a) General view.

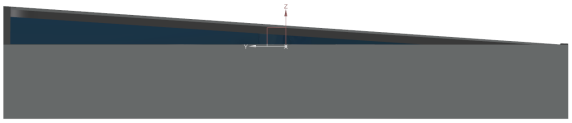

(b) Plane yz view.

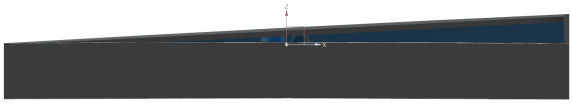

(c) Plane xz view.

Figure C.2: CAD model of the mold obtained using the MM for the flat plate under pure torsion.

- **Z-shaped part under spring-in deformation**

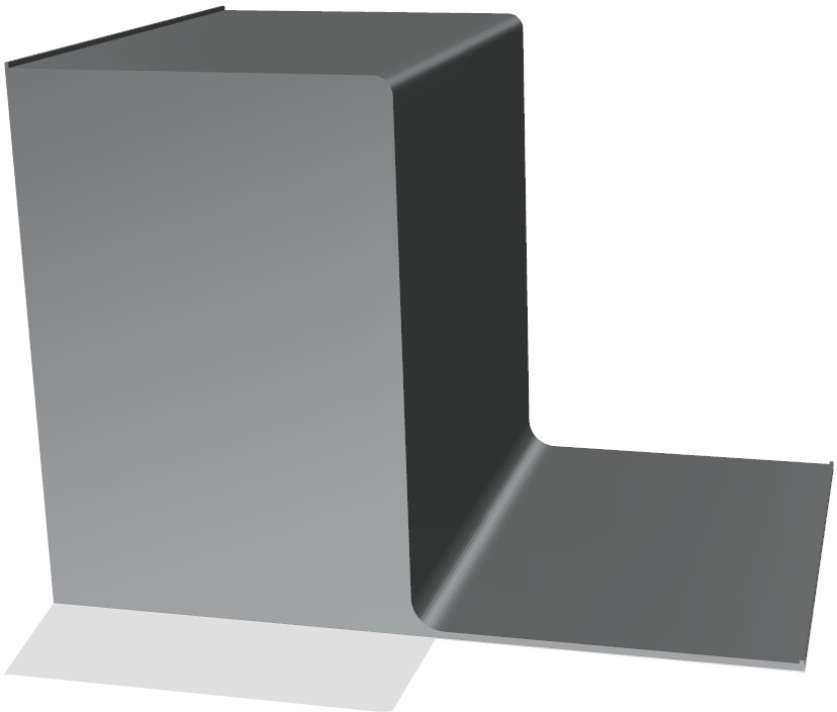

Figure C.3: CAD model of the mold obtained using the MM for the Z-shaped part under spring-in deformation.

List of Figures

List of Tables

List of Abbreviation and Symbols

Abbreviations

CAD	Computer-Aided Design
CAE	Computer-Aided Engineering
CAM	Computer-Aided Manufacturing
CHILE	Cure-Hardening Instantaneous Linear Elasticity
CLT	Classical Laminate Theory
CPM	Control Points Method
CP	Control Point
CTE	Coefficient of Thermal Expansion
D.O.F	Degrees of Freedom
DMA	Dynamics Mechanical Analysis
DMM	Distortion Modes Method
DSC	Differential Scanning Calorimetry
FEM	Finite Element Method
MM	Mirror Method
RTM	Resin Transfer Molding
SQRTM	Same Qualified Resin Transfer Molding
UD	Unidirectional
VARTM	Vacuum-Assisted Resin Transfer Molding

Symbols

α	Coefficient of thermal expansion
β	Coefficient of chemical shrinkage

δ_{res}	Residual distance
δ_{res}^{max}	Maximum residual distance
$\dot{X}$	Cure rate
η	Precision/threshold
κ_i	Curvature
λ	Fitting parameter of the Di Benedetto model of the glass transition temperature
$\mathcal{M}$	Mesh
ν	Poisson's ratio
$\overrightarrow{v_i}$	Displacement vector
$\mathcal{P}$	Set of variables
ϕ	Twist (torsional) angle
ρ	Density
σ	Stress
θ	Spring-in/spring/back angle
ε	Strain
ε^E	Dilatational strain
ε_{ch}	Chemical strain
ε_{th}	Thermal strain
ξ	Relaxation factor
A_i	Frequencies for the kinetic constants
b_D	Fitting parameter of the diffusion function
C_{ijkl}	Elastic tensor
D_{min}	Averaged sum of squared distances
E	Young's modulus
f_d	Diffusion function
F_{obj}	Objective function

G	Shear modulus
h	Thickness
H_T	Maximum heat per unit mass released by the curing reaction
K	Hydrostatic compressive modulus
K_i	Kinetic constants
M	Traction
N	Moment
N	Number of control points
p	Line search step
P_i	Point position
R^2	Interpolation fitting parameter
S_i	Activation energy for the kinetic constants
T	Curing/cycle temperature
t	Time
T_g	Glass transition temperature
V_f	Fiber volume fraction
X	Degree of cure
x	Spatial position
X_{gel}	Gelation point

Bibliography

[1] A. P. Chatzimichali and K. D. Potter, "From composite material technologies to composite products: a cross-sectorial reflection on technology transitions and production capability," *Translational Materials Research*, vol. 2, no. 2, 2015. [Online]. Available: http://dx.doi.org/10.1088/2053-1613/2/2/026001

[2] B. Wucher, "Predicting and compensating distortions of composite parts," Ph.D. dissertation, 2016.

[3] "Autoclave Design." [Online]. Available: http://netcomposites.com/guide-tools/guide/manufacturing/autoclave-design/

[4] "Fabrication methods." [Online]. Available: http://www.compositesworld.com/blog/post/fabrication-methods

[5] "LMS Samcef Documentation." [Online]. Available: http://lgintranet.lmsintl.com/v99/index.html

[6] R. Hill, "Theory of mechanical properties of fibre-strengthened materials—III. self-consistent model," *Journal of the Mechanics and Physics of Solids*, vol. 13, no. 4, pp. 189–198, 1965.

[7] Z. Hashin and S. Shtrikman, "On some variational principles in anisotropic and nonhomogeneous elasticity," *Journal of the Mechanics and Physics of Solids*, vol. 10, no. 4, pp. 335–342, 1962.

[8] Wolfram—Alpha. [Online]. Available: http://www.wolframalpha.com/widgets/view.jsp?id=372d3f309fef061977fb2f7ba36d74d2

[9] "Tractions and moments in a plate." [Online]. Available: http://www.mathworks.com/matlabcentral/mlc-downloads/downloads/submissions/44717/versions/6/screenshot.jpg

[10] J. N. Reddy, *Mechanics of Laminated Composite Plates - Theory and Analysis*. CRC Press, 1997.

[11] D. Roylance, "Laminated composite plates," 2000.

[12] M. Bruyneel, "Mechanics of composites - Classical laminate theory. Lecture notes."

[13] A. a. Johnston, "An integrated model of the development of process-induced deformation in autoclave processing of composite structures," Ph.D. dissertation, 1997.